From the Infrared to the Ultraviolet and Back Again

Manuel Meinrad Ettengruber

München 2024

From the Infrared to the Ultraviolet and Back Again

Manuel Meinrad Ettengruber

Dissertation
der Fakultät für Physik
der Ludwig-Maximilians-Universität
München

vorgelegt von
Manuel Meinrad Ettengruber
aus Vilsbiburg

München, den 14.02.2024

Erstgutachter: Prof. Dr. Gia Dvali
Zweitgutachter: Prof. Dr. Allen Caldwell
Tag der mündlichen Prüfung: 21.03.2024

Zusammenfassung

In dieser Arbeit wird die Frage diskutiert, wie Theorien, deren Energieskala höher ist als die des Standardmodells der Teilchenphysik, sich in Experimenten zeigen, die auf Energieskalen operieren, die im Vergleich viel niedriger sind als die der elektroschwachen Wechselwirkung. Da der neutrinolose doppelte Betazerfall ein etabliertes Beispiel für solch einen Prozess ist, wird zunächst diskutiert, inwieweit es möglich ist, dass die dazu bereits geplanten Experimente ein Signal detektieren würden, wenn die normale Massenordnung für Neutrinos in der Natur realisiert ist. Die Wahrscheinlichkeit einer Detektion wird in Abhängigkeit von der Masse des leichtesten Neutrinos und der daraus resultierenden Abhängigkeit von kosmologischen Tests der Neutrinomassensumme diskutiert. Der weitere Teil dieser Arbeit befasst sich mit einer Klasse von Theorien, die die Energieskala der Gravitation von der Planckskala auf Terraelektronenvolt absenken, um das Hierarchieproblem zu lösen. Zunächst wird eine allgemeingültige Herangehensweise vorgestellt, wie der Neutrinosektor in solchen Theorien behandelt werden kann. Anschließend wird diese verwendet, um die Phänomenologie solcher Theorien in der Neutrinophysik zu bestimmen. Die Vorhersagen der Dvali-Redi-Theorie mit vielen Kopien des Standardmodells werden im Anschluss zum ersten Mal experimentell überprüft. Dazu wird eine kombinierte Datenanalyse von mehreren Experimenten durchgeführt. Es wurden keine Signale dieser Theorie gefunden, und daraus werden mögliche Werte der relevanten Parameter ausgeschlossen. Ein weiteres Teilchen, das von diesen Theorien potenziell beeinflusst wird, ist das Neutron. Diese Möglichkeit wird im Hinblick auf das Arkani-Hamed-Dimopoulos-Dvali-Modell mit großen extra Dimensionen diskutiert, und abhängig vom spezifischen Szenario ist es möglich, den verfügbaren Parameterbereich erheblich einzuschränken oder Vorhersagen für Neutronenoszillationsexperimente zu machen. Ein Resultat ist, dass solche Experimente sensitiv genug sind, um mit anderen experimentellen Möglichkeiten diese Modelle zu überprüfen konkurrenzfähig zu sein. Zum Abschluss werden theoretische Überlegungen angestellt, wie die Existenz vieler dunkler Yang-Mills-Sektoren, wie im Dvali-Redi-Modell, die Physik der hy-

pothetischen Axionen beeinflussen kann. Aus der Anforderung, das starke CP-Problem für jeden zusätzlichen Yang-Mills-Sektor zu lösen, entspringt die Notwendigkeit eines Axions pro Yang-Mills-Sektor. Dies hat zur Folge, dass eine kosmologische Produktion über den Misalignment-Mechanismus die Anzahl von zusätzlichen Axionen von oben beschränkt. Darüber hinaus führt ein mögliches kinetisches Mixen der Axionen zu Abweichungen in der Masse und im Kopplungsverhalten im Vergleich zum Fall mit nur einem Axion.

Abstract

This work discusses how theories with energy scales higher than that of the Standard Model of particle physics manifest in experiments operating at much lower energy scales compared to the electroweak scale. Since neutrinoless double beta decay serves as an established example of such a process, the discussion initially explores the possibility of detecting a signal in experiments already planned if the normal mass hierarchy for neutrinos in nature is realized. The probability of detection is discussed in relation to the mass of the lightest neutrino and its dependence on cosmological tests of the neutrino mass sum. The subsequent part of this work focuses on a class of theories that lower the energy scale of gravity from the Planck scale to the teraelectronvolt scale to solve the hierarchy problem. Initially, a general approach is introduced on how the neutrino sector can be addressed in such theories. This approach is then utilized to determine the phenomenology of such theories in neutrino physics. The predictions of the Dvali-Redi theory with many copies of the Standard Model are experimentally tested for the first time through a combined data analysis of multiple experiments. No signals of this theory were found, leading to the exclusion of possible values for the relevant parameters. Another particle potentially influenced by these theories is the neutron. This possibility is discussed concerning the Arkani-Hamed-Dimopoulos-Dvali model, and depending on the specific scenario, it is possible to significantly narrow down the available parameter space or make predictions for neutron oscillation experiments. One result is that such experiments are sensitive enough to be competitive with other experimental approaches to this model. Finally, theoretical considerations are made regarding how the existence of many dark Yang-Mills sectors, as in the Dvali-Redi model, can influence the physics of hypothetical axions. From the requirement to solve the strong CP problem for each additional Yang-Mills sector arises the necessity of one axion per Yang-Mills sector. This implies that cosmological production via the misalignment mechanism limits the number of additional axions from above. Furthermore, possible kinetic mixing of axions leads to deviations in mass and coupling behavior compared to the case with only one axion.

Projects and Publications

This thesis is based on completed and ongoing projects to which I have contributed during my research conducted at the Ludwig–Maximilians–Universit¨at München and the Max Planck Institute for Physics from January 2021 to March 2024. The projects resulted in a series of papers [1, 2, 3, 4] that have already been published or are in preparation. The authors are listed alphabetically by convention in particle physics and share the principal authorship. Although some new aspects were added and discussions were rephrased for a better understanding, a substantial part of this thesis is an ad verbatim reproduction with respect to equations, figures, and tables of these papers:

- M. Ettengruber, M. Agostini, A. Caldwell, P. Eller, and O. Schulz, "Discovering neutrinoless double-beta decay in the era of precision neutrino cosmology," Phys. Rev. D 106 no. 7, (2022) 073004, arXiv:2208.09954 [hep-ph].
- M. Ettengruber, "Neutrino physics in TeV scale gravity theories," Phys. Rev. D 106 no. 5, (2022) 055028, arXiv:2206.00034 [hep-ph]
- M. Ettengruber and E. Koutsangelas, "Consequences of Multiple Axions in Theories with Dark Yang-Mills Groups," arXiv:2307.10298 [hep-ph]
- G. Dvali, M. Ettengruber, and A. Stuhlfauth, "Kaluza-Klein Spectroscopy from Neutron Oscillations into Hidden Dimensions," arXiv:2312.13278 [hep-ph]
- M. Ettengruber, A. Zander, and P. Eller, "Testing the Number of Neutrino Species with a Global Fit of Neutrino Data," arXiv:2402.00490 [hep-ph]

The following papers I contributed but are not included in this thesis are:

- A. Caldwell, M. Ettengruber, A. Merle, O. Schulz, and M. Totzauer, "Global Bayesian analysis of neutrino mass data," Phys. Rev. D 96 no. 7, (2017) 073001, arXiv:1705.01945 [hep-ph]

- A. Zander, M. Ettengruber, and P. Eller, "How Many Dark Neutrino Sectors Does Cosmology Allow?," arXiv:2308.00798 [hep-ph]

The following paper in preparation is not included in this thesis:

- G. Dvali, M. Ettengruber, A. Jankowsky, in preparation

Danksagung

Während dem Verfassen dieser Dissertation wurde ich von vielen Menschen unterstützt, um letztendlich dieses Projekt erfolgreich zum Abschluss zu bringen.

Mein erster Dank geht an meine beiden Doktorväter, die mir die Gelegenheit und Inspiration gegeben haben, um meine Forschung erfolgreich zu betreiben. Prof. Dvali hat mich gelehrt, wie man in der theoretischen Physik neue Wege beschreitet und gleichzeitig die Rigorosität seiner Forschung nie aus den Augen verliert. Durch seine nach dem akademischen Ideal geprägte Betreuung konnte ich als junger Wissenschaftler an meinen Herausforderungen wachsen; Er gab mir so viel Freiheit wie möglich und Betreuung wo nötig.

Prof. Caldwell eröffnete mir das Feld der experimentellen Teilchenphysik und dadurch hat sich mein Horizont der Physik enorm erweitert. Die Option seine eigenen Theorien einem experimentellen Test zu unterziehen ist eine Fähigkeit, die durch eine immer stärkere Trennung zwischen Theoretikern und Experimentalphysikern nicht oft anzutreffen ist, und ich bin dankbar, dass das Experiment mir Beides beizubringen versucht wurde und nun auch geglückt ist.

Darüber hinaus möchte ich all meinen Kollegen danken, mit denen ich zusammen Antworten auf die Fragen der Physik gesucht habe. Es war mir eine Ehre und Freude, mit Philipp Eller, Oliver Schulz, Alan Zander, Matteo Agostini, Emmanouil Koutsangelas, Anna Jankowsky und Anja Stuhlfauth zusammenzuarbeiten. Ich habe viel von unseren Diskussionen gelernt; Mögen viele weitere folgen und uns neue physikalische Abenteuer erwarten.

Mein Doktorat am Max-Planck-Institut für Physik werde ich immer als eine äußerst glückliche Zeit in Erinnerung behalten und das liegt vor allem an den Menschen, die ich währenddessen kennenlernen durfte, die diesen Ort zu etwas Besonderem gemacht haben. Dafür danke ich, Anja Stuhlfauth, Giacomo Contri, Emmanouil Koutsangelas, Maximilian Bachmaier, Juan Sebastian Valbuena Bermudes, Ana Alexandre, Anna Jankowsky, Lucy Komisel, Lasha Berezhiani, Anna Bertolini, Francesca Pucci, Johannes Diehl, Dominik

Fuchs, Vera Kudrin und Vielen mehr. Ein besonderer Dank geht an meinen langjährigen Bürokollegen Giordano Cintia, mit dem ich einige Schachpartien geschlagen habe, wenn wir mal eine kurze Auszeit von der Physik brauchten.

Auch meinen ehemaligen Mathematik- und Physiklehrern, Monika und Harald Hoiß, möchte ich an dieser Stelle dafür danken, dass sie in mir das Interesse an der Physik geweckt haben und mich dazu ermutigt haben, dieses Studium zu ergreifen. Es war offensichtlich die richtige Entscheidung.

Schließlich, aber nicht zuletzt, möchte ich meiner Familie dafür danken, dass sie mich während all dieser Jahre uneingeschränkt unterstützt hat. Mit dies als Gewissheit fällt es einem leichter, Wege zu beschreiten, an denen man auch scheitern kann, aber deren Endresultate dafür umso besser sind. Meinen letzten Dank habe ich für Lidiia Renkas aufgespart. Ihre bedingungslose Liebe und Unterstützung ist ein Quell von Wärme, Stärke und Freude.

Contents

Chapter 1

Introduction

As soon as a new method in science is discovered the path for scientific progress and success is clear. The cooking recipe is: "Take the current scientific problems, throw the new method on it and it is quite likely that you find something great!". This is true in engineering with the steam engine developed by Savery, Newcomen, and Watt which opened the door for industrialization and it is true for quite current developments like the CRISPR/-Cas method by the Nobel laureates Charpentier and Doudna which allows humanity to manipulate genes of organisms in such an efficient way that one can build a whole industry on it.

But after the pioneering phase and the following phase of triumph comes a time when new problems appear that are difficult to solve with the current method if it is not impossible. Of course, looking at such developments from a historical point of view looks clearer to the reader of a lexicon than to the protagonists of that time.

The field of elementary particle physics is right now in the stage where its triumph is a long ongoing story both from the theoretical point of view with the implementation of gauge groups and quantum field theory in particle physics with the Standard Model of Particle Physics (SM) as its crowning moment as well as on the experimental site where one can nowadays measure the predictions of the theory with such a precision that the computing power for the theoretical predictions is the actual bottleneck.

But already during its success, appeared problems on the horizon for elementary particle physics that show quite a resistance to be solved using the usual attempts of particle physics even after decades of intensive research in theory and experimental physics. Some of the problems of modern physics, and also the most severe problems from the personal point of view of the author, are the prominent Dark Matter (DM)/-Energy (DE) problem, the open question of the nature of neutrino masses, the strong CP Problem, and

the Hierarchy Problem.

Here a short explanation is in order what we call a "problem". First one has to mention that no terrestrial experiment gives us a signal that one could not explain with the SM. The roots of the above-mentioned problems come either from astrophysical observations like in the DM/DE case [5], from the interplay of theory and observations like in the neutrino case (massive neutrinos in the SM are not a problem per se but the nature and the size of the mass term remains an open question) [6] or address theoretical inconsistencies like the strong CP problem [7, 8] or the hierarchy problem [9].

Following the cooking recipe of success of elementary particle physics on started to think about models with an extended gauge sector compared to the one of the SM. These models were typically linked with an energy scale well above the scale of the SM to avoid contradiction with experiments. Very prominent examples of such models are the left-right symmetric model [10], Supersymmetry [11], and grand unified theories [12]. Each of these models follow a very tempting principle in order to solve some of the questions mentioned above. Because all these models have an inherent energy scale lying above the electro-weak scale one calls such models "UV-models" or "UV solutions".

Even though they are following the cooking recipe of success so far no imprints of these theories have been found in experiments. Some models experiments could rule out quite quickly, like an unbroken supersymmetry, for others, they were able to give tighter and tighter bounds on the available parameter space for different theories. The situation that no hints of the UV theory of nature show up in our terrestrial experiments is not an issue from a consistency point of view but some may wonder if the path a lot of people in the community are following is the right one.

Maybe particle physics is at a stage right now where a new concept is needed to solve the current problems. One Ansatz that we will investigate in this work further is the idea that new physics is not introduced at a high energy scale but by lowering the gravitational scale of nature from the Planck scale, M_P, down to a new scale, M_*, which lies around TeV. At first glance this ansatz has two tempting characteristics: 1) By lowering the scale of gravity down to TeV one solves the hierarchy problem and 2) One does not have to introduce unmotivated new types of interactions but one stays with the one of the SM and of gravity.

The first framework that could lower the scale of gravity was the theory of large extra dimensions which was introduced by Arkani-Hamed, Dimopoulos, and Dvali and is therefore called ADD model [13, 14]. Later a second framework was discovered that could achieve the same thing by adding a large number of additional species within a theory [15, 16]. One specific model that

realized this mechanism was proposed by Dvali and Redi (DR model) who introduced many copies of the SM [17]. Further research showed that these two frameworks are not just able to solve the hierarchy problem but can also give answers to some of the above-mentioned problems [18, 19, 20, 17, 21]. I will discuss these two frameworks later in great detail but let me just state here that these two theories follow a very different philosophy from the ones discussed before. In these theories, the problems are solved by lowering a scale lying in the UV down to TeV scale and the new additional states are lighter than the cutoff of the theory. Therefore, we call such attempts "IR-models".

Of course, these frameworks rely on concepts that have not yet been observed in nature but they offer a different perspective on how one can solve the same problems with very different philosophies. If now the UV- or the IR solutions or even a possibility not yet thought of will be the answer to current questions time will show but at this stage, one cannot tell which way to go is the right one. Therefore, in this thesis, I will follow the path of IR-models and present my corresponding research conducted at the Max-Planck Institut für Physik in the last three years.

In the following chapter 2 I present the findings of [1] in which we have calculated the discovery probability for next-generation neutrinoless double beta decay experiments in the scenario of three light Majorana neutrinos which is a very prominent IR signal of new physics. We have performed this analysis in a Bayesian manner and discussed the dependency of the discovery power of the different experiments with respect to the theoretical uncertainties in the nuclear matrix element calculations and the dependency on the lightest mass eigenstate. Because cosmology is able to constrain or measure the latter quantity with high precision in the upcoming future we discuss in detail how neutrinoless double beta decay ($0\nu\beta\beta$) searches are entangled with cosmological surveys.

The chapter 3 starts the discussion about IR solutions and it begins with presenting [2]. In this work, the neutrino sector of such theories is investigated. The mass mechanism generating neutrino masses in such theories has been generalized and extended to a realistic three-flavor case. This has then been applied to the ADD model and the many species model to calculate the oscillation behavior of neutrinos in such theories.

Chapter 4 is based on [22] where we used the findings of [2] to perform a global fit of neutrino data to test the DR model and give the first lower bound on the number of additional neutrino species.

We discuss in chapter 5 the possibility that within the ADD model also neutrons and not just neutrinos as proposed so far can mix with bulk fields and oscillate into states of the KK-tower. By using the long lifetime of neu-

trons in bound states it is possible to draw powerful conclusions regarding the parameters of the theory. Moreover, we outline how current neutron experiments are already testing the parameter space motivated by the Hierarchy Problem. This chapter is based on [4].

Complementary to the experimental probe of the DR model we pursue in chapter 6 the deeper theoretical investigation of models which consist of multiple additional Yang-Mills (YM) groups like the DR model. Due to consistency with Quantum Gravity (QG) an extra axion is required per additional YM group and the phenomenology of many axions is discussed in detail. Among other results, one important one is that this enables us to give an upper bound on the number of additional YM groups by demanding that production via the misalignment mechanism should not exceed existing DM bounds. This result is based on [3].

All the necessary background knowledge to understand the chapters is introduced in the chapters themselves. Therefore it is possible to read the chapters by themselves in a consistent way. If a specific framework is investigated in several chapters the introduction to it is done in the first one. Also, the motivation for specific physical problems which are discussed within this thesis will be discussed when they show up the first time.

Chapter 2

Discovering Neutrinoless Double-Beta Decay in the Era of Precision Neutrino Cosmology

2.1 Neutrinoless double beta decay and Majorana Neutrinos

As promised in the title we start in the low-energy regime of neutrinoless double beta decay ($0\nu\beta\beta$). It is a nuclear process that goes as

$$n + n \to p + p + 2e^{-}. \tag{2.1}$$

This process is not allowed in the SM because it breaks $U(1)_{B-L}$ which is an accidental symmetry of the SM. But if we take a look at physics beyond the SM one sees that there are theories that can make such a process take place. The most prominent way $0\nu\beta\beta$ decay can be realized is the possibility that the neutrino forms a Majorana mass term. Majorana noticed in [23] that there is the following possibility to form a Lorentz-invariant mass term with a four-component spinor, Ψ, defined with the condition

$$\Psi = \Psi^{c}. \tag{2.2}$$

The upscript c is the so-called "charge conjugation transformation", and is defined as

$$\Psi^{c} = C\bar{\Psi}^{T}, \tag{2.3}$$

and takes a particle to its anti-particle. Now we understand that from (2.2) one cannot distinguish a Majorana particle from its own antiparticle. The free, Lorentz invariant, Lagrangian for such a spinor looks like the following

$$\mathcal{L} = i\bar{\Psi}\gamma^{\mu}\partial_{\mu}\Psi + m\bar{\Psi}\Psi. \tag{2.4}$$

If one introduces the notion of chiral Weyl-spinors, u_L, one can show that we can express our Ψ as

$$\Psi = \begin{pmatrix} u_L \\ -i\sigma_2 u_L^* \end{pmatrix}, \tag{2.5}$$

and we can rewrite the mass term (2.4) into

$$\frac{1}{2}m(u_L^T i\sigma_2 u_L + h.c.). \tag{2.6}$$

Now let us identify our generic u_L with the left-handed up quark of the SM. Even though this term is Lorentz invariant it is not invariant under the gauge group of the SM. Every particle that carries a charge under this group will violate the symmetry condition and one can therefore not write down this term in the SM Lagrangian.

The situation is different for the neutrino. In the SM a neutrino, ν_L, is the doublet partner of the left-handed electron, e_L, under $SU(2)_L$

$$\begin{pmatrix} \nu_L \\ e_L \end{pmatrix}. \tag{2.7}$$

The e_L can form a Dirac mass term with e_R but the SM does not contain ν_R and therefore predicts, that the neutrino is massless.

Nevertheless, nowadays the situation has evolved from the time the SM was proposed. Due to the observed phenomenon of neutrino oscillations [24] we know nowadays that the neutrino has a mass that is unequal to zero due to its specific E/L behavior that is characteristic for the theory of Pontecorvo where the oscillation behavior comes from a mismatch between the flavor interaction states and the mass states [25, 26]. A deeper discussion about the theory of neutrino oscillations is presented in chapter 3.

For now, it is important to note that the neutrino has a mass and can form additional to a Dirac mass term, like the rest of the particles in the SM, also a Majorana mass term. In order to do so one has to introduce right-handed neutrinos into the matter content of the SM. Because the Majorana mass term breaks Lepton number by two units it is possible to write down the diagram 2.1.

This process describes how two left-handed down-quarks can decay into two left-handed up-quarks and two left-handed electrons by the insertion of

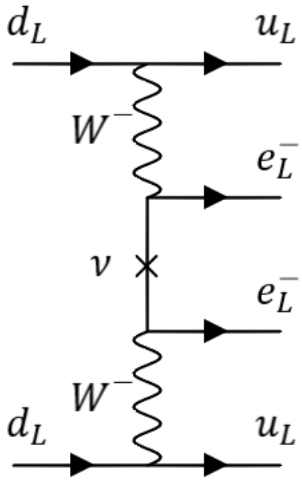

Figure 2.1: A process that violates Lepton number by two units which results from the inserted majorana mass vertex for the neutrino.

a Majorana mass vertex for the neutrino. Because of the fermion content of the neutron, udd, and the proton, uud, this diagram can cause a nuclear decay as we described in (2.1). Of course, if we want to calculate the decay probability one has to keep in mind that it is not enough to just evaluate the Feynman diagram but one has to also consider nuclear physics effects. Nevertheless, let us pick out the Majorana neutrino propagator which is special in this diagram, and investigate it further. From the SM we know that the interaction Lagrangian does not produce a diagonal mass matrix. In order to define consistent propagators one has to choose the basis in which the mass matrix is diagonal. The following discussion about the mismatch between the interaction basis and the propagating basis relies on the review [27] and the discussion about the related $0\nu\beta\beta$ on [28]. The so-called mass basis can be found by diagonalizing the mass matrix of the neutrinos with the following Ansatz

$$diag(m_1, m_2, m_3) = V_R^{\nu\dagger} M V_L^{\nu}. \tag{2.8}$$

Then it is possible to rewrite the mass term in the Lagrangian as the following

$$-\mathcal{L} = \sum_{k=1}^{3} m_k \bar{\nu}_k \nu_k \tag{2.9}$$

where we assumed a three-neutrino scenario. In this basis, we can rewrite

the weak doublet components of the neutrino as

$$\nu_{Li} = P_L \sum_j^3 V^{\nu}_{Lij} \nu_j, \tag{2.10}$$

where P_L is the left-handed projector. In the same manner, we can diagonalize the charged lepton mass matrix

$$diag(m_e, m_\mu, m_\tau) = V_L^{l\dagger} M_l V_R^l \tag{2.11}$$

Therefore, the weak doublet component,l^w, of the charged lepton can also be written in term of mass eigenstates, l_j, as

$$l^w_{Li} = P_L \sum_{j=1}^3 V^l_{ij} l_j. \tag{2.12}$$

Then one can rewrite the charged current interaction term in the Lagrangian as

$$\mathcal{L}_{CC} \propto \begin{pmatrix} \bar{e}^w_L & \bar{\mu}^w_L & \bar{\tau}^w_L \end{pmatrix} \gamma^\mu \begin{pmatrix} \nu_{eL} \\ \nu_{\mu L} \\ \nu_{\tau L} \end{pmatrix} W^+_\mu = \begin{pmatrix} \bar{e}_L & \bar{\mu}_L & \bar{\tau}_L \end{pmatrix} \gamma^\mu U \begin{pmatrix} \nu_1 \\ \nu_2 \\ \nu_3 \end{pmatrix} W^+_\mu. \tag{2.13}$$

The matrix U is called the lepton mixing matrix and relates the mass basis with the interaction basis. It is expressed by combining (2.10) and (2.12)

$$U_{ij} = P_{l,ii} V^{l\dagger}_{ik} V^{\nu}_{Lkj} (P_{\nu,jj}). \tag{2.14}$$

The additional matrices P_l and P_ν represent the possible field redefinition in the lepton and neutrino fields. Lepton fields which are Dirac particles can absorb three phases. As mentioned before neutrinos can be Majorana particles. These particles cannot absorb phases in their redefinition because the mass term is not invariant under it. Therefore, we are left with $6(n-2)$ parameters in the Majorana case and $5n-11$ in the Dirac case where n is the number of neutrino mass eigenstates.

Now back to the Majorana propagator in the neutrinoless double beta decay. As argued above we have to redefine the propagator from the interaction basis into the mass basis which is done in the following

$$\begin{aligned} \langle 0| \, T(\nu_{eL}(x_1)\nu^T_{eL}(x_2)) \, |0\rangle &= -\frac{1-\gamma_5}{2} \sum_i U^2_{ei} \, \langle 0| \, T(\nu_i(x_1)\bar{\nu}_i(x_2)) \, |0\rangle \, \frac{1-\gamma_5}{2} C \\ &= -\frac{i}{(2\pi)^4} \sum_i \int d^4q e^{-iq(x_1-x_2)} \frac{U^2_{ei} m_i}{q^2 - m_i^2} \frac{1-\gamma_5}{2} C. \end{aligned} \tag{2.15}$$

We can pull out the factor of $U_{ei}^2 m_i$ in front of the integral and simplify the remaining integral by taking into account that $q > m_i$. Then one can define the quantity with which the propagator is scaling as

$$m_{\beta\beta} = \sum_i U_{ei}^2 m_i = |c_{12}^2 c_{13}^2 m_1 + s_{12}^2 c_{13}^2 m_2 e^{i\alpha_1} + s_{13}^2 m_3 e^{i\alpha_2}|, \tag{2.16}$$

and this is the so-called "effective Majorana mass". The parameters result from the lepton mixing matrix

$$U = \begin{pmatrix} 1 & 0 & 0 \\ 0 & c_{23} & s_{23} \\ 0 & -s_{23} & c_{23} \end{pmatrix} \begin{pmatrix} c_{13} & 0 & s_{13}e^{i\delta_{CP}} \\ 0 & 1 & 0 \\ -s_{13}e^{i\delta_{CP}} & 0 & c_{13} \end{pmatrix} \begin{pmatrix} c_{12} & s_{12} & 0 \\ -s_{12} & c_{12} & 0 \\ 0 & 0 & 1 \end{pmatrix} \begin{pmatrix} e^{i\alpha_1} & 0 & 0 \\ 0 & e^{i\alpha_2} & 0 \\ 0 & 0 & 1 \end{pmatrix}, \tag{2.17}$$

where $c_{ij} = \cos\theta_{ij}$ and $s_{ij} = \sin\theta_{ij}$ and θ_{ij} are the so called mixing angles, δ_{CP} is the CP violating phase and $\alpha_{1/2}$ are the so called Majorana phases.

Doing the exact calculations, evaluating the whole Feynman diagram, and including the kinematics and nuclear effects one arrives at the final equation for the half-life, $T_{1/2}$, of isotopes that can perform neutrinoless double beta decay

$$\frac{1}{T_{1/2}} = G\, g_A^4\, \mathcal{M}^2 \left(\frac{m_{\beta\beta}}{m_e}\right)^2, \tag{2.18}$$

where G is the kinematically allowed phase space factor, $g_A^4 \simeq 1.276$ is the axial-vector coupling, $\mathcal{M}$ the nuclear matrix element (NME) accounting for the nuclear physics effects, and m_e the electron mass. From this equation, we see that it is absolutely crucial to determine the parameters of the lepton mixing matrix and the masses of the participating mass eigenstates.

The first category of experiments that are doing this are so-called neutrino oscillation experiments. These experiments measure the flavor of a neutrino after it propagated over a specific length. Due to neutrino oscillations, there exists a probability that the neutrino changes its flavor along this way. The actual probabilities of the different possibilities ($\nu_e \to \nu_e$, $\nu_e \to \nu_\mu$, ...) are always slightly different but the general behavior is that the amplitude is determined by the parameters of U and the frequency of the oscillation depends on $\Delta m_{ij}^2 = m_i^2 - m_j^2$ so the differences in the mass squares. The important point is that neutrino oscillation experiments cannot determine the absolute mass values of the neutrino mass eigenstates but are just sensitive to Δm_{ij}^2. This leaves us with the situation that we can distribute the masses in two different ways as seen in Fig. 2.2. One calls the ordering with $m_1 \ll m_2 \ll m_3$ the "normal ordering" (NO) and the situation $m_3 \ll m_1 \ll m_2$ is called the "inverted ordering" (IO). The determination of these parameters and the

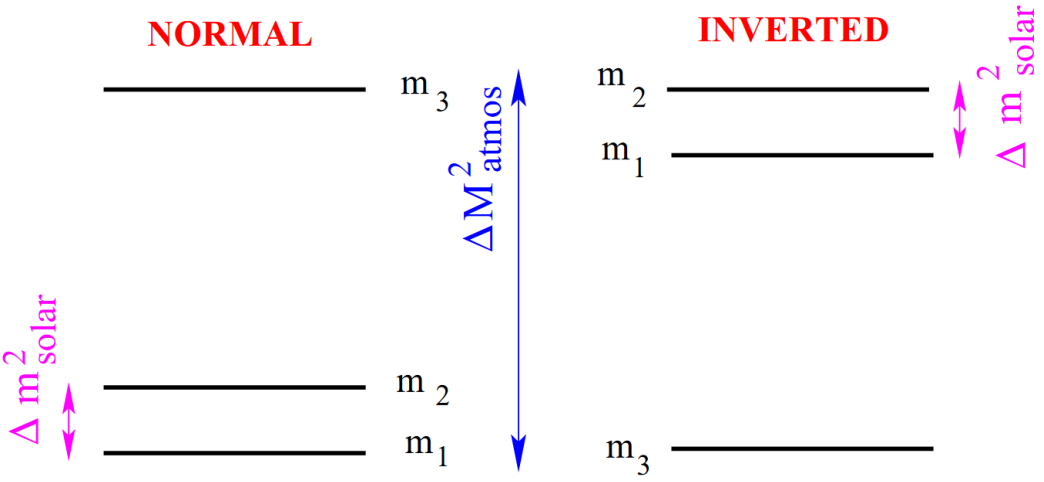

Figure 2.2: Mass schemes in a 3ν scenario. The nomenclature of the mass splitting can be either done by the numeration of the mass eigenstates or by the type of experiments that are measuring this specific mass splitting [27].

mass ordering is a worldwide endeavor and the current status can be found in [29].

So to be able to determine $m_{\beta\beta}$ one also needs the actual values, m_1, m_2, and m_3. Actually, due to the knowledge of their mass differences from neutrino oscillation experiments, the actual open question is the mass of the lightest neutrino mass eigenstate m_{lightest}. The leading experiment in determining absolute values of neutrino masses is the KATRIN experiment in Karlsruhe [30]. The observable under investigation is the so-called effective electron neutrino mass

$$m_{\nu_e}^2 = \sum_i m_i^2 U_{ei}^2 \tag{2.19}$$

and as soon this quantity is measured, m_{lightest} can be determined depending on the ordering of neutrino masses. So far in [30] only an upper bound could be given of

$$m_\nu < 0.8eV. \tag{2.20}$$

The last two parameters influencing $m_{\beta\beta}$ are the majorana phases α_1 and α_2. These two phases are only accessible via the possible Majorana property of the neutrino. The nature of the neutrino mass is still an open question and therefore these phases are still unconstrained.

So what would be the experimental signature of a neutrinoless double beta decay compared to its SM cousin the double beta decay with two neutrinos in the final state ($2\nu\beta\beta$)? The answer is that compared to $2\nu\beta\beta$ which has a continuous energy spectrum, $0\nu\beta\beta$ on the other hand has a discrete

spectrum. $0\nu\beta\beta$ is basically a two-body decay into two electrons because the much heavier daughter nucleus does not absorb significant portions of kinetic energy. The expected sum of energies of the emitted electrons can be calculated then as

$$Q = M_{\text{nucleus}}^{\text{parent}} - M_{\text{nucleus}}^{\text{daughter}} - 2m_e. \tag{2.21}$$

Therefore, we are left with a very clear signal in case neutrinos are their own anti-particles as proposed by Majorana. Additionally to the question of the nature of the neutrino mass, $0\nu\beta\beta$ decay could play an important role in explaining the matter-antimatter asymmetry observed in our universe due to the lepton number violation by two units [31]. These scientific questions caused a broad program of experimental searches for $0\nu\beta\beta$ [32]. The next generation of $0\nu\beta\beta$ experiments are designed to be able to test the possible $m_{\beta\beta}$ values in the case of inverted mass hierarchy.

2.2 Bayesian statistics

At the beginning of data analysis, one has to decide what statistical technique one uses to extract the information the data tells you. Two main schools of thought are on the market namely Bayesian and frequentist. Here we discuss the Bayesian way of reasoning. A review on this topic is [33]. The master equation of this school of thought is Bayes Theorem

$$P(\lambda|D, M) = \frac{P(D|\lambda, M)P_0(\lambda|M)}{P(D|M)}, \tag{2.22}$$

where the model under investigation is M, λ is the set parameters describing the model and the experimental data is D. The quantities in (2.22) are:

- $P(D|\lambda, M)$ is called the likelihood. This quantity describes the probability of the data as a function of the parameters of the model.
- $P_0(\lambda|M)$ is called the prior. It is a probability function we assign prior to the analysis to the parameters of the theory. This is a feature of the Bayesian analysis that we will discuss further.
- $P(D|M)$ is called the Bayesian evidence and is defined as

$$P(D|M) = \int P(D|\lambda, M)P_0(\lambda|M)d\lambda. \tag{2.23}$$

- $P(\lambda|D, M)$ is called the posterior probability distribution. It represents a probability distribution for the parameters of the model given the data.

The advantage of this school of thinking is that the question "What is the probability of a parameter given the data?" can be answered. The answer is just the posterior probability distribution. A frequentist analysis is not able to answer this question. Actually in a frequentist way of thinking this is not even a valid question which seems very odd.

A criticism regarding the Bayesian approach is the dependency of the analysis on the choice of priors. Indeed the resulting posterior can depend heavily on which prior was plugged in (2.22). So how can a mathematical consistent statistical analysis of experimental data depend on the subjective choice on a prior? This seems as counter-intuitive as the fact that the frequentist approach cannot answer the question of how probable a parameter value is.

I want to present two arguments that are usually made against this criticism. First, one has to point out that the dependency on the prior is strong when the data is weak. If the data is strong the resulting posterior is basically independent of the choice of the prior. So the fact that a potential analysis depends on the choice of priors actually just expresses the fact that the data is not strong enough to draw conclusive statements from it. Secondly, also in frequentist statistics the analyzer has to make some choices on how to actually perform the analysis. A very common choice is the different options one has in choosing a test statistic. These choices are more abstract than assigning probabilities to different parameter values like in choosing a prior but the final result will also depend on these choices. Therefore, one can argue that the choice of a prior is actually just more honest than hiding subjective preferences behind a mathematical concept.

Another nice feature of Bayesian statistics is that it offers a simple way to compare two hypotheses and decide which one is more likely. The quantity of interest to do so is the so-called Bayes Factor. Imagine one wants to compare two hypotheses H_1 and H_0 with each other. Given the data, we can define the posterior odds as

$$\mathcal{O}_1 = \frac{P(H_1|D)}{P(H_0|D)}. \tag{2.24}$$

This quantity is larger than one if H_1 is more likely and smaller than one if H_0 is. If we assume that these two hypotheses are the only ones possible we can use Bayes theorem and we have

$$P(H_0|D) = \frac{P(D|H_0)P_0(H_0)}{P(D|H_1)P_0(H_1) + P(D|H_0)P_0(H_0)}, \tag{2.25}$$

$$P(H_1|D) = \frac{P(D|H_1)P_0(H_1)}{P(D|H_1)P_0(H_1) + P(D|H_0)P_0(H_0)}. \tag{2.26}$$

Then we can rewrite (2.24) as

$$\mathcal{O}_1 = \frac{P(D|H_1)}{P(D|H_0)}\mathcal{O}_0 \tag{2.27}$$

where

$$\mathcal{O}_0 = \frac{P_0(H_1)}{P_0(H_0)}$$

are the prior odds. The factor $\frac{P(D|H_1)}{P(D|H_0)}$ is known as the 'Bayes Factor'.

In order to give an example of how this works explicitly we assume we have a number of experiments, i, that perform a counting of signal events, with expectation value ν_i, and background events with expectation value λ_i. Then the two hypotheses we would like to compare with each other would be H_0, the data seen is just sourced by background, or H_1, the data also includes signal events. The likelihood of counting experiments that just count background events is modeled with a Poisson distribution as

$$P(D|H_0) = P(\{n\}|H_0) = \prod_i e^{-\lambda_i}\frac{\lambda_i^{n_i}}{n_i!}, \tag{2.28}$$

where the λ_i's are the background expectation, which is given for each experimental setup individually and $\{n\}$ is the collection for the counts reported by the experiments. For hypothesis H_1, one has to add the signal expectation ν_i which is related to the experimental setups for $0\nu\beta\beta$ searches by

$$\nu_i = \frac{N_A\, ln2}{m_i}\frac{\mathcal{E}_i\,\epsilon_i}{T_{1/2}}, \tag{2.29}$$

with the Avogadro number N_A, the molar mass of the enriched isotope m_i, the exposure $\mathcal{E}_i$ and the detection efficiency ϵ_i of the experiment. For simplicity we shall call henceforth the collection of relevant parameters for $0\nu\beta\beta$ decay

$$\theta = (m_1, \Delta m_{12}, \Delta m_{13}, s_{12}, s_{13}, \alpha_1, \alpha_2, \mathrm{NME}). \tag{2.30}$$

Then

$$P(\{n\}|\theta, H_1) = P(\{n\}|\nu(\theta), H_1) = \prod_i e^{-(\lambda_i+\nu_i)}\frac{(\lambda_i+\nu_i)^{n_i}}{n_i!}, \tag{2.31}$$

With these definitions we can calculate $P(D|H_1)$ via

$$P(D|H_1) = P(\{n\}|H_1) = \int P(\{n\}|\nu(\theta))P(\theta|H_1)d\theta = E(P(\{n\}|\nu(\theta)))_{P(\theta)}. \tag{2.32}$$

Now we have both expressions we need to calculate the Bayes Factor. If one assumes that both hypotheses are equally likely then we are left with the situation that the Bayes Factor is the same quantity as the posterior odd.

Now we can discriminate between different hypotheses. One can carry on with this way of thinking and ask the question: Given a possible experimental setup where the experimental parameters are known, can one predict how likely it is that this experiment reports a discovery?

First, we have to define what we mean by discovery. How more likely must H_1 be than H_0? We define a discovery when the posterior odds

$$\mathcal{O}_1 = \frac{E(P(\{n\}|\nu(\theta)))_{P(\theta)}}{P(\{n\}|H_0)} \tag{2.33}$$

is greater than 10. The following indicator function

$$I = \begin{cases} 1, & \text{if } \mathcal{O}_1 \geq 10 \\ 0, & \text{otherwise} \end{cases} \tag{2.34}$$

gives then either 1 in case of a discovery as defined and 0 when no discovery would be reported. To calculate now the discovery probability P_D, we have to create samples of possible counts the different experiments could report. We also need to sample over the possible parameter values from the analysis of available data. The resulting mathematical expression is

$$P_D = E\left[E\left[I\left(\frac{E[P(\{n\}|\theta)]_{P(\theta)}}{P(\{n\}|H_0)}\right)\right]_{P(\{n\}|\theta)}\right]_{P(\theta)}. \tag{2.35}$$

In the following section we use 3000 Markov chain Monte Carlo samples from the posterior probability distribution of the neutrino parameters from the analysis of available neutrino data for each investigated scenario. Then we create 3000 samples from the investigated experiments for each of these parameter sets. In the last step, we average over the parameter samples again while keeping the specific set of counts fixed. By calculating the posterior odds for every single created event, we can decide if this specific sample we call a discovery or not and evaluate how many of the investigated samples lead to a discovery. This procedure was followed for the single experiment case already in [34].

2.3 Discovering neutrinoless double-beta decay in the era of precision neutrino cosmology

One question we want to answer in the next section is if next-generation $0\nu\beta\beta$ experiments can probe also the parameter space of $m_{\beta\beta}$ in case of normal ordering (NO) and how Cosmology is entangled with the search for $0\nu\beta\beta$. The results of this work have been published in [1] and we follow this paper very closely in this section.

Neutrinos affect Big Bang Nucleosynthesis and the large-scale structure of the universe by introducing characteristic signatures in the relative abundance of elements as well as in the power spectra of the cosmic microwave background (CMB) and baryon acoustic oscillations (BAO) [35]. Using these effects one can put upper bounds on the sum of the neutrino mass ($\Sigma = m_1 + m_2 + m_3$). The current best results indicate that $\Sigma < 120$ meV, with a 95% credible interval, resulting from the data from Planck, along with its amalgamation with lensing and BAO data [36]. Excitingly, upcoming surveys like DESI [37] and EUCLID [38] are expected to achieve a remarkable precision of 20 meV in measuring Σ, even under the assumption of its minimum allowable value. This significance extends to $m_{\beta\beta}$ since Σ and $m_{\beta\beta}$ are intrinsically connected, as demonstrated in equation (2.16).

Our ability to predict decay half-lives is constrained by two main factors. The first factor pertains to the precision and accuracy of the many-body computations employed to estimate the Nuclear Matrix Element (NME) values. In the field, four principal many-body methods have historically been utilized: the Nuclear Shell Model (NSM), the Quasiparticle Random-Phase Approximation (QRPA) method, the Energy-Density Functional (EDF) theory, and the Interacting Boson Model (IBM). Multiple calculations exist for each method, each characterized by distinct assumptions and approximations. These calculations can yield results that vary by as much as a factor of three for a given isotope, and even within each method, significant disparities can be observed [39].

The second factor that constrains the accuracy of our predictions is the value of $m_{\beta\beta}$. While neutrino oscillation parameters have been accurately measured, critical pieces of information are still missing, such as the Majorana phases and the value of the lightest neutrino mass eigenstate [29]. Furthermore, the ordering of the neutrino mass eigenstates remains unknown. Current global fits [40] suggest a mild preference for the normal ordering, but its significance is subject to ongoing debate [41, 42]. Cosmological constraints on the sum of neutrino masses disfavor parts of the parameter space for the

inverted ordering, while the parameter space for normal ordering remains largely unaffected.

In the case of the inverted ordering, $m_{\beta\beta}$ is constrained, with its minimum allowed value being 18.4 ± 1.3 meV [43]. However, in the scenario of a normal ordering, it is theoretically possible for $m_{\beta\beta}$ to vanish, although this would require a precise adjustment of the Majorana phases to cancel the terms in (2.16) [44, 45]. Achieving the sensitivity to probe $m_{\beta\beta}$ down to at least the minimum value allowed for the inverted ordering has been the long-standing goal of $0\nu\beta\beta$-decay experiments for two decades.

The quest for $0\nu\beta\beta$ decay is currently at a turning point. The scientific community has developed experimental approaches aimed at exploring the entire parameter space associated with the inverted ordering of neutrino mass states. Discussions within the community are actively underway to delineate the next steps in this endeavor.

As part of this ongoing process, the United States Department of Energy recently conducted a comprehensive portfolio review of ton-scale experiments. This review has culminated in a summit that brought together the Astroparticle Physics European Consortium (APPEC), American and European funding agencies, and the scientific community. Notably, three experiments, CUPID [46], LEGEND [47], and nEXO [48], have already advanced to the conceptual design stage and are poised for further development. These experiments employ different isotopes and have the potential to conduct independent and complementary measurements. The importance of utilizing multiple isotopes extends beyond the confirmation of any future discoveries; it significantly enhances the overall discovery potential and mitigates systematic uncertainties associated with both detection methodologies and nuclear many-body calculations. Furthermore, such multi-isotope experiments could shed light on the underlying mechanism governing the decay process [49, 50].

In this study, we investigate the potential for discovering $0\nu\beta\beta$ decay in the context of a future, global, multi-isotope effort. While a discovery is virtually guaranteed in the case of inverted-ordered Majorana neutrinos, our primary focus is on assessing the likelihood of discovery for normal-ordered neutrinos. To achieve this, we leverage all available neutrino data to place constraints on $m_{\beta\beta}$ and compute Bayesian discovery probabilities for future searches under various scenarios.

In this type of analysis, two parameters are key: the Majorana phases and the value of the lightest mass eigenstate, m_1. The prior distributions assigned to these parameters substantially influence the analysis outcomes. Following the approach proposed in reference [45], we address the lack of information regarding the phases by adopting a uniform prior distribution. We find this to be the most reasonable choice given the available information

and constraints.

We have adopted a different approach in handling the prior choice for m_1 compared to our previous work [51, 34]. In this study, we initially present the discovery probabilities as a function of m_1, explicitly highlighting the substantial dependence on this parameter. Subsequently, we proceed to assume a uniform prior distribution for m_1 and explore scenarios where cosmological constraints on Σ indirectly provide information about m_1. This approach helps to reduce the influence of the prior choice.

Specifically, after considering the current constraints on Σ, we examine two extreme hypothetical scenarios related to future measurements by DESI and EUCLID. In one scenario, we consider $\Sigma = 100 \pm 20\,\mathrm{meV}$, which is just below current limits. In the other scenario, we investigate $\Sigma = 59 \pm 20\,\mathrm{meV}$, situated at the lower end of the expected parameter range that allows for a significant probability of $m_1 \approx 0\,\mathrm{meV}$.

When the oscillation parameters are held constant, Σ and m_1 are linked by a bijective function, enabling the analytical computation of probability distributions through a change of variables [52, 53]. To illustrate this, Figure 2.3 presents the probability distributions of m_1 corresponding to the two Gaussian probability distributions for Σ. The Jacobian transformation introduces asymmetry into the distributions, generating tails on their left side and shifting their mode towards larger values.

In our analysis, we combined the likelihoods from the most sensitive $0\nu\beta\beta$-decay experiments which are CUORE [54], EXO-200 [55], GERDA [56], and KamLAND-Zen [57]. None of these have reported hints for a signal and have set lower limits on its half-life at the level of $10^{25} - 10^{26}$ years, corresponding to upper limits on $m_{\beta\beta}$ of the order of 100 meV. We also include the likelihood from the latest analysis of KATRIN [30] on the electron neutrino mass $m_\beta = (c_{12}^2\, c_{13}^2\, m_1^2 + s_{12}^2\, c_{13}^2\, m_2^2 + s_{13}^2\, m_3^2)^{1/2}$.

The oscillation parameters are incorporated into the analysis using Gaussian terms with central values and uncertainties taken from Ref. [29].

Our approach involves the sampling of both the likelihood function and the prior probability distributions, allowing us to generate pseudo-data sets that simulate the outcomes of future $0\nu\beta\beta$-decay experiments. Subsequently, we assess the average probability of these pseudo-data sets yielding a discovery, as originally suggested in [58].

To replicate the anticipated performance of future experiments, we employ a Poisson counting analysis with fixed background expectations, following the methodology outlined in [39]. In this context, we also adopt the background levels and signal efficiencies as input parameters from that reference. Furthermore, we assume a uniform ten-year operation duration for all experiments, aligning with the community's objectives for achievement

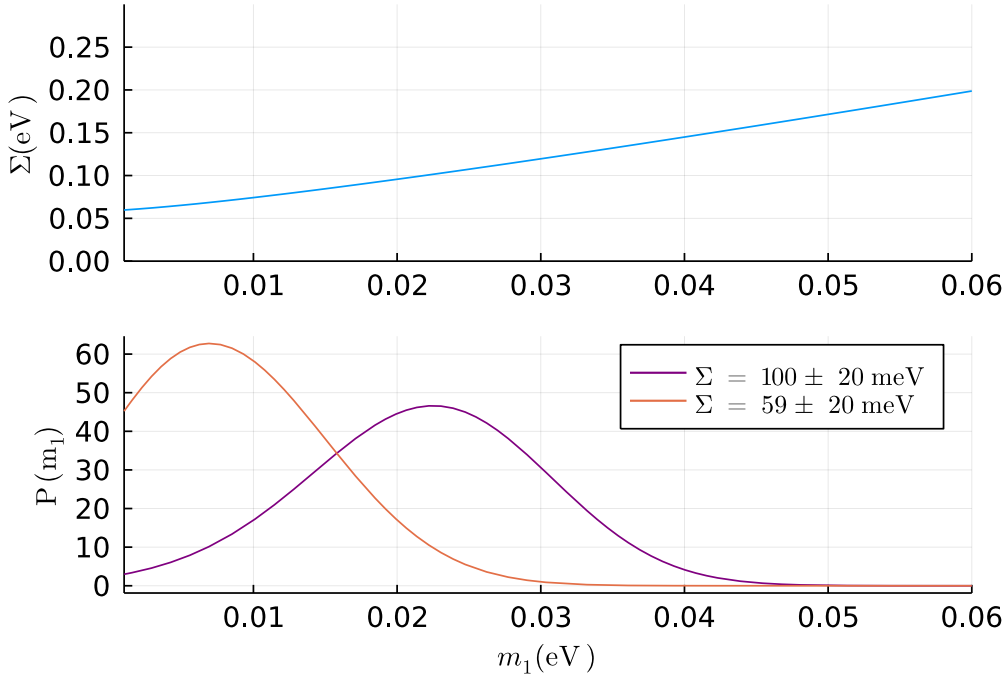

Figure 2.3: (Top) Correlation between Σ and m_1 assuming the best fit values for the neutrino oscillation angles and mass splittings [29]. Assuming neutrino masses follow the normal ordering, Σ is constrained to be larger than 59 meV. (Bottom) Gaussian probability distributions of Σ transformed into probability distributions of m_1 through a change of variable using the best fit of the neutrino oscillation parameters. The Gaussian distributions $\Sigma = 59 \pm 20$ meV and 100 ± 20 meV correspond to the two extreme measurements that DESI and EUCLID can perform.

within the next two decades. The discovery criteria is defined by requiring the posterior odds to be above a certain threshold, i.e.:

$$\mathcal{O}_1 = \frac{P(D|H_1)}{P(D|H_0)} \frac{P(H_1)}{P(H_0)} > 10, \tag{2.36}$$

where $P(D|H)$ are the probabilities of the data given the hypothesis that $0\nu\beta\beta$ decay exists (H_1) or not (H_0). $P(H_1)$ and $P(H_0)$ are their corresponding priors assumed to be equal. This criterion corresponds to the requirement that H_1 is ten times more likely than H_0, assuming they have equal prior probabilities initially. Subsequently, we define the discovery probability as the proportion of pseudo-datasets that meet our discovery criteria. Our calculations are executed using the BAT software kit, along with its built-in

Metropolis-Hastings sampling algorithm [59]. Notably, we have determined that the discovery criteria employed in this study yield results that are numerically comparable to those obtained through a 3σ frequentist rejection test of H_0.

In our calculations, we adopt fixed sets of Nuclear Matrix Element (NME) values, each sourced from a specific many-body calculation. We specifically consider calculations from references [60, 61, 62, 63, 64, 65, 66] that provide results for all isotopes relevant to our analysis, namely ^{76}Ge, ^{100}Mo,^{130}Te, and ^{136}Xe. This choice excludes certain Nuclear Shell Model (NSM) and Quasiparticle Random-Phase Approximation (QRPA) calculations for which the NME value for ^{100}Mo is currently unavailable. However, this approach has the advantage of incorporating correlated systematic uncertainties for each element within an NME set, which partially offset when combining data from various isotopes [67, 49].

The disparity among the discovery probabilities computed for different sets of NME values provides a rough estimate of the uncertainty attributed to the diverse many-body methods employed. Nonetheless, it should be noted that this approach does not comprehensively account for effects that uniformly impact all methods, such as the absence of the contact operator [68] or the phenomena related to "g_A quenching" [39], which we will discuss later.

The upper panel of Figure 2.4 displays the posterior probability distributions for $m_{\beta\beta}$ computed as part of a scan across fixed m_1 values, ranging from 10^{-4} to 10^{-2} eV. It is important to note that these distributions should not be interpreted as two-dimensional distributions, but rather as a set of connected one-dimensional conditional probability distributions for $m_{\beta\beta}$, each normalized independently.

The probability distributions are confined to well-defined regions within the parameter space, thanks to the precision of measurements concerning neutrino oscillation parameters. The remaining width in the $m_{\beta\beta}$ probability distributions can be attributed to the degrees of freedom associated with the Majorana phases. Our choice of employing a uniform prior for these phases tends to favor the largest possible $m_{\beta\beta}$ values at each fixed m_1 value. This includes the region spanning from $10^{-3} - 10^{-2}$ eV, where specific values of the Majorana phases can lead to vanishing $m_{\beta\beta}$ values. As the chosen m_1 value decreases, the maximum allowable $m_{\beta\beta}$ value also decreases, reaching a minimum of 3.7 meV for $m_1 = 0$ meV.

$0\nu\beta\beta$-decay experiments effectively truncate the upper portion of these probability distributions, presently ruling out $m_{\beta\beta}$ values above 156 meV [57], thereby indirectly constraining m_1 to be less than or approximately 100 meV. Future experiments are anticipated to achieve discovery sensitivities down to $m_{\beta\beta}$ values of 6 meV, contingent upon the Nuclear Matrix Element (NME)

values [43].

The lower panel of Figure 2.4 illustrates the combined discovery probability for CUPID, LEGEND, and nEXO as a function of m_1, considering all sets of Nuclear Matrix Element (NME) values under examination. The discovery probability starts at zero when m_1 falls below 1 meV, and steadily increases as m_1 advances, ultimately reaching nearly 100% when m_1 exceeds approximately $\sim$60 meV. Notably, the discovery probability exhibits fluctuations depending on the specific set of NME values in the range of m_1 from 5 to 50 meV. Larger NME values correspond to higher discovery probabilities within this m_1 range. However, as m_1 falls below 5 meV or rises above 50 meV, the discovery probabilities tend to converge.

When we possess a theoretical prediction for the value of m_1, determining the discovery probabilities in the realm of $0\nu\beta\beta$-decay becomes straightforward using the plot in Figure 2.4. However, our current understanding of fermion masses lacks a comprehensive model and theoretical guidance on the value of m_1 is limited. Therefore, it is crucial to consider scenarios where m_1 is treated as a free parameter, albeit weakly constrained by indirect information. However, this approach comes with a caveat. If the information available regarding m_1 is not sufficiently robust, the outcomes of any analysis are profoundly influenced by the choice of its prior probability distribution. Specifically, the adoption of a scale-invariant log-flat prior would result in a non-normalizable posterior distribution unless a cutoff on m_1 is implemented, as done in Ref. [34]. Alternative approaches, such as effectively constraining m_1 to be similar to the other two mass eigenvalues, have also been explored in prior studies as in [51, 69]. In our analysis, we opt for a uniform prior distribution spanning from 0 to 600 meV for m_1. This particular choice favors $m_{\beta\beta}$ values closer to the parameter space probed by experiments, serving as a reasonable approach when no other guidance regarding the parameter range of m_1 is available. Nonetheless, incorporating cosmological constraints on Σ can alter the probability distribution for m_1, rendering analyses that include cosmological data less sensitive to the chosen prior for m_1.

Figure 2.5 presents the discovery probabilities for CUPID, LEGEND, nEXO, and their combined efforts across four distinct scenarios, considering each set of Nuclear Matrix Element (NME) values. The initial two scenarios showcase the influence of incorporating the current cosmological constraint on Σ. In scenarios where cosmological models extend beyond Λ_{CDM}, significantly larger neutrino masses are permissible [70]. In this context, the most stringent information regarding m_1 is derived from current $0\nu\beta\beta$-decay experiments and the KATRIN experiment. Consequently, discovery probabilities can be as high as 80%, as the uniform prior for m_1 assigns substantial probability mass to larger m_1 values. In other words, disregarding stan-

dard cosmological bounds and assuming a flat prior for m_1 suggests that the discovery of $0\nu\beta\beta$-decay is quite likely. However, when we introduce the likelihood constraint of $\Sigma < 120\,\text{meV}$, this penalizes the consideration of large m_1 values, leading to a reduction in discovery probabilities, which now range between 20% and 60%.

The speculative scenarios involving future measurements of Σ offer promising prospects for discovery. In the event that Σ hovers just below the current constraints, for example, at 100 meV, forthcoming $0\nu\beta\beta$-decay experiments are poised to detect a signal with a high probability, ranging from 20% to 80%. Even if $\Sigma = 59 \pm 20\,\text{meV}$, which represents the lower limit of its permissible parameter space, the discovery probabilities remain substantial, spanning from a few percentage points to over 40%. Notably, these discovery probabilities in these two scenarios exhibit only modest sensitivity to the prior choice for m_1, primarily because measurements of Σ provide robust information regarding m_1 (as depicted in Figure 2.3). For instance, we have estimated that implementing a log-prior on m_1 with a cutoff, as seen in [34], would reduce these discovery probabilities by a maximum of 30%. This suggests that regardless of the specific value reported for Σ by DESI and EUCLID, the next-generation $0\nu\beta\beta$-decay experiments will explore a complementary parameter space. In this space, both the detection of a signal and its exclusion will offer invaluable insights and information.

The discovery probabilities for individual experiments exhibit a degree of similarity, with the maximal spread observed for nEXO and the least spread for LEGEND. This pattern aligns consistently with the variation in available Nuclear Matrix Element (NME) values for xenon (Xe) and molybdenum (Mo). In scenarios where cosmological data are not incorporated, m_1 is predominantly constrained by the existing $0\nu\beta\beta$-decay experiments. In such cases, increasing the NME values has a dual effect: it shifts the probability distribution for $m_{\beta\beta}$ towards lower masses while simultaneously enabling future experiments to explore lower $m_{\beta\beta}$ values. The impact of this interplay diminishes in scenarios where Σ is constrained, and the existing $0\nu\beta\beta$-decay experiments exert a lesser influence on the probability distribution for $m_{\beta\beta}$.

The significant spread in results attributed to the uncertainty in Nuclear Matrix Elements (NME) remains noteworthy, especially considering that our analysis excludes Quasiparticle Random-Phase Approximation (QRPA) calculations for which results regarding ^{100}Mo are not currently available. It is important to highlight that ongoing efforts within the nuclear theory community are actively striving to enhance the accuracy and precision of NME values.

Promising developments include *ab initio* calculations for light and medium-sized nuclei [71], with forthcoming calculations expected to encompass the

heavier isotopes of interest. These new calculations aim to incorporate more realistic nuclear correlations and corrections, such as two-body currents, to refine the leading-order operator in chiral effective field theory. Preliminary results from these calculations suggest a reduction in NME values [72]. Furthermore, the inclusion of the so-called "g_A quenching" physics can be at least partially compensated for by the previously unaccounted-for contact term, as introduced in Ref. [73]. This compensation leads to discovery probabilities akin to those depicted in Figure Figure 2.5. Indeed, we have computed that an overall scaling of the NME values for all isotopes by 20% ((equivalent to a $\sim$10% variation in g_a) would result in a 5% to 10% change in the discovery probabilities, without altering the fundamental conclusions of our study. Importantly, the impact of such an overall scaling is minimal, as it uniformly affects both current and future experiments.

When we combine the results from all the experiments, we observe an average enhancement of discovery probabilities by approximately 20% compared to the average probabilities obtained from individual experiments. Furthermore, the range of values for the combined probabilities is considerably narrower compared to the spread seen among individual experiments. This outcome aligns with our expectations, as it reflects the partial compensation of fluctuations in Nuclear Matrix Element (NME) values across the three different isotopes. Combining the experiments serves to alleviate the challenges posed by the least favorable NME values that lead to very low discovery probabilities in individual experiments. Another significant advantage of amalgamating multiple experiments is an increase in confidence regarding potential discoveries. For instance, systematic uncertainties linked to mischaracterized background components predominantly impact only a single experiment but are mitigated in a combined analysis. Additionally, statistical fluctuations tend to balance out, reducing the likelihood of false discoveries. In fact, we have estimated the chance of false discoveries to be as low as 0.2%. All these considerations underscore the importance of conducting several large-scale $0\nu\beta\beta$ experiments, as they provide numerous advantages, including enhanced discovery potential and increased confidence in results.

In conclusion, the realms of precision neutrino cosmology and the pursuit of $0\nu\beta\beta$-decay are intricately linked and offer complementary insights. In the context of the minimal extension of the Standard Model of particle physics, if neutrinos are Majorana particles and the mass ordering is inverted, it becomes clear that future $0\nu\beta\beta$-decay experiments will unmistakably detect a signal. The situation is more nuanced for the normal mass ordering, where the outcomes from future cosmological experiments will significantly narrow down the permissible ranges for m_1. Consequently, this will impact the

discovery probabilities for the next-generation $0\nu\beta\beta$-decay experiments. If cosmological data continue to establish upper bounds on Σ in the future, the discovery probability for upcoming $0\nu\beta\beta$-decay searches will remain moderate, leaving the question of whether neutrinos are Majorana particles still open. However, if future cosmological observations report a value for the sum of neutrino masses, Σ, exceeding 59 meV, the prospect of discovering $0\nu\beta\beta$-decay becomes highly significant, even for the normal mass ordering. In such a scenario, a non-observation of $0\nu\beta\beta$-decay would strongly suggest that neutrinos are Dirac particles.

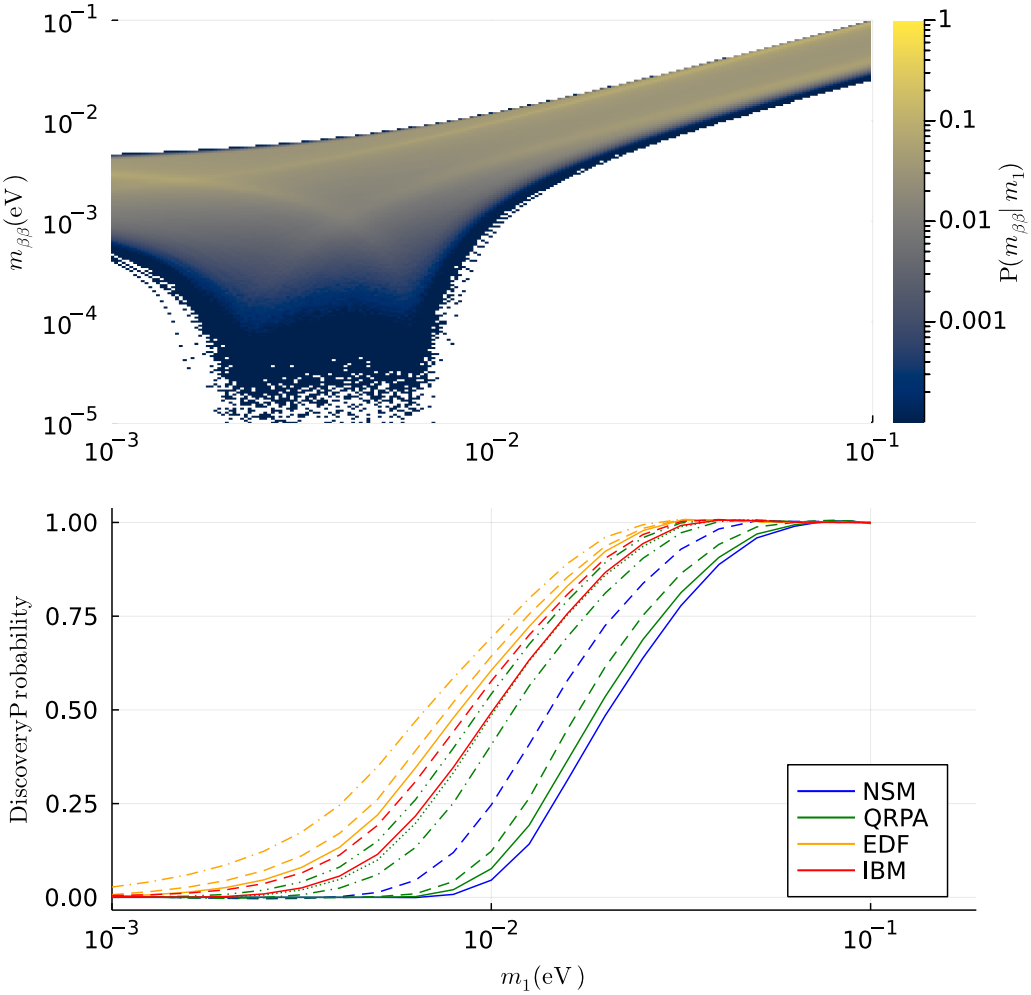

Figure 2.4: (Top) Conditional one-dimensional posterior probabilities for $m_{\beta\beta}$ computed for a scan of fixed m_1 values, assuming all available data on neutrinos, normal ordering and a uniform prior on the effective Majorana phases. (Bottom) Discovery probability for a combined analysis of CUPID, LEGEND, and nEXO as a function of the true value of m_1. The probability is computed for different sets of NME values yielding a band for the discovery probability. The different line styles therefore correspond to different calculations methods of the NME values within a model.

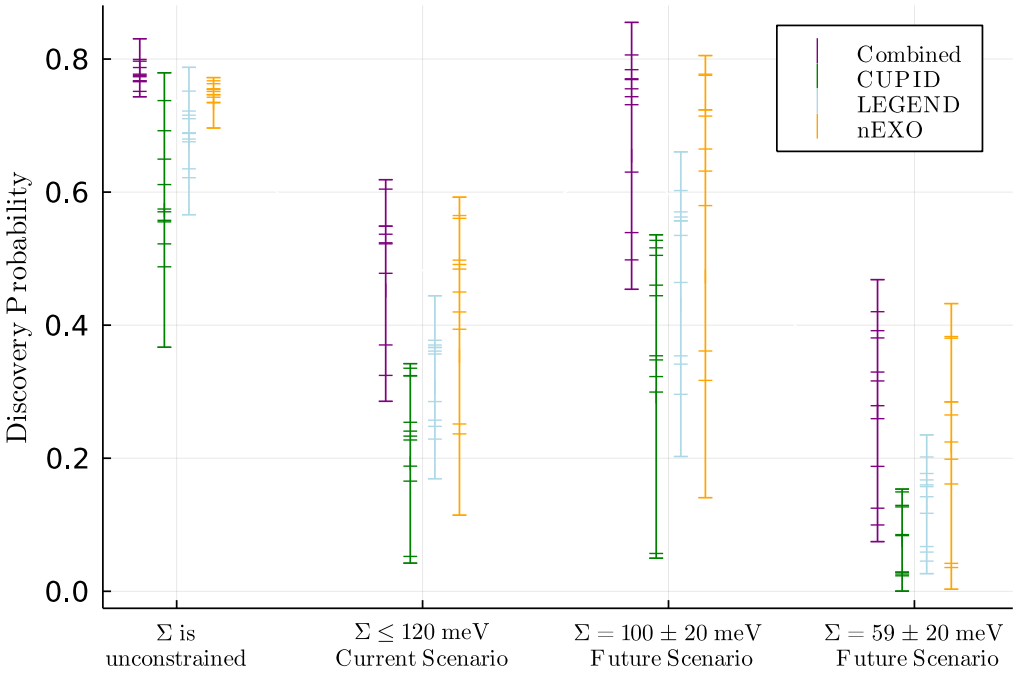

Figure 2.5: Discovery probabilities for a selection of proposed experiments and their combination under different scenarios and set of NME values. The scenarios differ because of the information included on Σ, respectively no information, current upper limit, and two possible measurements at the extreme of the currently allowed parameter space. The calculation has been performed using fixed sets of NME values, and each result is shown as a horizontal tick.

Chapter 3

Neutrino Physics in TeV Scale Gravity Theories

The $0\nu\beta\beta$ decay is just one example of how UV physics can lead to effects in the IR. In the following, I will discuss how gravity could induce such effects on neutrinos. To understand the motivation for theories that can achieve these effects one has to understand the Hierarchy Problem which we will discuss first.

3.1 The Hierarchy Problem

In this section, I will briefly describe the foundations of the Hierarchy Problem of Particle Physics. Reviews on this can be found in several textbooks. I will rely on [74].

To understand the hierarchy problem one has to understand how scalar masses are calculated in QFT. In order to do so we investigate the Lagrangian

$$\mathcal{L} = -\frac{1}{2}\phi(\Box + m^2)\phi + \lambda\phi\bar{\psi}\psi + \bar{\psi}(i\partial\!\!\!/ - M)\psi, \tag{3.1}$$

where the bare mass of the scalar, ϕ, is m and the bare mass of the fermion, ψ, is M. We now want to calculate the contribution to the scalar mass on the first loop level. The Feynman diagram of interest is shown in Fig.3.1 and the mathematical expression is

$$i\Sigma_2(p\!\!\!/) = (i\lambda)^2 \int \frac{d^4k}{(2\pi)^4} \frac{Tr[(p\!\!\!/ + k\!\!\!/ + M)(k\!\!\!/ + M)]}{[(p+k)^2 - M^2 + i\epsilon][k^2 - M^2 + i\epsilon]}. \tag{3.2}$$

This expression becomes after regularization the following

$$\Sigma_2(p^2) = \frac{3\lambda^2}{4\pi^2} \int_0^1 dx \left([M^2 - p^2x(1-x)] \ln \frac{M^2 - p^2x(1-x)}{\Lambda^2} + \Lambda^2 \right), \tag{3.3}$$

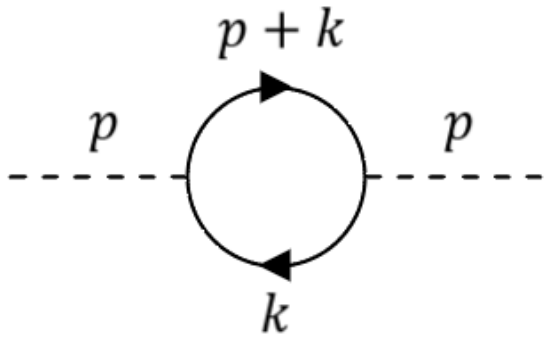

Figure 3.1: First loop contributing to the scalar mass.

where Λ is a UV cutoff. After renormalization, the end result becomes in the limit $p^2, m_P^2 << M^2$

$$\Sigma_2(p^2) = \frac{\lambda^2}{4\pi^2}\left[\frac{(p^2-m^2)^2}{20M^2} + \mathcal{O}\left(\frac{m^6}{M^4}\right)\right]. \tag{3.4}$$

We can see that the UV dependence drops out due to the process of renormalization. This also means that within the SM the mass of the Higgs-boson is a perfect finite quantity which once measured can be seen as an input parameter of the SM.

Now assume that the SM is not the final theory of nature. Actually, we know that this cannot be the case because the SM does not include gravity in its description. We even expect that the SM description breaks at least at the scale M_P due to the classicalization of fundamental particles heavier than M_P [75]. So if we take this seriously the UV cutoff Λ cannot be treated anymore as a mathematical artifact that can be taken care of by renormalization because this cutoff is physical now. Therefore, the divergence in (3.3) should also be physical. The expression for the pole mass, m_P, will then depend on the UV cutoff via

$$m_P^2 = m^2 - \Sigma(m^2) \approx m^2 - \Lambda^2. \tag{3.5}$$

The actual physical quantity measured in experiments is m_P which is around $m_P \approx 125$ GeV for the Higgs Boson. Setting $\Lambda = M_P \approx 10^{19}$ GeV one finds the expression for the bare mass

$$m^2 = (1 + 10^{-34})\Lambda^2. \tag{3.6}$$

Now per se one could say that this is just the result but on the other hand it looks odd that a theory parameter like the bare mass in the Lagrangian has to

be precisely set up to the 34th digit in order to explain the mass of the Higgs being around the electroweak scale. Such a behavior of parameters we call fine-tuning. It means that one has to tune the parameters in a very specific way to accommodate phenomenological aspects. This can leave somebody unsatisfied because such a precise choice of a parameter is not motivated by first principles at all.

The problem of fine-tuning often arises when experimental results are applied to theoretical frameworks. Often these theories can evade current experimental bounds by tuning the parameters in such a way that experiments cannot rule them out completely. From a philosophical point of view highly fine-tuned theories are not as attractive as not fine-tuned models. The reason is that a specific choice in the parameter space of a theory just replaces the original physics question with the question of why this specific choice should be made.

Now in the case of the Higgs mass, the situation is even more peculiar. We have seen that within the SM scalar masses can be renormalized and a Higgs mass around the scale of electroweak symmetry breaking sounds reasonable. The problem of fine-tuning just arises when one introduces a UV cutoff in the SM. The mass of a scalar like the Higgs gets quadratic contributions of this cutoff and it would therefore make more sense if the mass of the Higgs would then be around the scale of Λ. The fact that the Higgs "sees" the cutoff of the theory is often called "UV-sensitivity". The problem that the Higgs is UV sensitive as soon a UV cutoff is introduced which would result in a highly fine-tuned situation for the bare mass parameter is called the "hierarchy problem" or the "electroweak hierarchy problem".

Now, how serious is the hierarchy problem? The answer is that there are people who take it extremely seriously and some do not. The argument why one should not worry too much goes as follows: We do not know the physics that lies beyond the UV cutoff. Therefore, we do not know what kind of non-perturbative effects may spoil our perturbative loop expansion as we did for scalar masses. Of course, this argument should be acknowledged but from my personal point of view, this looks a little bit like closing the eyes and hoping for the best. Especially the second answer to the question is much more appealing.

Let us take the hierarchy problem seriously because that is what QFT tells us. The consequence would be that one should not take Λ too far away from the electroweak scale otherwise one runs into fine-tuning problems as discussed above. This interpretation would then suggest that new physics should be around the corner and not be placed at M_P which would be very unfortunate for physics. This standpoint is much more optimistic and was the motivation for the theories we discuss in the next sections.

3.2 TeV scale gravity theories

Now that we have established that the Hierarchy Problem should be taken seriously we can proceed by discussing possible solutions to solve it. Because there are plenty of attempts on the market who could give an answer to it I want to focus on theories which are called "TeV scale gravity theories". We have seen that gravity plays a crucial role in the Hierarchy Problem but instead of searching for an explanation in the UV where new physics appears at a scale M_X, one could tackle it from the opposite side and ask if gravity really just gets effective at the Planck scale.

Imagine a world where not M_P defines the scale where gravity becomes nonnegligible but another scale. Let us call this new scale the fundamental scale of gravity M_f. If this new scale would lie much closer to M_w than to M_P the Hierarchy Problem would be resolved. The difference with theories that are lying in the UV to solve the hierarchy problem is that the different nature of gravity itself is the answer to the problem. The philosophy of this attempt is different because instead of giving a UV explanation one answers the problem by bringing the root of the problem which lies in the UV down to the IR by introducing new light states and we therefore call these kinds of solutions "IR solutions".

So far two models are known that can split M_P and M_f and bring M_f down to the TeV scale and therefore offer a solution to the Hierarchy Problem. These two models are the so-called Arkani-Hamed-Dimopoulos-Dvali (ADD) [13, 76, 14] model and the Many Species framework [15, 16]. In the following, we give a short introduction to these models.

3.2.1 The ADD model and small neutrino masses

The ADD model, also known as Large Extra Dimensions, takes as the first axiom the existence of n extra spatial dimensions. How this model works we describe in the following and we rely next to the original papers also on [77]. These extra dimensions have of course to be compactified because, in our daily lives, we do not experience the existence of these dimensions. We, therefore, write the spacetime manifold, $\mathcal{M}$, as

$$\mathcal{M} = \mathcal{M}_4 \times K_n \tag{3.7}$$

where $\mathcal{M}_4$ is the four-dimensional Minkowski space and K_n is the compactified manifold. In the ADD model, these extra dimensions are compactified on circles with the radii $R_1, ..., R_n$.

This means that all fields have to be defined in this higher dimensional space. For simplicity let us demonstrate the effects of the circular compacti-

fication on a massless scalar field in $(4+1)$ scenario. The results nevertheless can be generalized to higher-spin fields in more dimensions. First, one imposes the boundary conditions

$$\Phi(x^\mu, Z) = \Phi(x^\mu, Z + 2\pi R), \tag{3.8}$$

where x^μ is the four dimensional coordinate and Z is the extra dimensional coordinate. Due to the periodicity of the boundary condition, a Fourier representation is possible and looks like

$$\Phi(x^\mu, Z) = \sum_{k=0,\pm1,\ldots} \phi(x^\mu) e^{ikZ/R}. \tag{3.9}$$

The expansion coefficients, $\phi(x^\mu)$, only depend on the four-dimensional coordinate and are called modes. Using the five-dimensional Klein-Gordon equation

$$\Box_5 \Phi(x^\mu, Z) = \left(\partial_\mu^2 - \frac{\partial^2}{\partial Z^2}\right) \Phi(x^\mu, Z) = 0, \tag{3.10}$$

and plugging the Fourier expression into this equation one gets

$$\left(\Box_4 + \frac{k^2}{R^2}\right) \phi_k(x^\mu) = \left(\partial_\mu^2 + \frac{k^2}{R^2}\right) \phi_k(x^\mu) = 0. \tag{3.11}$$

Now something interesting is happening to the originally 5-dimensional massless scalar field. The four-dimensional modes with $k \neq 0$ get a mass of

$$m_k = \frac{k}{R}. \tag{3.12}$$

The mode with $k = 0$, also known as zero mode, stays massless and is accompanied by the massive non-zero modes. This construction of more and more massive modes on top of the massless zero mode is the so called Kaluza-Klein tower or KK-tower. This equation can be generalized to a situation with more extra dimensions of different sizes and then it becomes

$$m_{\vec{k}} = \sqrt{\frac{k_1^2}{R_1^2} + \cdots + \frac{k_N^2}{R_N^2}}\,. \tag{3.13}$$

In the ADD model the known SM particles are confined on $\mathcal{M}_4$, also called "brane", because obviously, these particles do not propagate into these extra dimensions. This means also that these particles are not accompanied by a KK-tower. The graviton on the other hand is not charged under the SM

and can dilute into these extra dimensions. The space spanned by the extra dimensions we call "bulk". The action for gravity one can write therefore as

$$S = \frac{\mathcal{M}_f^{2+n}}{2} \int d^4x \int_0^{2\pi R} d^n Z \sqrt{G} R_{4+n}, \tag{3.14}$$

where G is the $(4+n)$ dimensional metric and R_{4+n} the scalar curvature.

Now we want to investigate this action in two different extreme cases. First, we turn to the case where the distance we are probing this gravitational action is much smaller than the radii of the extra dimensions $r \ll R$. Then one can approximate at such distances the geometry as a 4+n dimensional Minkowski space and this implies that the static gravitational potential looks like the following

$$V(r) = -\frac{m_1 m_2}{r^{1+n} M_f^{2+n}}. \tag{3.15}$$

In the other case where $r \gg R$ the gravitons that are probed at this distance have not enough energy to excite the higher modes of the KK-tower. Therefore, the only mode of interest is the zero mode and then one can take G being independent of the Z coordinate. Then one can perform the integration over the extra dimensions and (3.14) reduces to

$$\frac{1}{2} M_f^{2+n} V_n \int d^4x \sqrt{g} R, \tag{3.16}$$

where g and R are the well known 4-dimensional Minkowski metric and Ricci scalar respectively. V_n is the volume of the extra space which is

$$V_n = (2\pi R)^n. \tag{3.17}$$

Of course we know, that at large distances, the gravitational potential takes the usual Newton form

$$V(r) = -G_N \frac{m_1 m_2}{r}. \tag{3.18}$$

G_N here is the Newtonian constant. In our case we can identify this constant in our reduced gravitational action (3.16) with

$$G_N = (M_f^{2+n} V_n)^{-1}. \tag{3.19}$$

A four dimensional observer would, as usual, relate G_N with $1/M_P^2$, and then the following relation holds

$$M_f^{2+n} V_n = M_P^2. \tag{3.20}$$

Now by requiring that the radius of these extra dimensions is reasonably small in order to not be ruled out immediately we can solve this equation for R and get

$$R = \frac{1}{2\pi M_f}\left(\frac{M_P}{M_f}\right)^{2/n}. \tag{3.21}$$

For a scenario $n = 2$ and a submillimeter scale for R one sees that M_f should be around 10 TeV. This scale would be then the cutoff of the SM and it marks the scale where perturbative QG breaks down not M_P. Therefore, the ADD model solves the Hierarchy Problem.

Let me comment briefly on a widespread misconception about the ADD model and the hierarchy problem because I have heard this many times during my Ph.D. time. Some people told me: "The ADD scenario does not solve the hierarchy problem because it replaces one hierarchy with another. Instead of the ratio Λ/m_{Higgs} one is left with R/L_{Planck}". Going back to the section dedicated to the hierarchy problem we can immediately see why this argument is wrong. The thing that makes the hierarchy problem special is that the Higgs actually gets quantum corrections proportional to the cutoff. This is the reason why we started worrying in the first place. The parameter R of the ADD model does not get any quantum corrections of this form and is therefore not UV-sensitive like the Higgs. This is the core of the problem and this gets often confused with small value puzzles like why is the electron Yukawa coupling much smaller than the one of the top quark? Or why is an ant much smaller than a giraffe? Good questions indeed but intrinsically different than the hierarchy problem.

Now let us carry on with investigating the ADD model deeper. We want to go a step further by realizing that the bulk is not just the natural habitat for the graviton but for any particle that is not charged under SM gauge group and is therefore also not confined on the brane [13]. The fact that bulk fields cannot be charged under the SM is a consistency requirement imposed by gauge invariance and also a feature of the localization mechanism of the gauge field on the brane [78]. Likewise, when SM gauge fields are localized on the brane, it inherently excludes the presence of bulk modes carrying those charges. Notably, sterile neutrinos emerge as prominent examples, acting as the right-handed counterparts to the familiar left-handed neutrinos within the SM. This framework can give an alternative way to generate small neutrino masses as was described in [18, 79].

This mass arises from the mixing between the right-handed component of a bulk field Ψ and the SM left-handed neutrino ν_L, which is confined to the brane.

The field $\Psi(x, y)$ is a function of four space-time coordinates x and N

extra space coordinates y. It transforms in the spinor representation of the $4+N$-dimensional Poincare symmetry. For simplicity, we shall choose it as the smallest representation of this sort.

From the perspective of the four-dimensional Lorentz group acting on space-time coordinates denoted by x, the bulk fermion Ψ encompasses both chiralities. The procedure for defining a high-dimensional spinor and projecting it onto a four-dimensional observer on the brane is elucidated in the appendix of [80].

A notable finding within that context is that $4+N$-dimensional chirality is exclusively defined in even space-time dimensions. In the current context, this stipulates that N can be expressed as $N = 2n$, where n is an integer, while there is no meaningful definition for chirality when N is expressed as $N = 2n-1$. It is noteworthy that the dimensionalities of the irreducible massless spinors in both $N = 2n$ and $N = 2n-1$ are identical and equal to 2^{2+n-1}.

The reduction of a generic $4+N$-dimensional spinor into the irreducible representations of ($4D$-Lorentz)$\times SO(N)$ symmetry has the following schematic form,

$$2^{2+n-1} \;\to\; 2_L \times 2^{n-1} + 2_R \times 2^{n-1}\,, \tag{3.22}$$

where numbers indicate the dimensionalities of the representations and only the 4-dimensional chiralities are labeled explicitly by L, R. The chiralities with respect to the internal $SO(N)$-symmetry depend on the type of the initial spinor, as discussed above.

Thus, a massless bulk fermion Ψ under the 4-dimensional Lorentz symmetry decomposes into 2^{n-1} left-handed and 2^{n-1} right-handed fermions:

$$\Psi \;\to\; \sum_{A} \Psi_L^{(A)} \;+\; \sum_{\bar{A}} \Psi_R^{(\bar{A})}\,, \tag{3.23}$$

where $A, \bar{A}$ label the basic $SO(N)$-spinors [1].

The above decomposition takes place for each KK level separately,

$$\Psi(x,y) \;\to\; \frac{1}{\sqrt{V_N}} \sum_{\vec{k}} e^{\frac{i\vec{k}\vec{y}}{R}} \left(\sum_{A} \Psi_{\vec{k},L}^{(A)}(x) \;+\; \sum_{\bar{A}} \Psi_{\vec{k},R}^{(\bar{A})}(x) \right)\,. \tag{3.24}$$

A bulk fermion Ψ with canonical normalization exhibits a mass dimension of $\frac{3+N}{2}$, while the KK modes denoted as $\Psi_{\vec{k}}$ possess a mass dimension of $\frac{3}{2}$.

Through dimensional reduction from $4+N$ to 4-dimensional space-time, the extra-dimensional component of the Dirac operator, represented by $\bar{\Psi}\vec{\gamma}\vec{\partial}_y\psi$,

[1] That is, indices $A, \bar{A}$ label the types of spinors forming a proper complete basis in the $SO(N)$ spinor space, not to be confused with a spinor index.

contributes the Dirac mass terms for the KK modes. During this process, at each KK level, the left and right chiralities form pairs, giving rise to a tower of massive Dirac fermions:

$$\sum_{\vec{k}} m_{\vec{k}} \sum_{A=\bar{A}=1}^{2^{n-1}} \bar{\Psi}^{(A)}_{\vec{k},L}(x)\Psi^{(\bar{A})}_{\vec{k},R}(x)\,. \tag{3.25}$$

The notation $A = \bar{A}$ is assumed such that the spinors undergo appropriate filtering through the high-dimensional $\vec{\gamma}$-matrix. Specifically, each non-zero KK level, denoted as $\vec{k} \neq 0$, gives rise to 2^{n-1} massive Dirac fermions.

The fermions corresponding to the KK level $\vec{k} = 0$, they remain massless. However, a specific superposition of their right-handed components takes on the role of the right-handed partner of the SM neutrino, imparting a Dirac mass to the latter. Let us delve into a more detailed discussion of this phenomenon.

The mass term for the neutrino emerges through a Yukawa-type interaction involving the left-handed lepton doublet $L = (\nu_L, e_L)$, the bulk fermion Ψ, and the Higgs doublet field $H = (H^0, H^-)$.

$$\mathcal{L}_{\text{int}} \;=\; \frac{1}{M_*^{N/2}} H(x)\,\bar{L}(x)\,\Psi(x, y=0)\,. \tag{3.26}$$

The brane is situated at $y = 0$. The previous expression is presented in a schematic form and necessitates additional specification.

To ensure the consistency of the four-dimensional effective field theory, a crucial requirement is its invariance under both the four-dimensional Poincaré symmetry and the gauge symmetry of the SM.

The invariance of (3.26) under the SM gauge symmetry uniquely fixes Ψ to be a gauge-neutral degree of freedom.

Simultaneously, the four-dimensional Poincaré invariance dictates that only the right-handed components $\Psi^{(\bar{A})}_{\vec{k},R}(x)$ (or the charge conjugates of the left-handed ones) of the bulk fermion Ψ are involved in the aforementioned Yukawa coupling. However, this requirement alone does not completely determine the specific form of the coupling due to the following reason.

As the brane introduces a breaking of the higher-dimensional Poincaré symmetry, it is not obligated to obey its $SO(N)$ subgroup. Essentially, the brane functions as a spurion capable of absorbing the $SO(N)$-spinor index. In general, the specific manner of this breaking determines the superposition of bulk spinors $\Psi^{(\bar{A})}_R$ to which the SM neutrino couples.

Within the framework of the effective field theory, this specific information is not readily available. It hinges on factors such as the origin of the

brane and the dynamics responsible for localizing the 4-dimensional chiral fermions on it. In our phenomenological analysis, we will consider this as an external input.

It is noteworthy that the smallness of the SM neutrino's mass is largely indifferent to the precise form of the $\Psi_R^{(\bar{A})}$ superposition to which it couples. The primary contribution to the neutrino's mass predominantly arises from the $\vec{k} = 0$ mode. Nevertheless, the mixing with higher energy states in the KK tower is influenced by this superposition.

Upon taking into account the Higgs vacuum expectation value $\langle H \rangle = (v, 0)$, the above coupling reduces to a mass term that mixes the active left-handed neutrino, with the tower of KK modes,

$$\mathcal{L}_{\text{int}} \;=\; \alpha_\nu \, \bar{\nu}_L(x) \sum_{\vec{k}} \nu_{k,R} \,, \tag{3.27}$$

where

$$\alpha_\nu \;\equiv\; \frac{v}{\sqrt{M_*^N V_N}} \,, \tag{3.28}$$

and

$$\nu_{k,R} \;\equiv\; \sum_{\bar{A}} c_{\bar{A}} \Psi^{(\bar{A})}_{\vec{k},R}(x), \tag{3.29}$$

denotes the superposition of spinors from each KK level to which ν_L mixes. In general, the coefficients c_A can also depend on the level k. However, for the sake of simplicity, we will make the assumption that the $\nu_{k,R}$ are eigenstates of the KK masses. Under this assumption, the orthogonal superpositions effectively decouple from our problem and can be neglected.

The mixing of ν_L with the tower of $\nu_{k,R}$ results in the generation of the neutrino mass, given by $m_\nu \simeq \alpha_\nu \sqrt{\sum_{\bar{A}} |c_{\bar{A}}|^2} \sim \alpha_\nu$. This mass, for $M_* \sim M_f$, is approximately:

$$m_\nu \sim \frac{v M_f}{M_P} \,. \tag{3.30}$$

For $M_f \sim 10$TeV, this value is in the right phenomenological ballpark.

The neutrino's mass is primarily generated through its mixing with the right-handed components of the $\vec{k} = 0$ level, which themselves lack intrinsic masses. Nonetheless, the mixing with higher members of the Kaluza-Klein tower induces oscillations of the neutrino into these states. Such oscillations can potentially lead to observable effects, as discussed in works such as [18, 79].

Certainly, for simplicity, let us consider the impact of this effect for one relevant extra dimension with radius R. In this analysis, we will closely follow

the approach presented in [79]. In this specific case, the indices A and $\bar{A}$ are not necessary, and we can express the relevant expressions as follows,

$$\Psi(x,y) = \frac{1}{\sqrt{2\pi R}} \sum_{k=-\infty}^{k=\infty} e^{\frac{iky}{R}} \left(\Psi_{k,L}(x) \; + \; \Psi_{k,R}(x)\right) . \tag{3.31}$$

Notice that the hierarchy $M_f/M_P \sim 10^{15}$ is still maintained by assuming the existence of additional $N-1$ dimensions with much smaller radii. The corresponding KK excitations associated with these extra dimensions are heavy and effectively decouple from the neutrino mass problem.

Due to the degeneracy under the reflection $k \to -k$ for each $k \neq 0$ level, the active neutrino mixes with the modes $\nu_{kR} \equiv \frac{1}{\sqrt{2}}(\psi_{k,R} + \psi_{-k,R})$, while the orthogonal superpositions, $\frac{1}{\sqrt{2}}(\psi_{k,R} - \psi_{-k,R})$, decouple and can be disregarded.

Then, the part of the Lagrangian describing the relevant mass terms is

$$\mathcal{M}_\nu = \alpha_\nu \nu_L \left(\nu_{0R} \; + \; \sqrt{2}\sum_{k=1}^{\infty} \nu_{kR}\right) + \sum_{k=1}^{\infty} \frac{k}{R} \bar{\nu}_{kL} \nu_{kR} \, . \tag{3.32}$$

Thus, we have the mass matrix of the following form,

$$\begin{pmatrix} 0 & \alpha_\nu & \sqrt{2}\alpha_\nu & \sqrt{2}\alpha_\nu & ... \\ 0 & 0 & 0 & 0 & ... \\ 0 & 0 & 1/R & 0 & ... \\ 0 & 0 & 0 & 2/R & ... \\ ... & ... & ... & ... & ... \end{pmatrix} . \tag{3.33}$$

Each $k \neq 0$ mixes with SM neutrino with an angle given by $\tan\varphi_k = \frac{\alpha_\nu R}{k}$. Thus, the modes with higher values of k quickly decouple and the main effect is concentrated in the part of the KK tower with $k \sim 1$.

The active (left-handed) SM neutrino represents a superposition of the mass eigenstates of the form

$$\nu_L \; = \; \frac{1}{\mathcal{N}} \Big(\nu'_L + \sum_{k=1}^{\infty} \frac{\alpha_\nu R}{k} \nu'_{k,L}\Big), \tag{3.34}$$

where $\mathcal{N}^2 = 1 + \sum_k \frac{(\alpha_\nu R)^2}{k^2} \simeq 1$ is a normalization factor. The mixing with the KK tower results in the oscillations of the active flavor into the KK modes. The survival probability is

$$P_{\rm surv}(t) = |\langle \nu_L | \nu_L(t) \rangle|^2 = \frac{1}{\mathcal{N}^4} \Big| 1 + \sum_{k=1}^{\infty} \frac{(\alpha_\nu R)^2}{k^2} \exp\left(i\phi_k\right) \Big|^2 . \tag{3.35}$$

As a result, we obtain an interference pattern from an infinite number of oscillating modes with increasing frequencies proportional to k^2 and decreasing amplitudes proportional to $1/k^2$. Due to this behavior, in practice, the higher-frequency modes can be effectively averaged out, and only a few low-frequency modes remain observable.

The implications of this phenomenon, particularly for solar neutrinos, were discussed in detail in [79]. More recent experimental constraints and updates can be found in [81] and subsequent papers, with the latest bounds presented in [82].

It is important to note that assuming the alignment of the interaction (3.29) and mass (3.25) eigenstates, the analysis reproduced above from [79] can be readily extended to an arbitrary number of relevant dimensions. This allows for a straightforward generalization of the discussed phenomena in the context of higher-dimensional scenarios.

Now before we proceed let us discuss current bounds on the ADD model. In general, there are two parameters of interest that get tested by experiments. The high energy cutoff M_f gets tested at LHC and ATLAS [83] and CMS [84] give a lower bound to this scale of

$$M_f \gtrsim 10\text{TeV}\,. \tag{3.36}$$

The second parameter is R which can be measured by searching for deviations from Newtons´s law at small lengthscales. Current experiments report [85, 86, 87, 88]

$$R_{max} \lesssim 30\,\mu\text{m}\,. \tag{3.37}$$

3.2.2 Many Species Theory and Small Neutrino Masses

The many species framework is the second case which lowers the scale of QG to TeV scale. It was developed after the ADD model and in this section, we want to present first the arguments why the fundamental scale gets lowered in theories with many light species and then present the mechanism of how small neutrino masses can be generated.

There is more than one way that can demonstrate the following equation

$$M_p^2 \geq N M_f^2, \tag{3.38}$$

where N is the number of light species. This is the master equation for the many species framework and one can easily see how it solves the hierarchy problem by decoupling M_f from M_P like the ADD model. One just has to make N large enough. If one takes $N \approx 10^{32}$, M_f is then at the TeV scale. This fact was first pointed out in the papers [15, 16] and one of the proofs

presented in these papers I show in the following. The proof has two steps. First, we will show that the Planck mass obeys the bound

$$M_p^2 \geq N\Lambda^2, \tag{3.39}$$

where Λ is the mass scale of the introduced species. Then it was shown that Λ is the scale of new gravitational dynamics proofing (3.38).

Consider N species of the bosonic quantum fields Φ_j , j = 1, 2, ...N, of mass Λ. We shall first assume that the system is invariant under an exact discrete $Z_2^N \equiv Z_2^{(1)} \times Z_2^{(2)} \times ... \times Z_2^{(N)}$ symmetry, under the independent sign flips of the fields. That is, under any given $Z_2^{(j)}$-factor only one particular field changes the sign,$\Phi_j \to -\Phi_j$, whereas all the other fields are invariant. We shall now prove that in such a case the Planck mass must satisfy the bound (3.38). In order to prove the relation (3.38) we can perform the following thought experiment. Taking an arbitrarily large number of N-species particles, we can prepare an arbitrarily large black hole. This black hole will carry the information about the amount of the conserved charge carried by the particles. In order to avoid entering the discussions on the black hole information loss issues, it is useful to think of these Z_2-s as the gauged discrete symmetries [89, 90, 91]. The information about the absorbed charge then can be monitored by the Aharonov-Bohm effect at infinity, using the probe Z_2-cosmic strings [92], and cannot be lost. Because the conserved quantum number is Z_2^N , we can store maximum N units of the charge in such a black hole. For this, we will need N particles, each belonging to a different species. Any further increase of the number of the initial particles, will not increase the amount of the conserved discrete charge stored by the black hole. Thus, we shall focus on a minimal size black hole carrying the maximum possible discrete charge. The mass of such a black hole is

$$M_{BH} = N\Lambda \tag{3.40}$$

Because of the conservation, the information about the Z_2^N-charge hosted by the black hole must be revealed after its evaporation. For a black hole of the Hawking temperature T_H, the probability of the emission of a heavy particle of mass $\Lambda >> T_H$ is exponentially suppressed by a Boltzmann factor $\sim \exp -\frac{\Lambda}{T_H}$. Thus, our black hole with N units of the Z_2^N-charge can start emitting N-species particles, only after its temperature drops to $T_H \sim \Lambda$. At this point, the mass of the black hole is $M_{BH}^* \sim \frac{M_P^2}{\Lambda}$. Starting from this moment, the black hole can start revealing back the stored charge, in the form of the N-species particles. However, by conservation of energy, the maximum number of particles that can be emitted by the black hole is

$$n_{max} \sim \frac{M_P^2}{\Lambda^2} \tag{3.41}$$

These states should carry the same Z_2^N-charge as the original N-particles. Thus, $n_{max} = N$, which proves the equation (3.39). In other words, the key point of the proof is that the amount of the maximal discrete charge that is stored in the initial black hole scales as N, but the temperature at which the black hole starts giving back this charge essentially does not scale with N. Hence the only way to avoid inconsistency is the scaling of the M_P^2 as $\sim N$.

Now one has to do the second step which shows that this scale Λ is the scale where gravitational physics changes.

To see this, consider a BH with temperature $T_H \approx \Lambda$. Let us assume first that the BH does not carry the conserved charge of species number. In semi-classical approximation the decay rate of the BH is

$$\frac{dM_{BH}}{dt} \approx -NT_H^2 \tag{3.42}$$

Using the relation between the black hole mass and the temperature $T_H \approx M_P^2/M_{BH}$, we can re-express this as

$$\tau_{BH} \approx \frac{1}{N}\int_0^{M_{in}} \frac{M_{BH}^2}{M_P^4} dM_{BH} \tag{3.43}$$

where M_{in} is the initial mass, which for the black hole of size $\Lambda^{-1}$is $M_{in} \approx \frac{M_P^2}{\Lambda}$. This gives,

$$\tau_{BH} \approx \frac{M_{BH}^3}{NM_P^4} \approx \frac{1}{\Lambda}. \tag{3.44}$$

If the BH has N units of the conserved charge, this calculation has to be slightly modified to take into account the fact that due to the conservation of charge, the number of species available for emission decreases as the BH evaporates. In this case,

$$\frac{dM_{BH}}{dt} \approx -n(M_{BH})T_H^2 \tag{3.45}$$

where $n(M_{BH}) = \frac{M_{BH}}{\Lambda}$ is the number of available species. Going through the same steps as above one finds that the lifetime of the BH is again given by (3.44). The fact that the lifetime becomes comparable to the size of the BH implies that they cannot be treated as semi-classical four-dimensional BHs with well-defined Hawking temperature, since the temperature T_H itself changes on the time-scale $\approx T_H^{-1}$. Therefore, we conclude that Λ determines the critical scale beyond which new gravitational dynamics must appear and we can identify $\Lambda = M_F$.

This is one argument but more have been given in the papers [15, 16, 93, 94, 95]. This new scale of gravity has been incorporated in string theory where it is known as the "species scale" [94, 95].

The first specific model that used this mechanism to solve the hierarchy problem was the Dvali-Redi (DR) model which introduced 10^{32} SM copies as the largest possible extension of the SM [17]. In this model, it was also demonstrated how small neutrino masses can be generated and we present its results in the following.

As already said, the framework represents N identical copies of the SM. The copies are permuted under $P(N)$. It is useful to visualize the copies as placed on equidistant sites in the space of species. Fermions of each sector are charged under their own gauge group. The exceptions are sterile neutrinos, which represent the right-handed partners of corresponding active left-handed neutrinos. We shall denote them by ν_{Rj}, where $j = 1, 2, ..., N$ is the label of the SM copy. These particles do not carry any charges under the SM gauge groups. Thus the notion of "belonging" is defined by their transformation properties under the permutation group $P(N)$ as well as by their couplings to particles of specific SM copies. In particular, the gauge charges do not forbid sterile neutrinos to interact with neutrinos of the other copies. One can say that sterile neutrinos are not confined to specific sites in the space of species. The most generic renormalizable coupling has the following structure,

$$(HL)_i \lambda_{ij} \nu_{Rj} + h.c., \tag{3.46}$$

where H and L stand for the Higgs and lepton doublets of the i-th copy. Here λ_{ij} is a $N \times N$ Yukawa matrix interaction in the space of species. This Yukawa coupling matrix is restricted by the permutation symmetry group $P(N)$ and has therefore the following form:

$$\lambda_{ij} = \begin{pmatrix} a & b & b & \dots \\ b & a & b & \dots \\ b & b & a & \dots \\ \dots & \dots & \dots & \ddots \end{pmatrix}. \tag{3.47}$$

For the calculation of the mass matrix of neutrinos, one has to have a closer look at the Higgs doublet H_i. The simplest case for calculation is when the permutation symmetry is unbroken by the electroweak vacua. This means, that the VEV of the Higgs doublet in every copy of the SM takes the same value v. In this section, we shall focus on this case. The generalization to the case of broken permutation symmetry will be given later.

For now, let us, therefore, take v as the VEV of the Higgses for all copies. Then, the mass matrix takes the form $m_{ij} = \lambda_{ij} v$.

This mass matrix has the eigenvalues

$$m_1' = (a - b)v, \tag{3.48}$$

$$m_H = [a + (N-1)b]v, \tag{3.49}$$

corresponding to the eigenvectors

$$\nu_1' = \sqrt{\frac{N-1}{N}}\nu_1 - \frac{1}{\sqrt{N}}\nu_h, \tag{3.50}$$

and

$$\nu_H = \frac{1}{\sqrt{N}}\nu_1 + \sqrt{\frac{N-1}{N}}\nu_h. \tag{3.51}$$

It is worth noticing for later convenience that the light eigenvalue is $N-1$ times degenerated. Because

$$b \leq \frac{1}{\sqrt{N}}, \tag{3.52}$$

and $a \approx 1000b$ we see that the mass of the neutrino is suppressed by the number of species. The mechanism presented here can explain the smallness of the neutrino mass but has no phenomenological implications which can be tested by experiments due to the huge mass of the heavy state which scales with the number of species which is of order $N \approx 10^{32}$.

Before we proceed to the basics of neutrino oscillations let me mention here that additionally to the ADDM and DR model there exists another IR attempt to solve the neutrino mass problem via the gravitational anomaly [96] which will be not discussed in this work. In the following, I will focus on TeV scale gravity theories which have a different motivation rooted in the hierarchy problem.

3.3 Basics of Neutrino Oscillation

In this part, the theoretical background of Neutrino Oscillation is described. For more detailed references see the reviews I am relying on [97, 98]. Neutrino oscillation is an observed phenomenon that shows that neutrinos can change their favor without collisions. The reason for this is in principle a rather simple quantum mechanical phenomenon.

For demonstration let us assume a quantum mechanical 2-level system with the stationary states $|\Psi_1\rangle$ and $|\Psi_2\rangle$. Then their time evolution is

$$|\Psi_i(t)\rangle = e^{-iE_i t}\,|\Psi_i\rangle\,. \tag{3.53}$$

If one takes the following initial state

$$|\Psi(0)\rangle = a\,|\Psi_1\rangle + b\,|\Psi_2\rangle\,, \tag{3.54}$$

and let it evolve in time it looks like

$$|\Psi(t)\rangle = ae^{-iE_i t}\,|\Psi_1\rangle + be^{-iE_2 t}\,|\Psi_2\rangle\,. \tag{3.55}$$

The probability of finding the system in the initial state after time t can be calculated then like

$$\begin{aligned} P_{surv} = |\,\langle\Psi(0)|\,|\,|\Psi(t)\rangle\,|^2 &= ||a|^2 e^{-iE_1 t}\,|\Psi_1\rangle + |b|^2 e^{-iE_2 t}\,|\Psi_2\rangle\,|^2 \\ &= 1 - 4|a|^2|b|^2 \sin^2[(E_2 - E_1)t/2]. \end{aligned} \tag{3.56}$$

A similar calculation one has to do for neutrinos. The crucial point is that the initial state is a superposition of the energy eigenstates. In the case of neutrinos, the interplay between different states is caused by the flavor and the mass basis. Therefore, a neutrino of a given flavor is a superposition of different mass eigenstates. In the SM the connection between flavor and the mass basis in the leptonic sector are given by the Pontecorvo-Maki-Nakagawa-Sakata-Matrix **U** which is the analogue of the Cabibbo-Kobayashi-Maskawa-Matrix of the quark sector.

Therefore, one can write the flavor eigenstates as

$$|\nu_\alpha\rangle = \sum_i U^*_{\alpha i}\,|\nu_i\rangle\,, \tag{3.57}$$

where α stands for the flavor and i for the mass eigenstates. From this one can find the general expressions for oscillation as

$$P_{\alpha\beta} = |\sum_i U_{\beta i} e^{-i\frac{\Delta m^2_{ik}}{2p}L} U^*_{\alpha i}|^2, \tag{3.58}$$

where L is the propagation length of the neutrinos, $\Delta m^2_{ik} = m^2_i - m^2_k$ is the mass splitting and p is the momentum. In the 2×2 case of mixing between two different flavors the survival probability becomes

$$P_{\alpha\to\alpha} = 1 - 4|U_{\alpha 2}|^2(1 - |U^2_{\alpha 2}|)\sin^2\left(\frac{\Delta m^2 L}{2E}\right). \tag{3.59}$$

The core of the mechanism we have now understood in the previous example. Nevertheless, the case for neutrinos is slightly more complicated because we know from Quantum Mechanics that particles are described by a wave packet. But let us start with describing the neutrino by plane waves and do the generalization to a wave packet afterward. The time-evolved state of a neutrino looks then like the following

$$|\nu(t,\vec{x})\rangle = \sum_i U^*_{\alpha i} e^{-ip_i x}\,|\nu^{\text{mass}}_i\rangle \tag{3.60}$$

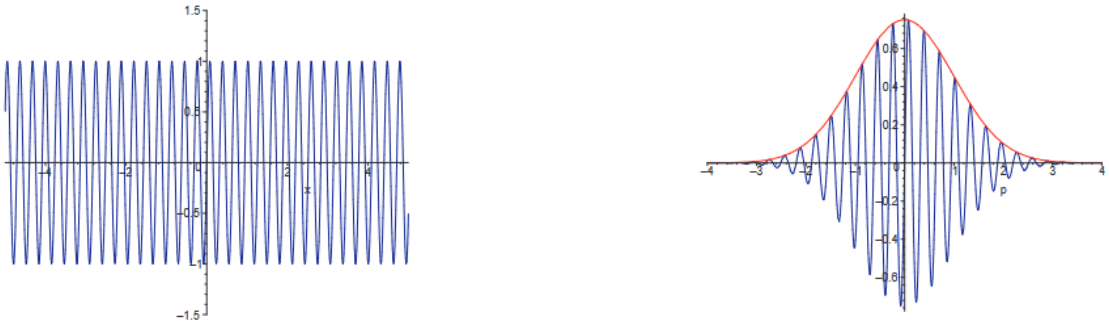

Figure 3.2: Comparison between a plane wave (left) and a wave packet (right) [98].

The phase factor every mass eigenstate picks up is $e^{-i\phi_i}$ with

$$\phi_i = E_i t - \vec{p}_i \vec{x}. \tag{3.61}$$

Physical relevance is the relative phase between the different mass eigenstates. Therefore, one is interested in the differences of the phases of the mass eigenstates and one has to calculate $\Delta\phi_{ik}$ as

$$\Delta\phi_{ik} = \Delta E_{ik} t - \Delta\vec{p}_{ik} \vec{x}. \tag{3.62}$$

Due to the different masses of the eigenstates, they cannot have the same energy and momentum but usually, one either assumes the same energy or momentum to simplify the calculation. Both lead to the same result. So let us take $\Delta\vec{p} = 0$ and plug it in (3.62). Together with the approximation for ultra-relativistic neutrinos, $E_i = \sqrt{\vec{p}^2 + m_i^2} \approx p + \frac{m_i^2}{2p}$ one gets for the oscillation phase

$$\Delta\phi = \Delta E \approx \frac{\Delta m^2}{2p} t, \tag{3.63}$$

where we suppressed the indices. Because neutrinos are relativistic one can do the replacement $t \approx L$ and we find the oscillating phase like in the sin in (3.59).

This ansatz is called the "Same Momentum Approach". Similarly, there is a "Same Energy Approach" which leads to the same result. In general, this result is correct even with the unnatural plane wave assumption. A more elaborate way of describing neutrinos is via a wave packet approach.

Figure 3.2 shows the differences between a plane wave description and a wave packet approach. In the latter model, one is able to describe local particles with a momentum $\vec{p}_0$ and a momentum spread of σ_p. With the

Heisenberg uncertainty follows $\sigma_p \geq 1/\sigma_x$. A free particle with momentum spread, location spread σ_x and a mass m_i is described by

$$\Psi_i(t,\vec{x}) = \int \frac{d^3p}{(2\pi)^3} f_{\vec{p}_0}(\vec{p}) e^{i\vec{p}\vec{x} - iE_i(p)t}. \tag{3.64}$$

Here $f_{\vec{p}_0}$ is the momentum distribution. Its form is usually taken to be a Gaussian

$$f_{\vec{p}_0} = \frac{1}{(2\pi\sigma_p^2)^{3/4}} e^{-\frac{(\vec{p}-\vec{p}_0)^2}{4\sigma_p^2}}. \tag{3.65}$$

When one neglects the spreading of the packet and calculates the wave packet from (3.64) the result is

$$\Psi_i(t,\vec{x}) = e^{i\vec{p}_0\vec{x} - iE_i(p_0)t} \frac{1}{(2\pi\sigma_p^2)^{3/4}} e^{-\frac{(\vec{x}-\vec{v}_{gi}t)^2}{4\sigma_x^2}}, \tag{3.66}$$

with the group velocity $\vec{v}_{gi} = [\partial E_i(p)/\partial\vec{p}]_{\vec{p}=\vec{p}_0} = \vec{p}_0/E_i(\vec{p}_0)$. With this, we can write down an evolved expression of the neutrino state

$$|\nu(\vec{x},t)\rangle = \sum_i U^*_{\alpha i} |\nu_i(\vec{x},t)\rangle = \sum_i U^*_{\alpha i} \Psi_i(\vec{x},t) |\nu_i\rangle . \tag{3.67}$$

In order now to calculate the correct oscillation phase for the wave packet approach one has to take into account that usually neutrinos are highly relativistic or/and the masses of the mass eigenstates are nearly degenerate. So one can do the following expansion

$$\Delta E = \frac{\partial E}{\partial p}\Delta p + \frac{\partial E}{\partial m^2}\Delta m^2 = v_g \Delta p + \frac{1}{2E}\Delta m^2. \tag{3.68}$$

Plugging this into (3.62) results in

$$\Delta\phi = -(L - v_g t)\Delta p + \frac{\Delta m^2}{2E} t. \tag{3.69}$$

One immediately sees that adopting the same momentum approach leads again to the standard oscillation phase. Moreover, the factor $(L - v_g t)$ cannot exceed σ_x because otherwise, the wave function goes to 0. Therefore, the first term is small and leads to

$$\sigma_x |\Delta p| \ll 1. \tag{3.70}$$

With the Heisenberg uncertainty one gets

$$|\Delta p| \ll \sigma_p. \tag{3.71}$$

If one uses the same energy approach and follows the same procedure one finds

$$|\Delta E| \ll \sigma_E. \tag{3.72}$$

These are necessary conditions that must be satisfied to make neutrino oscillations possible. This is one of the properties of neutrino oscillations which one can just obtain by the more elaborated wave packet approach. Nevertheless, for almost all practical purposes the first term of the equation (3.69) is negligibly small and the oscillation conditions are satisfied for sure.

The effect of neutrino oscillation appears basically because of the small Δm of the mass eigenstates one cannot choose a specific eigenstate due to the QM uncertainties. So as long as the uncertainties are bigger than Δm the effect appears. Because the masses are fixed on just has to worry about the changing of the QM uncertainties. They are influenced by three events. These are the production, the detection, and the propagation of the neutrinos between the two locations. First, we focus on the production and detection process.

The uncertainties in the production or detection process are σ_E and σ_p. When we assume that the uncertainties are independent of $E^2 = \vec{p}^2 + m^2$ and choose the process with the smaller uncertainty one gets the minimal uncertainty of

$$\sigma_{m^2} = [(2E\sigma_E)^2 + (2p\sigma_p)^2]^{1/2}. \tag{3.73}$$

As long this quantity satisfies $\sigma_{m^2} \gg |\Delta m^2|$ it is impossible to resolve the different mass eigenstates. If the mass differences are too large the oscillation effect gets suppressed. This is also the reason why leptons do not oscillate due to their large masses which are much bigger than their QM uncertainties. The fact that a too accurate measurement of neutrino energy and momentum destroys neutrino oscillation was first shown in [99].

Another way the coherence of the wave packet could be lost is due to the propagation of the wave packet [100]. Because of the different masses, the group velocities of the different eigenstates that compose are flavor eigenstate are different. Therefore, the wave packet separates due to the velocity difference Δv_g. If the spatial separation exceeds σ_x coherence and therefore neutrino oscillation is lost. With this picture, one can define the coherence length l_{coh} and time t_{coh} which gives the information until coherence holds and when the wave packet starts losing it. The conditions are

$$\Delta v_g t_{\text{coh}} \simeq \sigma_x, \tag{3.74}$$

with

$$l_{\text{coh}} \simeq v_g t_{\text{coh}}. \tag{3.75}$$

Here v_g stands for the averaged group velocity of the different mass eigenstates. For ultra relativistic neutrinos $\Delta v_g = \frac{\Delta m^2}{2E^2}$ holds and one gets

$$l_{\text{coh}} \simeq \frac{v_g}{|\Delta v_g|}\sigma_x \simeq \frac{2E^2}{|\Delta m^2|\sigma_x}. \tag{3.76}$$

Recapitulating the discovered conditions for oscillations we have now two different restrictions on them. First, one has to ensure that in the production and detection, a coherent state is produced or detected respectively. The second part is the loss of coherence due to propagation in space. Now we compare them with each other and check if they can be satisfied simultaneously. Taking the production/detection condition $\Delta E \ll \sigma_E$ and $L \ll l_{\text{coh}}$ one gets for Δm^2

$$\Delta E \sim \frac{\Delta m^2}{2E} \ll \sigma_E \tag{3.77}$$

and

$$\frac{\Delta m^2}{2E^2} L \ll \sigma_x \simeq v_g/\sigma_E. \tag{3.78}$$

Therefore, one finds the necessary condition for oscillation

$$\frac{\Delta m^2}{2E} \ll \sigma_E \ll \frac{2E^2}{\Delta m^2 L}. \tag{3.79}$$

3.4 Neutrino Physics in TeV Scale gravity Theories

In this section we present the results of my work which was published in [2] and we rely on it very closely in the following. In this project, I worked out a general framework for how neutrino physics can be treated in TeV scale Quantum Gravity theories as ADDM or the DR model are. Moreover, we will generalize this framework to a realistic three-flavour case and investigate their effects on low-energy phenomena and observables such as neutrino oscillations into the hidden modes and possible deviations from the Standard Model PMNS matrix which can be tested by nowadays experiments.

3.4.1 Generalisation of Neutrino Masses

We have demonstrated that in ADDM and in DR one can generate small neutrino masses by introducing a right-handed neutrino which is uncharged under the SM gauge group and can therefore propagate into an additional space which was introduced in this class of theories. In the case of ADDM,

this space is represented by the bulk of large extra dimensions, and in the DR it is described as the "space of species". In both cases, the neutrino mass is suppressed by the large effective volume of this extra space.

This common structure we want to investigate further. We shall make a rather general assumption regarding the presence of an additional space through which the sterile neutrino can propagate. Also, we assume that this extra space lowers the scale of gravity via

$$M_*^2 = \frac{M_P^2}{\Lambda}, \tag{3.80}$$

where Λ is the volume of the extra space measured in fundamental units. In ADDM the size of the extra space is a function of R $\Lambda(R)$ and in DR of N $\Lambda(N)$.

The underlying assumption here is that particles devoid of any charge under the Standard Model gauge symmetries have the capability to move through this additional space. Essentially, their interactions and couplings are distributed relatively evenly throughout this space. Consequently, their coupling to individual copies is suppressed.

Within the established framework, two potential candidates for such particles emerge. Firstly, the graviton is a natural choice since gravity exhibits universal interactions. The second candidate is the sterile neutrino. Currently, it remains uncertain whether the neutrino is purely a Majorana particle. If it is not, it implies the existence of a sterile partner denoted as ν_R, which, when combined with the standard left-handed neutrino, forms a Dirac state. This sterile neutrino does not carry any gauge quantum numbers associated with the Standard Model group. Consequently, it is not constrained to the location of our Standard Model, similar to gravity. These particles can disperse throughout the entire extra space, regardless of whether that space represents extra spatial dimensions or the space of species.

This natural dispersion results in a suppression of the coupling between the sterile fermion and the Standard Model neutrino, leading to the generation of a small Dirac mass. The reduced coupling with numerous mixing partners is a consequence of the principle of unitarity and was demonstrated in a prior study [101]. This is the key mechanism behind the small neutrino mass both in ADDM [18] as well as in DR [17].

A possible operator for neutrino mass of the SM neutrino is the Dirac operator

$$yH\bar{\nu}_L\nu_R, \tag{3.81}$$

where y is a Yukawa coupling and H is the SM Higgs doublet. In this framework, the left-handed neutrinos of the Standard Model have the capacity to

mix with various types of right-handed neutrinos that reside in the additional space. So ν_R is a superposition of all possible mixing partners

$$\nu_R = \frac{1}{\sqrt{\Lambda}} \sum_n c_n \nu_{nR} \,. \tag{3.82}$$

Of course, the superposition has to be normalized and this depends on the size of the extra space the right-handed neutrinos live in. Therefore the different contributions of all mixing partners have to be divided by the volume of space in which they can propagate. The resulting form of (3.81) is then

$$yH\bar{\nu}_L\nu_R = \frac{yv}{\sqrt{\Lambda}}\bar{\nu}_L \sum_n c_n \nu_{nR} \,. \tag{3.83}$$

With (3.80) one gets

$$\frac{M_f}{M_P} yv\bar{\nu}_L \sum_n c_n \nu_{nR}. \tag{3.84}$$

The factor in front of the operator represents the effective Dirac mass of neutrino which we can denote by

$$m_D = \frac{M_f}{M_P} yv \,. \tag{3.85}$$

I would like to emphasize that this prefactor is subject to suppression by the Planck mass. As a result, it generates a small Dirac mass for neutrinos. This mechanism encapsulates a fundamental method for generating small neutrino masses within the ADDM framework [18] and the DR framework [17], in a manner that transcends specific theories. Thus, it becomes apparent that the small mass of neutrinos is an inherent property of this class of theories.

What sets this approach apart is that the suppression of the neutrino mass arises from the dimensions of the extra space to which the sterile neutrino can propagate. This is distinct from the commonly used method of introducing a heavy Majorana particle, as in the case of the see-saw mechanism. In essence, the solution we present for the smallness of neutrino mass operates in the infrared domain rather than relying on an ultraviolet solution involving the introduction of an exceedingly heavy particle.

Of course, such mixing can also occur between ν_{Rj} and the left-handed inhabitants, ν_{Li}, of the extra space. Therefore, we also include the mass terms of the following form,

$$m_{ij}\bar{\nu}_{Li}\nu_{Rj}. \tag{3.86}$$

Let us label the neutrino of the SM with $i = 1$. Moreover, let us assume that the interactions among certain pairs of neutrinos are stronger than the

mixing with other types. We shall organize such mass terms as the diagonal entries m_{ii}. Correspondingly the off-diagonal entries μ_{ij} will denote mixings with other species. The resulting mass matrix is

$$\begin{pmatrix} m_D & \mu_{12} & \dots & \dots \\ \mu_{21} & m_{22} & \mu_{23} & \dots \\ \vdots & \dots & \ddots & \dots \end{pmatrix}, \tag{3.87}$$

with $\mu_{1i} = c_i m_D$, and we ordered the diagonal entries according to their hierarchy

$$m_D < m_{22} < \dots < m_{kk}. \tag{3.88}$$

Assuming that the mixing angles, due to off-diagonal entries, are small, we can split this matrix into the diagonal and off-diagonal parts and treat the latter one as a perturbation

$$\begin{pmatrix} m_D & \mu_{12} & \dots & \dots \\ \mu_{21} & m_{22} & \mu_{23} & \dots \\ \vdots & \dots & \ddots & \dots \end{pmatrix} = \begin{pmatrix} m_D & 0 & \dots & \dots \\ 0 & m_{22} & 0 & \dots \\ \vdots & \dots & \ddots & \dots \end{pmatrix} + \begin{pmatrix} 0 & \mu_{12} & \dots & \dots \\ \mu_{21} & 0 & \mu_{23} & \dots \\ \vdots & \dots & \ddots & \dots \end{pmatrix}, \tag{3.89}$$

and we denote

$$V \equiv \begin{pmatrix} 0 & \mu_{12} & \dots & \dots \\ \mu_{21} & 0 & \mu_{23} & \dots \\ \vdots & \dots & \ddots & \dots \end{pmatrix}. \tag{3.90}$$

With this, we find that the eigenvalues do not become corrected in the first order in mixing

$$m_i = m_{ii} + \langle n_i | V | n_i \rangle = m_{ii} + \mathcal{O}^2. \tag{3.91}$$

The correction to the mass eigenstates has the following form

$$|m_1\rangle = |1^{(0)}\rangle + \sum_{k=2} \frac{\mu_{1k}}{m_1^{(0)} - m_k^{(0)}} |k^{(0)}\rangle, \tag{3.92}$$

where the $|n\rangle$ are the eigenstates of the unperturbed matrix. Of course, one has to normalise the expression with

$$Norm^2 = 1 + \sum_{k \neq n} \left(\frac{\mu_{nk}}{m_n^{(0)} - m_k^{(0)}}\right)^2. \tag{3.93}$$

This leads then to the following expression for the mass eigenstates

$$|\vec{m}\rangle = \begin{pmatrix} 1 & \frac{\mu_{12}}{m_1 - m_2} & \dots \\ \frac{\mu_{21}}{m_2 - m_1} & 1 & \dots \\ \vdots & \dots & \ddots \end{pmatrix} |\vec{n}\rangle, \tag{3.94}$$

symbolically

$$|\vec{m}\rangle = U\,|\vec{n}\rangle\,. \tag{3.95}$$

Now one has to invert U in order to find the expression for the space states. In order to invert the matrix U, we use the equation

$$(A+X)^{-1} = A^{-1} + Y, \tag{3.96}$$

with

$$Y = -A^{-1}XA^{-1}, \tag{3.97}$$

and X being in this case the perturbation matrix V. One, therefore, gets for U^{-1}

$$U^{-1} = \begin{pmatrix} 1 & -\frac{\mu_{12}}{m_1-m_2} & \dots \\ -\frac{\mu_{21}}{m_2-m_1} & 1 & \dots \\ \vdots & \dots & \ddots \end{pmatrix}. \tag{3.98}$$

This is how the mixing with the states of extra space takes place in the case of a single flavour of SM neutrino. In particular, the above reproduces the results of such mixings in ADDM [18] and in DR [17] for the case of a single flavour.

3.4.2 Generalisation to three flavour case

Let us now extend our discussion to the scenario with three flavors of SM neutrinos. The most straightforward, though somewhat unrealistic, case occurs when each of the three flavor neutrinos has its distinct mixing partners within the extra space. In such a scenario, the mass matrix assumes the following block-diagonal structure

$$\mathcal{M} = \begin{pmatrix} M_e & 0 & 0 \\ 0 & M_\mu & 0 \\ 0 & 0 & M_\tau \end{pmatrix}, \tag{3.99}$$

where the M_α stands for the mass matrices of the different flavours. Each of them has a form analogous to (3.87). Certainly, we must consider mixing among the different flavors of neutrinos to maintain phenomenological consistency, especially in enabling the three-flavor neutrino oscillations within the Standard Model. To accommodate this phenomenon, we need to deviate from the block-diagonal structure mentioned earlier. We therefore write,

$$\mathcal{M} = \begin{pmatrix} M_e & e\mu & e\tau \\ e\mu & M_\mu & \mu\tau \\ e\tau & \mu\tau & M_\tau \end{pmatrix}, \tag{3.100}$$

where we denote with the $\alpha\beta$ ($\alpha, \beta = e, \mu, \tau$) entries the mixing matrices among the different space state partners of different flavours. To enhance the accuracy of the perturbative calculation, we handle the mixing of flavor ground states, which includes the direct mixing among Standard Model neutrinos, as a component of the perturbed matrix itself, rather than incorporating it into the perturbation matrix V. This leads to the following expressions for the mass eigenstates of the three active neutrinos (we denoted the entries of the SM-like mixing elements as U_{ei}^{-1})

$$|m_1^e\rangle = U_{e1}^{-1}|e\rangle + U_{e2}^{-1}|\mu\rangle + U_{e3}^{-1}|\tau\rangle + \sum_{k=2} \frac{U_{e1}^{-1}\mu_{1k}^e + U_{e2}^{-1}e\mu_{1k} + U_{e3}^{-1}e\tau_{1k}}{m_1^e - m_k^e}|k_1^e\rangle +$$

$$\sum_{k=2} \frac{U_{e1}^{-1}e\mu_{1k} + U_{e2}^{-1}\mu_{1k}^\mu + U_{e3}^{-1}\mu\tau_{1k}}{m_1^e - m_k^\mu}|k_1^\mu\rangle + \sum_{k=2} \frac{U_{e1}^{-1}e\tau_{1k} + U_{e2}^{-1}\mu\tau_{1k} + U_{e3}^{-1}\mu_{1k}^\tau}{m_1^e - m_k^\tau}|k_1^\tau\rangle\,. \tag{3.101}$$

This expression represents the mass eigenstate corresponding to the lightest neutrino, which we associate with the primary mass eigenstate for the electron neutrino. To proceed, we need to invert this expression in a similar manner to the one-flavor case and in order to do so we assume that

$$U_{e1} >> U_{e2}, U_{e3} >> e\mu_{1i}, e\tau_{1i}. \tag{3.102}$$

Then we can write the interaction eigenstate approximately as

$$|\nu_e\rangle = U_{e1}|m_1^e\rangle + U_{e2}|m_1^\mu\rangle + U_{e3}|m_1^\tau\rangle - U_{e1}\Big(\sum_{k=2} \frac{U_{e1}^{-1}\mu_{1k}^e + U_{e2}^{-1}e\mu_{1k} + U_{e3}^{-1}e\tau_{1k}}{m_1^e - m_k^e}|m_k^e\rangle$$

$$+ \sum_{k=2} \frac{U_{e1}^{-1}e\mu_{1k} + U_{e2}^{-1}\mu_{1k}^\mu + U_{e3}^{-1}\mu\tau_{1k}}{m_1^e - m_k^\mu}|m_k^\mu\rangle + \sum_{k=2} \frac{U_{e1}^{-1}e\tau_{1k} + U_{e2}^{-1}\mu\tau_{1k} + U_{e3}^{-1}\mu_{1k}^\tau}{m_1^e - m_k^\tau}|m_k^\tau\rangle\Big). \tag{3.103}$$

If we assume that U_{ei} are already normalized, the normalisation looks as follows,

$$N_e^2 = 1 + U_{e1}\left(\sum_{k=2}\frac{U_{e1}^{-1}\mu_{1k}^e + U_{e2}^{-1}e\mu_{1k} + U_{e3}^{-1}e\tau_{1k}}{m_1^e - m_k^e}\right)^2 +$$

$$\left(\sum_{k=2}\frac{U_{e1}^{-1}e\mu_{1k} + U_{e2}^{-1}\mu_{1k}^\mu + U_{e3}^{-1}\mu\tau_{1k}}{m_1^e - m_k^\mu}\right)^2 + \left(\sum_{k=2}\frac{U_{e1}^{-1}e\tau_{1k} + U_{e2}^{-1}\mu\tau_{1k} + U_{e3}^{-1}\mu_{1k}^\tau}{m_1^e - m_k^\tau}\right)^2 . \tag{3.104}$$

We can further simplify the expression for the flavor neutrino by making the assumption that the masses of the bulk states in the diagonal entries are identical for all flavors. This means that

$$m_k^e = m_k^\mu = m_k^\tau = m_k. \tag{3.105}$$

We also want to assume that different cross-mixing elements among different flavours have the same structure as the mixing of bulk states with their own flavour. This means that also the mixing parts $\alpha\beta_{1k}$ and μ_{1k}^α look like

$$\mu_{1k}^\alpha = \mu f(m_D^\alpha), \tag{3.106}$$

with the same overall constant μ and the same function f depending on the induced Dirac mass just differing by the argument. This leads then to the following expression for the flavour eigenstate

$$|\nu_e\rangle = U_{e1}\,|m_1^e\rangle + U_{e2}\,|m_1^\mu\rangle + U_{e3}\,|m_1^\tau\rangle - U_{e1}\sum_{\alpha=1}^{3}\sum_{k=1}\frac{\mu_{1k}^e U_{e1}^{-1} + \mu_{1k}^\mu U_{e2}^{-1} + \mu_{1k}^\tau U_{e3}^{-1}}{m^e - m_k}\,|k^\alpha\rangle\,. \tag{3.107}$$

Now let us drop the assumption (3.102) and give for the simplified equation (3.107) the expression for a larger cross mixing among the SM neutrinos which is a more realistic scenario. Then the equation gets modified in the following way

$$|\nu_e\rangle = U_{e1}\,|m_1^e\rangle + U_{e2}\,|m_1^\mu\rangle + U_{e3}\,|m_1^\tau\rangle - \sum_{\alpha=1}^{3}\sum_{k=1}\frac{\overrightarrow{U_e}\overrightarrow{C}}{m^e - m_k}\,|k^\alpha\rangle\,, \tag{3.108}$$

with

$$\overrightarrow{U_e} = \begin{pmatrix} U_{e1} \\ U_{e2} \\ U_{e3} \end{pmatrix}, \tag{3.109}$$

and

$$\overrightarrow{C} = \begin{pmatrix} \mu_{1k}^e U_{e1}^{-1} + \mu_{1k}^\mu U_{e2}^{-1} + \mu_{1k}^\tau U_{e3}^{-1} \\ \mu_{1k}^e U_{\mu 1}^{-1} + \mu_{1k}^\mu U_{\mu 2}^{-1} + \mu_{1k}^\tau U_{\mu 3}^{-1} \\ \mu_{1k}^e U_{\tau 1}^{-1} + \mu_{1k}^\mu U_{\tau 2}^{-1} + \mu_{1k}^\tau U_{\tau 3}^{-1} \end{pmatrix}. \tag{3.110}$$

In an analog way, the equation (3.103) can get modified.

Having established these analytical tools, we can now compute a comprehensive expression for a flavor eigenstate of a neutrino that undergoes mixing with a significant number of additional states, while also considering mixings with other flavor states. This approach, which we have applied to non-degenerate, non-perturbed eigenstates, is applicable to the ADDM scenario, and through cross-verification, we can reproduce the one-flavor equation previously derived in [79].

In the subsequent section, we will demonstrate how to compute the flavor states in the case of a highly degenerate mass matrix, which is of particular relevance to the DR scenario.

3.4.3 Highly Symmetric Mass Matrices

Up to this point, we have explored the scenario of a very general mass matrix that includes mixing with all the states within the extra space. However, it is also valuable to examine cases where these mass matrices exhibit specific structures and high levels of symmetry. An illustrative instance of this is the "Many Species Theory", which involves exact copies of the Standard Model.

Now, we will outline an approach to handle matrices of this kind when they are organized into blocks within the mass matrix. To illustrate this method without loss of generality, we will use the example of the DR scenario.

In the DR scenario, the arrangement of various copies of the Standard Model can be based on the vacuum expectation values (VEVs) of the Higgs doublets. It is important to note that even if these copies obey a strict permutation symmetry, the VEVs of the Higgs doublets can spontaneously break this symmetry. This occurs because, due to the low cutoff and cross-couplings among different doublets, the potential can admit vacua where Higgs doublets from different copies exhibit distinct VEVs, represented as $\langle H_j \rangle = v_j$.

Also, because in principle a Majorana mass term for neutrinos is not forbidden neither by gauge nor by permutation symmetry, we will investigate additionally to the common Dirac operator

$$(HL)_i \lambda_{ij} \nu_{Rj}, \tag{3.111}$$

also a Weinberg operator of the form

$$(\bar{L^c} i\sigma_2 H)_i \lambda_{ij} (H i\sigma_2 L)_j \,. \tag{3.112}$$

In this context, the indices i and j denote different copies, and L represents the SU(2) doublet, with σ_2 operating within this space. As previously men-

tioned, we assume that Yukawa couplings adhere to the $P(N)$-symmetry, and consequently, they adopt the form as described in equation (3.47).

It is important to recognize that the operators described in equation (3.112) explicitly break global lepton number symmetries.

The crucial step is to allocate distinct Higgs VEVs to individual Standard Model copies. We organize the copies with the same VEVs into diagonal blocks within the neutrino mass matrix.

Now, let us consider a minimal scenario of this nature in which the VEVs can adopt two possible values, denoted as v and v'. In this setup, we select a subgroup with a size of N, where N is less than the total number of species, denoted as N_{TOTAL}. To this subgroup, we assign the VEV v, while the remaining species, which amount to M species ($M = N_{TOTAL} - N$), are assigned the VEV v'.This assignment can be expressed as,

$$v_i = \begin{cases} v & \text{for } i \leq N \\ v' & \text{for } i > N\,. \end{cases} \tag{3.113}$$

Taking this into account and plugging it into the operators (3.111) and (3.112) one gets the following mass matrices respectively

$$M^{\text{Majorana}} = \begin{pmatrix} av^2 & bv^2 & bv^2 & ... & bv^2 & bv'v & & ... & & bv'v \\ bv^2 & av^2 & bv^2 & ... & bv^2 & \vdots & & \ddots & & \vdots \\ \vdots & & \ddots & & \vdots & \vdots & & \ddots & & \vdots \\ bv^2 & & ... & & av^2 & bv'v & & ... & & bv'v \\ bv'v & & ... & & bv'v & av'^2 & bv'^2 & bv'^2 & ... & bv'^2 \\ \vdots & & \ddots & & \vdots & bv'^2 & av'^2 & bv'^2 & ... & bv'^2 \\ \vdots & & \ddots & & \vdots & \vdots & & \ddots & & \vdots \\ bv'v & & ... & & bv'v & bv'^2 & & ... & & av'^2 \end{pmatrix}, \tag{3.114}$$

and

$$M^{\text{Dirac}} = \begin{pmatrix} av & bv & bv & ... & bv & bv & & ... & & bv \\ bv & av & bv & ... & bv & \vdots & & \ddots & & \vdots \\ \vdots & & \ddots & & \vdots & \vdots & & \ddots & & \vdots \\ bv & & ... & & av & bv & & ... & & bv \\ bv' & & ... & & bv' & av' & bv' & bv' & ... & bv' \\ \vdots & & \ddots & & \vdots & bv' & av' & bv' & ... & bv' \\ \vdots & & \ddots & & \vdots & \vdots & & \ddots & & \vdots \\ bv' & & ... & & bv' & bv' & & ... & & av' \end{pmatrix}. \tag{3.115}$$

The diagonalization of the above mass matrices will be performed in the next section.

Diagonalizing of the Majorana mass matrices

In this section, we will diagonalize the Majorana mass matrices. Due to the complexity of the resulting expressions, the diagonalization procedure will be conducted within certain limits. The two limits which will be discussed are $v' \gg v$, and $N \gg M$ or vice versa.

The symmetric breaking limit of the mass matrix

Here the focus lies on the Majorana mass matrix (3.114) and we make the assumption that the breaking of $P(N)$ is into two equally large sectors, $M = N$. In order to simplify the resulting equations even further, we will also assume that $v' \gg v$. we put the value v' close to the cutoff of the theory which is $\sim$TeV. This will lead later to very interesting phenomenological implications.

We start diagonalizing (3.114) noticing that it is a 2×2 block matrix. As the first step, we multiply the matrix with the following transformation matrix

$$U' = \begin{pmatrix} S & 0 \\ 0 & S \end{pmatrix}, \tag{3.116}$$

where S is the diagonalization matrix of a matrix of just ones (a matrix with the same entry everywhere)

$$S = \begin{pmatrix} 1 & -1 & \dots & \dots & \\ \vdots & 1 & 0 & \dots & \\ \vdots & 0 & \ddots & 0 & \dots \end{pmatrix}. \tag{3.117}$$

This leads then to the following expression

$$U'^{-1} M^{Majorana} U' = U'^{-1} \begin{pmatrix} A & B \\ C & D \end{pmatrix} U' = \begin{pmatrix} S^{-1}AS & S^{-1}BS \\ S^{-1}CS & S^{-1}DS \end{pmatrix}, \tag{3.118}$$

where the matrices A, B, D, and C denote the block entries of the mass matrix. One can separate the diagonal entries of the matrices A and D from the rest of the matrix and turn this one into a matrix with just the same entry

$$A = v\lambda_{ij} = \begin{pmatrix} (a-b)v^2 & 0 & \dots \\ 0 & \ddots & 0 \\ \vdots & \dots & (a-b)v^2 \end{pmatrix} + \begin{pmatrix} bv^2 & \dots & \dots \\ \vdots & \ddots & \vdots \\ \vdots & \dots & bv^2 \end{pmatrix}. \tag{3.119}$$

The diagonal part commutes with S and one is therefore left with the following matrix

$$\begin{pmatrix} (a-b)v^2+Nbv^2 & 0 & \dots & Nbvv' & 0 & \dots & 0 \\ 0 & (a-b)v^2 & 0 & \dots & 0 & \dots & 0 \\ \vdots & 0 & \ddots & 0 & & \dots & 0 \\ Nbvv' & 0 & \dots & (a-b)v'^2+Nbv'^2 & 0 & \dots & 0 \\ 0 & \dots & & 0 & (a-b)v'^2 & \dots & 0 \\ 0 & \dots & & \dots & 0 & \ddots & 0 \end{pmatrix}. \tag{3.120}$$

Now one can take out the diagonal element and can bring it down to a 2×2 matrix of the following form

$$\begin{pmatrix} Nbv^2 & Nbvv' \\ Nbvv' & Nbv'^2+(a-b)(v'^2-v^2) \end{pmatrix}. \tag{3.121}$$

In order to find the mass eigenstates, one has to manipulate (3.120) further with the following rotation matrix,

$$\begin{pmatrix} cos(\theta) & sin(\theta) \\ -sin(\theta) & cos(\theta) \end{pmatrix}, \tag{3.122}$$

with the rotation angle

$$\theta = \frac{1}{2}\arctan(2\frac{vv'}{v'^2-v^2}). \tag{3.123}$$

The rotation matrix multiplied with the U' matrix gives the transformation matrix of the mass matrix. The result is

$$U = \begin{pmatrix} cos(\theta) & -1 & \dots & -1 & sin(\theta) & 0 & \dots \\ cos(\theta) & 1 & 0 & \dots & sin(\theta) & 0 & \dots \\ \vdots & 0 & \ddots & & \vdots & 0 & \dots \\ -sin(\theta) & 0 & \dots & 0 & cos(\theta) & -1 & \dots \\ \vdots & 0 & \dots & 0 & \vdots & 1 \quad 0 & \dots \end{pmatrix}. \tag{3.124}$$

From this analysis, it becomes evident that only two states are influenced by the symmetry breaking, while the others remain degenerate with eigenvalues of $(a-b)v^2$ and $(a-b)v'^2$. Consequently, we can express the new heavy states in terms of the heavy states of the unbroken permutation subset, which we have previously encountered in equations (3.50) and (3.51). To facilitate the simplification of the rotation angle described in equation (3.123), we

will utilize the limit where v' is much larger than v. The result is then the following

$$n_H^b = n_H - \frac{v}{v'}\tilde{n}_H, \tag{3.125}$$

$$\tilde{n}_H^b = \tilde{n}_H + \frac{v}{v'}n_H, \tag{3.126}$$

where we used tilde for the v' sector. When one solves now for species states of the two different sectors one gets the following two expressions

$$n_1 = \sqrt{\frac{N-1}{N}}n_1' + \frac{1}{\sqrt{N}}n_H^b + \frac{1}{\sqrt{N}}\frac{v}{v'}\tilde{n}_H^b, \tag{3.127}$$

(notice that for the sake of simplicity the overall normalization factor is suppressed)

$$n_{N+1} = \sqrt{\frac{N-1}{N}}\tilde{n}_1' + \frac{1}{\sqrt{N}}\tilde{n}_H^b - \frac{1}{\sqrt{N}}\frac{v}{v'}n_H^b\,, \tag{3.128}$$

with the Eigenvalues of the mass eigenstates:

$$m_1' = (a-b)v^2, \tag{3.129}$$

$$\tilde{m}_1' = (a-b)v'^2, \tag{3.130}$$

$$m_H = 2(a-b)v^2, \tag{3.131}$$

$$\tilde{m}_H > M_P. \tag{3.132}$$

This is indeed an intriguing result with significant implications for phenomenology, which we will examine more closely later on. It is worth noting that the shared heavy eigenstate n_H has a mass that is independent of N, which is a departure from the original mechanism. This implies that the common heavy eigenstate is not extremely heavy, making neutrino oscillations into this state a feasible phenomenon.

Asymmetric breaking pattern with a large heavy sector

It is possible to break the symmetry in such a way that the sectors include different numbers of copies, where N represents the sector with a VEV of v, and M corresponds to the sector with a VEV of v'. To keep the expressions for the final results in a simplified form, we consider the limit $Mv'^2 \gg Nv^2$. After repeating the same diagonalization procedure, the matrix (3.120) in

this case has the following form

$$\begin{pmatrix} (a-b)v^2+Nbv^2 & 0 & \dots & Mbvv' & 0 & \dots & 0 \\ 0 & (a-b)v^2 & 0 & \dots & 0 & \dots & 0 \\ \vdots & 0 & \ddots & 0 & & \dots & 0 \\ Nbvv' & 0 & \dots & (a-b)v'^2+Mbv'^2 & 0 & \dots & 0 \\ 0 & \dots & & 0 & (a-b)v'^2 & \dots & 0 \\ 0 & \dots & & \dots & 0 & \ddots & 0 \end{pmatrix}. \tag{3.133}$$

Before we can perform the rotation, we have to make an intermediate step which brings the off-diagonal entries to the same value. Therefore one applies another transformation matrix of the following form

$$\begin{pmatrix} 1 & 0 & \dots & \dots & \dots & \dots \\ 0 & \ddots & 0 & \dots & \dots & \dots \\ \vdots & \dots & \kappa & 0 & \dots & \dots \\ \vdots & \dots & 0 & 1 & 0 & \dots \\ \vdots & \dots & \dots & 0 & \ddots & 0 \end{pmatrix}, \tag{3.134}$$

with κ being

$$\kappa = \sqrt{\frac{N}{M}}. \tag{3.135}$$

After this procedure the off-diagonal entries are equal and one can perform the rotation like in the symmetric case. Correspondingly one gets a mixing angle of the following form

$$\theta = \frac{1}{2}\arctan(-2\frac{\sqrt{N}\sqrt{M}bvv'}{Nbv^2 - Mbv'^2}). \tag{3.136}$$

The resulting transformation matrix is

$$U = \begin{pmatrix} cos(\theta) & -1 & \dots & -1 & sin(\theta) & 0 & \dots \\ cos(\theta) & 1 & 0 & \dots & sin(\theta) & 0 & \dots \\ \vdots & 0 & \ddots & & \vdots & 0 & \dots \\ -\kappa sin(\theta) & 0 & \dots & 0 & \kappa cos(\theta) & -1 & \dots \\ \vdots & 0 & \dots & 0 & \vdots & 1 \quad 0 & \dots \end{pmatrix}. \tag{3.137}$$

and θ simplified to

$$\theta = \sqrt{\frac{N}{M}}\frac{v}{v'}. \tag{3.138}$$

The resulting mass eigenstates are then

$$n_H^b = n_H - \frac{N}{M}\frac{v}{v'}\tilde{n}_H, \tag{3.139}$$

$$\tilde{n}_H^b = \tilde{n}_H + \frac{v}{v'}n_H, \tag{3.140}$$

with the eigenvalues

$$m_H = (a-b)v^2, \tag{3.141}$$

$$\tilde{m}_H > M_P. \tag{3.142}$$

The corresponding copy eigenstates are

$$n_1 = \sqrt{\frac{N-1}{N}}n_1' + \frac{1}{\sqrt{N}}n_H^b + \frac{1}{\sqrt{N}}\frac{N}{M}\frac{v}{v'}\tilde{n}_H^b, \tag{3.143}$$

$$n_{N+1} = \sqrt{\frac{M-1}{M}}\tilde{n}_1' + \frac{1}{\sqrt{M}}\tilde{n}_H^b - \frac{1}{\sqrt{M}}\frac{v}{v'}n_H^b. \tag{3.144}$$

We see that the mass m_H is the same as for the degenerated mass eigenstates.

Asymmetric breaking pattern with a large light sector

One can also investigate the case with a large light sector $Nv^2 \gg Mv'^2$. In this case, the procedure is the same and (3.133) stays untouched. The resulting mixing angle is

$$\theta = -\sqrt{\frac{M}{N}}\frac{v'}{v}. \tag{3.145}$$

The eigenvalues are

$$m_H = (a-b)v'^2, \tag{3.146}$$

$$\tilde{m}_H > M_P. \tag{3.147}$$

The corresponding eigenstates are given by

$$\tilde{n}_H^b = \frac{v}{v'}n_H + \tilde{n}_H, \tag{3.148}$$

$$n_H^b = \tilde{n}_H - \frac{Mv'}{Nv}n_H. \tag{3.149}$$

The copy eigenstates are

$$n_1 = \sqrt{\frac{N-1}{N}}n_1' - \frac{1}{\sqrt{N}}\frac{v'}{v}n_H^b + \frac{1}{\sqrt{N}}\frac{v'}{v}\tilde{n}_H^b, \tag{3.150}$$

$$n_{N+1} = \sqrt{\frac{M-1}{M}}\tilde{n}'_1 + \frac{1}{\sqrt{M}} n_H^b + \frac{1}{\sqrt{M}} \frac{M}{N} (\frac{v'}{v})^2 \tilde{n}_H^b. \tag{3.151}$$

Now the situation is reversed. The m_H goes to the eigenvalues of the degenerated states of the heavy sector. Taking v' close to the cutoff ($\sim$ TeV) the estimated values of m_H could be up to $\sim$keV.

Diagonalizing of the Dirac mass matrix

Let us now turn to diagonalization of the Dirac mass matrix which results from the operator (3.111). The procedure is similar but some details differ from the Majorana case. The first step is that one realizes that the overall structure of

$$M_{\text{Dirac}} M_{\text{Dirac}}^{\dagger} = \begin{pmatrix} A & B \\ B & D \end{pmatrix}, \tag{3.152}$$

is the same as in the Majorana case after a redefinition of the parameters a and b. Because the final expression for the composition of flavour eigenstates does not depend on them but on N their exact definition does not matter. Then one can apply the same procedure of diagonalization as in the Majorana case which leads to the same expressions as already presented in the previous section.

3.4.4 Phenomenology

Now, let us shift our focus to the phenomenological implications of the theoretical framework we have developed in the previous sections. We will carry out this analysis within the context of a specific theory. It is worth noting that initial steps in this direction were already taken in references [79] for ADDM and [17] for DR. However, these analyses were limited to the one-flavor case of the Standard Model neutrino. Our objective now is to extend this investigation to the three-flavor case, leveraging the general framework we have presented earlier.

Phenomenology of ADDM model

To begin our exploration of the Phenomenology of the ADDM scenario within a three-flavor context, we will adopt the framework presented in section 3 and employ our previously derived formulas to analyze the ADDM case. Our initial step involves establishing the mass matrix under investigation. To achieve this, we will utilize the Ansatz introduced in [79] and extend it to encompass the three-flavor scenario. In our endeavor to formulate the resultant mass matrix, we will make the crucial assumption that the flavor

symmetry remains intact within the bulk. This leads to the effect that the mixing among bulk states is diagonal. The resulting mass matrix is

$$\begin{pmatrix} m_{ee} & \sqrt{2}m_{ee} & \dots & \dots & m_{e\mu} & \sqrt{2}m_{ee} & \dots & m_{e\tau} & \sqrt{2}m_{ee} & \dots \\ 0 & \frac{1}{R} & 0 & \dots & \dots & \dots & \dots & \dots & \dots & \dots \\ 0 & 0 & \ddots & 0 & \dots & \dots & \dots & \dots & \dots & \dots \\ 0 & 0 & 0 & \frac{k}{R} & 0 & \dots & \dots & \dots & \dots & \dots \\ m_{\mu e} & \sqrt{2}m_{\mu\mu} & \dots & \sqrt{2}m_{\mu\mu} & m_{\mu\mu} & \sqrt{2}m_{\mu\mu} & \dots & m_{\mu\tau} & \sqrt{2}m_{\mu\mu} & \dots \\ 0 & \dots & \dots & \dots & 0 & \frac{1}{R} & 0 & \dots & \dots & \dots \\ \vdots & \dots & \dots & \dots & \dots & 0 & \ddots & 0 & \dots & \dots \\ m_{\tau e} & \sqrt{2}m_{\tau\tau} & \dots & \dots & m_{e\tau} & \sqrt{2}m_{\tau\tau} & \dots & m_{e\tau} & \sqrt{2}m_{\tau\tau} & \dots \\ 0 & \dots & \dots & \dots & \dots & \dots & \dots & 0 & \frac{1}{R} & \dots \end{pmatrix}. \tag{3.153}$$

In order to perform the diagonalization of this mass matrix, one has to define the parametrization of the U_{PMNS} matrix

$$U_{PMNS} = \begin{pmatrix} c_{12}c_{13} & c_{13}s_{12} & s_{13} \\ -c_{23}s_{12}e^{i\phi} - c_{12}s_{13}s_{23} & c_{12}c_{23}e^{i\phi} - s_{12}s_{13}s_{23} & c_{13}s_{23} \\ s_{23}s_{12}e^{i\phi} - c_{12}c_{23}s_{13} & -c_{12}s_{23}e^{i\phi} - c_{23}s_{12}s_{13} & c_{13}c_{23} \end{pmatrix}. \tag{3.154}$$

With this PMNS-matrix parametrization, we can use the formula (3.108) to calculate the expression for e.g., the muon neutrino. The result is

$$|\nu_\mu\rangle = U_{\mu 1}\,|m_1^e\rangle + U_{\mu 2}\,|m_1^\mu\rangle + U_{\mu 3}\,|m_1^\tau\rangle + \overrightarrow{U_\mu}\overrightarrow{C}\sum_\alpha \sum_k \frac{1}{k}\,|k_\alpha\rangle\,. \tag{3.155}$$

with $\overrightarrow{C}_{ADD}$

$$\overrightarrow{C}_{ADD} = \begin{pmatrix} \xi^e U_{e1}^{-1} + \xi^\mu U_{e2}^{-1} + \xi^\tau U_{e3}^{-1} \\ \xi^e U_{\mu 1}^{-1} + \xi^\mu U_{\mu 2}^{-1} + \xi^\tau U_{\mu 3}^{-1} \\ \xi^e U_{\tau 1}^{-1} + \xi^\mu U_{\tau 2}^{-1} + \xi^\tau U_{\tau 3}^{-1} \end{pmatrix}. \tag{3.156}$$

and the normalisation

$$N_\mu^2 = 1 + \frac{\pi^2}{2}(\overrightarrow{U_\mu}\overrightarrow{C})^2. \tag{3.157}$$

Notice that the parameters ξ^α are related to each other via

$$\xi^e \propto m_e \approx \mathcal{O}(1)m_\mu \approx \mathcal{O}'(1)m_\tau, \tag{3.158}$$

and therefore the key parameter in this expression is just the size of the dominant extra dimension R.

To gain insight into the variation in the composition of a muon neutrino from the Standard Model expectation, one can assess the survival probability. In this analysis, we make the assumption that only the lowest modes of the KK towers play a role in the oscillations, as the higher modes are effectively averaged out due to substantial mass splittings. Then the survival probability reads as

$$P(\nu_\mu \to \nu_\mu) = \frac{1}{|N_\mu|^4}\left[\sum_i \sum_j |U_{\mu i}|^2 |U_{\mu j}|^2 e^{\frac{i(m_i^2 - m_j^2)}{2E}} + 3|\overrightarrow{U_\mu}\overrightarrow{C}|^4 \left(\frac{\pi^4}{90} - 1\right)\right]. \tag{3.159}$$

with E being the energy of the investigated neutrino. This can be compared to the original result in [79] for the one flavour case

$$P = \frac{1}{(1 + (\pi^2/6)\xi^2)^2}\left[(1+\xi^2)^2 + \left(\frac{\pi^4}{90} - 1\right)\xi^4 - \xi^2 \sin^2 \frac{(m_n^2 - m_D^2)t}{4E}\right]. \tag{3.160}$$

By examining these two equations, one can discern that certain characteristics of the single-flavor scenario manifest in a modified fashion within the context of the three-flavor equation. A particularly intriguing aspect is the manner in which, in the context of the ADDM model, the modes that have been averaged out exert an influence on the survival probability, characterized by a term proportional to $\left(\frac{\pi^4}{90} - 1\right)$ when only the lowest mode remains unaveraged. Naturally, the experimental configuration and the specific mass differences dictate the extent to which multiple modes can be distinguished in the oscillations. As more modes become involved, the significance of the contribution from the averaged-out modes diminishes.

For comparison of the three flavour scenario with SM prediction, we take the latest results of the nu-fit collaboration [102] which are:

$$\theta_{12} = 33,44^\circ, \theta_{23} = 49,0^\circ, \theta_{13} = 8,57^\circ, \delta_{CP} = 195^\circ\,. \tag{3.161}$$

With this data, one can calculate the survival probability of a muon neutrino depending on the parameter ξ of the ADDM model. Figure 3.3 shows the result of this calculation and how it deviates from the SM case. Hence, the precise measurements of neutrino oscillations offer a means to establish constraints on the critical parameter ξ within the ADDM model. This constraint can be directly linked to the parameter R which has been the subject of investigation in numerous experiments [81, 103, 104, 105, 106, 107, 108, 109, 110, 111, 112, 113]. Presently, the most stringent constraint stands at $R < 0.81\mu m$.

By examining Figure 3.3, one gains insight into the remarkable sensitivity of neutrino probes. It becomes evident that a value of $R = 0.4\mu m$ exhibits

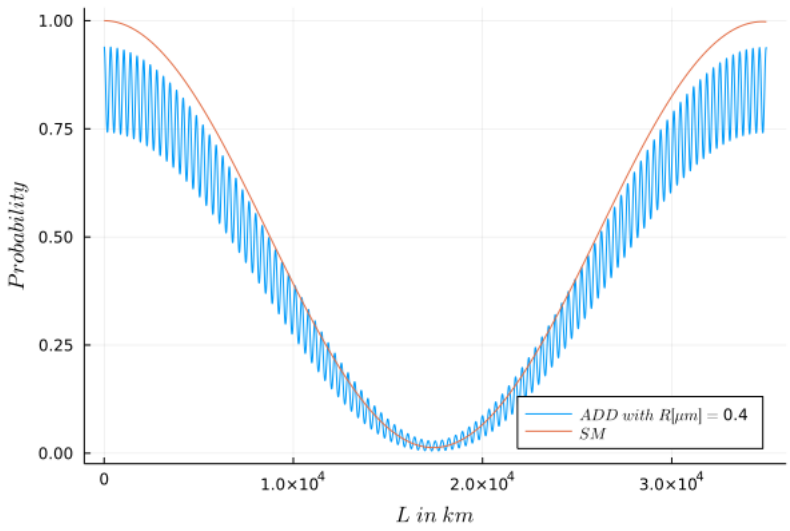

Figure 3.3: Survival probability of a muon neutrino in a three flavour ADD mixing scenario

significant deviations from the SM, underscoring the potential for modern neutrino experiments to establish constraints at the level of $R < 0.4\mu m$, or potentially even smaller.

A noteworthy feature of neutrino experiments is their capacity to measure the size of the largest extra dimension, in contrast to other experiments such as those focused on fifth forces, collider interactions, and astrophysical observations, which provide constraints on the fundamental scale of gravity denoted as M_f. According to [114], the constraints on M_f are as follows: $M_f > 4$ TeV for tabletop experiments, $M_f > 5.9 - 11.2$ TeV based on collider signals, and $Mf* > 1700$ TeV as estimated from neutron stars. The translation of these constraints into the actual size of the extra dimensions is contingent upon several factors, including the number of assumed extra dimensions and whether different scales are allowed among them.

Therefore, the measurement of parameter R through neutrino experiments serves as a complementary approach to assess the validity of the ADDM scenario. It offers a distinct perspective on the theory, enhancing our understanding of extra dimensions and their associated scales in the context of high-energy physics.

Furthermore, the deviation from the SM also has implications for the unitarity of the Lepton Mixing Matrix. In the SM, with its three known neutrino flavors, the neutrino sector is expected to be fully unitary. However, if there are more than three neutrino flavors, as posited in certain extensions

of the theory, the Lepton Mixing Matrix is no longer a simple 3×3 matrix but expands to a $(3+n) \times (3+n)$ matrix, where 'n' represents the number of additional neutrino flavors.

Nonetheless, in experiments that primarily detect active neutrino species, we still measure only the 3×3 subset of this complete Lepton Mixing Matrix. Since this subset, in general, will not be unitary when additional neutrino flavors are considered, we effectively observe a departure from unitarity. This departure is also observed in models like the ADDM, where neutrinos can oscillate into KK modes. Using the outcomes described above, the 3×3 segment of the full Lepton Mixing Matrix undergoes modification as follows

$$\begin{pmatrix} U_{ee}\frac{1}{N_e} & U_{e\mu}\frac{1}{N_e} & U_{e\tau}\frac{1}{N_e} \\ U_{\mu e}\frac{1}{N_\mu} & U_{\mu\mu}\frac{1}{N_\mu} & U_{\mu\tau}\frac{1}{N_\mu} \\ U_{\tau e}\frac{1}{N_\tau} & U_{\tau\mu}\frac{1}{N_\tau} & U_{\tau\tau}\frac{1}{N_\tau} \end{pmatrix}. \tag{3.162}$$

The objective at hand is to achieve highly precise measurements of the parameters within the well-established Pontecorvo-Maki-Nakagawa-Sakata (PMNS) matrix and explore potential deviations from unitarity. This feature is not exclusive to the ADDM model; it can manifest in various other theoretical frameworks as well. However, the example presented above offers a concrete and motivated framework for establishing constraints on unitarity-violating parameters and using them as a means to distinguish between different models.

In the following section, we will delve into the phenomenology of the DR model and compare it directly with the ADDM framework. This comparative analysis will shed light on how unitarity-violating parameters can be a valuable tool for differentiating between theoretical models and enhancing our understanding of the underlying physics.

Phenomenology of the Dvali-Redi model

The generalisation of the mass matrix in the DR scenario goes as follows. Of course, the general structure of the mass matrix is again similar to (3.100) but this time the off-diagonal block matrices have the following form

$$M_{\alpha\beta} = \begin{pmatrix} m_{\alpha\beta} & 0 & 0 & \dots \\ 0 & m_{\alpha\beta} & 0 & \dots \\ \vdots & 0 & \ddots & \vdots \end{pmatrix}. \tag{3.163}$$

This specific structure comes from the fact that in this theory the mixing among the different flavours can happen within a single copy since it is

determined by the physics of the SM. This leads to the following electron neutrino eigenstate

$$|\nu_e\rangle = \sqrt{\frac{N-1}{N}}(U_{e1}\,|m_1\rangle + U_{e2}\,|m_2\rangle + U_{e3}\,|m_3\rangle) + \frac{1}{\sqrt{N}}(U_{e1}\,|m_1^H\rangle + U_{e2}\,|m_2^H\rangle + U_{e3}\,|m_3^H\rangle). \tag{3.164}$$

The crucial parameter in this context is the number of active neutrino species. As previously demonstrated, we can categorize the total number of neutrino species into light and heavy sectors. This approach allows us to explore various scenarios in which different sectors contain varying numbers of neutrino copies. However, since our observations primarily pertain to our version of the SM, scenarios in which the sector containing our copy has a small number of active species are particularly intriguing.

For this reason, we place our focus on scenarios with sizable heavy sectors, as these scenarios result in a reduction of the number of active species in our sector. By investigating these scenarios, we can gain a deeper understanding of the implications and constraints related to the number of active neutrino species in our observable universe.

From (3.143) it becomes evident that the oscillation between sectors is suppressed by the number of active species in the large sector. Consequently, this contribution can be safely neglected.

In the one-flavor case, as discussed in [17], the survival probability is then expressed as

$$P(t) = 1 - \frac{4}{N}\sin^2(\frac{\Delta m^2 t}{2E}). \tag{3.165}$$

In this situation, the challenge of detecting the impact has transitioned from the substantial suppression caused by amplitude to the exceedingly low frequency resulting from minuscule differences among the mass eigenstates. Nonetheless, this circumstance remains highly intriguing for long-baseline experiments involving neutrino oscillations. Astrophysical sources emitting intense neutrino fluxes could serve as valuable contenders for evaluating such scenarios. Naturally, the ability to identify deviations from the anticipated neutrino flux in the standard model necessitates a profound comprehension of the operational mechanisms of these sources with exceptional precision.

Integrating out scenario

In scenarios involving a small light sector, we have observed that the suppression of amplitude behaves counter to the frequency of oscillations. To address this, we introduce the “integrating out” scenario, which offers a path

to bringing both of these parameters within the realm of easier experimental investigation.

The objective here is to amalgamate the advantages of various scenarios we have examined previously into a unified configuration. Suppose we have a permutation symmetry that is heavily broken between two sectors: one sector with a substantial number, denoted as M and another sector with a smaller count, denoted as N. This configuration has been discussed previously.

However, let us now consider a scenario where, due to additional breaking of the permutation symmetry, the smaller sector (N) is further divided into two sub-sectors, one with a number denoted as N' and the other with M'. It is important to note that the initial, primary breaking of the permutation symmetry into the M and N sectors remains the dominant factor. The secondary breaking, which splits the smaller sector, has a negligible impact, contributing effects only at the order of $\mathcal{O}(N/M)$, which are already exceedingly small. Consequently, this sector can be regarded as effectively decoupled from the other sectors.

Now, let us focus on the remaining copies that have been subdivided into two smaller sectors, denoted as N' and M'. In this context, we have the flexibility to determine which sector our SM copy belongs to.

In particular, we can assume that the number of copies in our sector, N', is significantly larger than the other sector, M'. While this choice does not substantially reduce the suppression of the amplitude, it does grant us the ability to set free the value of the common heavy eigenstate, denoted as m_H in which the neutrinos of both sectors undergo oscillations. This, in turn, allows us to increase the difference in mass, denoted as Δm to a level where the oscillation frequency becomes comparable to the typical oscillations of the SM. This scenario of splitting is analogous to the large light sector scenario.

Overall this integrating out scenario enables us to free both parameters of the theory. It allows us to bring down the number of copies and correspondingly oscillation frequencies to a scale that makes it observable for experiments.

We are now able to compute the oscillation in the three-flavor scenario with equal-size splitting. The equation representing the survival probability can be expressed as follows

$$P(\nu_\mu \to \nu_\mu) = \sum_{i=1}^{6}\sum_{j=1}^{6} |U_{\mu i}|^2 |U_{\mu j}|^2 e^{\frac{i(m_i^2 - m_j^2)}{2E}}. \tag{3.166}$$

Firstly, it is important to note that in this expression, no modes are averaged out as in the ADDM scenario. This lack of averaging is due to the inclusion

of just three additional mass eigenstates, whereas in ADDM scenarios, the KK tower can encompass a vast number of additional mass eigenstates. To go deeper into the analysis of equation (3.166), we break it down as follows:

$$P(\nu_\mu \to \nu_\mu) = \left(\frac{N-1}{N}\right)^2 \sum_{i=1}^{3}\sum_{j=1}^{3} |U_{\mu i}|^2 |U_{\mu j}|^2 e^{\frac{i(m_i^2 - m_j^2)}{2E}}$$

$$+ \frac{N-1}{N^2} \sum_{i=1}^{3}\sum_{j=4}^{6} |U_{\mu i}|^2 |U_{\mu j}|^2 e^{\frac{i(m_i^2 - m_j^2)}{2E}} + \frac{N-1}{N^2} \sum_{i=4}^{6}\sum_{j=1}^{3} |U_{\mu i}|^2 |U_{\mu j}|^2 e^{\frac{i(m_i^2 - m_j^2)}{2E}}$$

$$+ \frac{1}{N^2} \sum_{i=4}^{6}\sum_{j=4}^{6} |U_{\mu i}|^2 |U_{\mu j}|^2 e^{\frac{i(m_i^2 - m_j^2)}{2E}}. \quad (3.167)$$

In this expression, the first term corresponds to oscillations within the flavors, which are well-established in the SM. For large values of N these oscillations undergo only minor modifications. It is also evident that the primary contributions originate from oscillations into the hidden species at a level of approximately $\frac{1}{N}$, similar to the one-flavor case described in equation (3.166). The contributions solely from beyond the Standard Model (BSM) terms are suppressed by a factor of $\frac{1}{N^2}$. Figure 3.4 illustrates the results of the calculations for a muon neutrino. This figure clearly demonstrates that the differences compared to the SM can be quite significant. Consequently, we anticipate that current neutrino experiments have the potential to constrain the number of species to a range of $N > 10 - 100$. This is an exciting development because the LHC provides a lower bound on the value of M_*, which in turn establishes an upper limit on the number of species. On the other hand, neutrino experiments establish a lower bound on N. Therefore, using neutrinos to test the DR scenario complements the constraints provided by the LHC.

But not just the oscillator behavior of neutrinos get affected in this theory but the additional mass eigenstates will influence the effective mass of interacting neutrino states. This offers us another way to restrict the parameter space of the DR model by using the upper bound on the electron neutrino mass via the following formula

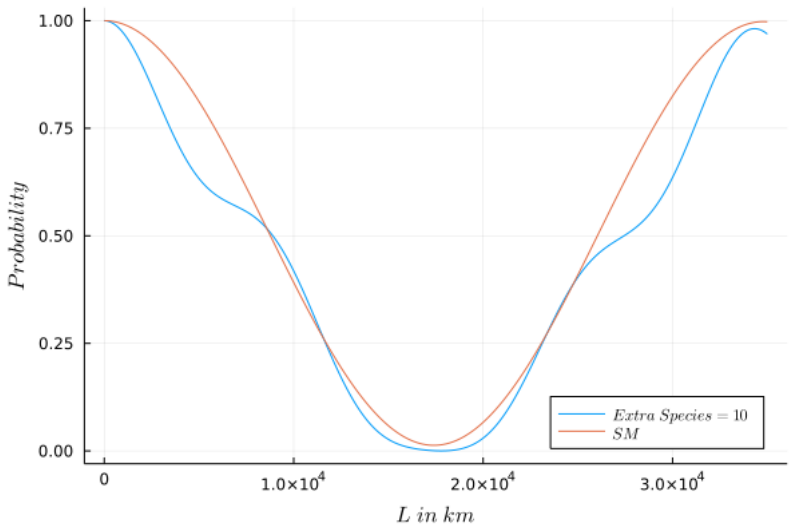

Figure 3.4: Survival probability of a muon neutrino in a three flavour case in DR model with an equal size splitting scenario.

$$m^2_{\nu_e} = m^2_{\text{lightest}} \left(\frac{N + \mu^2 - 1}{N} \right) + \frac{N-1}{N} (\Delta m^2_{12} U^2_{e2} + \Delta m^2_{13} U^2_{e3}) + \frac{\mu^2}{N} \left(\Delta m^2_{12} U^2_{e2} + \Delta m^2_{13} U^2_{e3} \right), \quad (3.168)$$

where μ is the parameter that relates the SM mass eigenstates with the BSM ones via

$$m^H_i = \mu m_i. \quad (3.169)$$

So we have two types of experiments to determine our DR parameters, neutrino oscillation experiments, and neutrino mass detection experiments.

To illustrate the unitarity violation in the SM lepton mixing matrix, as anticipated by the DR scenario, we need to examine formula (3.164). By isolating the 3×3 block matrix located in the upper left corner of the resulting mixing matrix, we can express it as follows:

$$\begin{pmatrix} \sqrt{\frac{N-1}{N}} U_{ee} & \sqrt{\frac{N-1}{N}} U_{e\mu} & \sqrt{\frac{N-1}{N}} U_{e\tau} \\ \sqrt{\frac{N-1}{N}} U_{\mu e} & \sqrt{\frac{N-1}{N}} U_{\mu\mu} & \sqrt{\frac{N-1}{N}} U_{\mu\tau} \\ \sqrt{\frac{N-1}{N}} U_{\tau e} & \sqrt{\frac{N-1}{N}} U_{\tau\mu} & \sqrt{\frac{N-1}{N}} U_{\tau\tau} \end{pmatrix}. \quad (3.170)$$

This matrix, as measured by experiments, clearly exhibits unitarity violation due to the presence of the overall factor $\sqrt{\frac{N-1}{N}}$. This characteristic signature

of the theory arises from the democratic oscillation into the common heavy eigenstates of the neutrino matrix.

In concluding the phenomenological section, it is important to briefly touch upon matter effects in the context of such theories. To calculate these effects, one can employ the standard framework for additional sterile neutrinos, leading to the formulation of an effective Hamiltonian, which can be expressed as follows

$$H_{eff} = \frac{1}{2E}\left[U\begin{pmatrix} m_e & 0 & 0 & 0 & 0 \\ 0 & m_\mu & 0 & 0 & 0 \\ 0 & 0 & m_\tau & 0 & 0 \\ 0 & 0 & 0 & m_4 & 0 \\ 0 & 0 & 0 & 0 & \ddots \end{pmatrix} U^\dagger + \begin{pmatrix} A & 0 & 0 & 0 & 0 \\ 0 & 0 & 0 & 0 & 0 \\ 0 & 0 & 0 & 0 & 0 \\ 0 & 0 & 0 & A' & 0 \\ 0 & 0 & 0 & 0 & \ddots \end{pmatrix}\right], \tag{3.171}$$

with $A = 2\sqrt{2}G_F N_e E$, $A' = -\sqrt{2}G_F N_n E$ and N_e, N_n being the densities of electrons, neutrons respectively. These considerations lead to the possibility of resonances for BSM modes, which can alter the oscillation pattern. While it is not guaranteed that resonance effects will manifest in experiments heavily influenced by matter effects, such as IceCube [115], there is still a chance that a favorable combination of experimental parameters can enhance the sensitivity of the experiment to detect these effects.

3.5 Conclusions

In this chapter, our primary focus has been on understanding neutrino masses within TeV scale gravity theories. In these theories, the reduction of the gravitational cutoff can be interpreted as a consequence of the "dilution" of the graviton wave function within a particular space characterized by a new coordinate. In both cases, the volume of this space is associated with the number of particle species present. Consequently, this new coordinate can be thought of as a species label. As shown in [15], in the context of ADD theory, the species correspond to the KK excitations, signifying that the additional space has a genuine geometric interpretation, specifically in the form of large extra spatial dimensions. On the other hand, in the "many species" solution to the hierarchy problem [15, 16], the species can encompass a wide range of arbitrary particles.

In both of these scenarios, it has previously been proposed that small neutrino masses naturally arise due to the dilution of the wave function of the sterile (right-handed) neutrino in the additional space. This concept was initially introduced within the context of ADDM theory [18] and its phe-

nomenological implications were explored in [79]. In the case of ADDM, the wave function of the sterile neutrino experiences dilution in the physically present geometric extra space. This leads to a significantly suppressed Yukawa coupling between the sterile and the active neutrinos in the Standard Model, resulting in the generation of tiny neutrino masses. Moreover, as demonstrated in [79], the mixing of an active left-handed neutrino with the KK tower of the sterile partner gives rise to a non-trivial oscillation pattern.

More recently, it has been demonstrated in [17] that a similar suppression mechanism for neutrino mass works in the context of the DR scenario [15, 16], in which species represent identical copies of the SM, and their label plays the role of an extra coordinate. Within this framework, it has been established that the dilution of the wave function of the sterile neutrino in the space of species leads to the generation of small neutrino masses [17]. However, it is worth noting that the phenomenological aspects of this scenario, are notably distinct from those in the case of [18], which relies on the ADDM framework.

In this chapter, we have expanded upon the original proposals mentioned above, introducing several generalizations. Notably, we have considered a more realistic scenario involving three SM neutrino flavors. We have employed a universal terminology, referring to "species" which enables us to encompass various aspects of the neutrino mixing matrix and compare and contrast different scenarios.

Moreover, we derived an approximate formula for the flavor eigenstates of a general mass matrix in the context of perturbation theory, focusing on the three-flavor scenario. Additionally, we demonstrated how highly symmetric mass matrices can be exactly calculated and explored various symmetry-breaking patterns for these highly symmetric mass matrices. We provided explicit expressions for flavor eigenstates in each of these cases.

Subsequently, we extended our analysis by applying the general formulas we had derived to specific theories of neutrino masses. These theories included the ADDM proposal [18, 79] within the ADD framework and the DR proposal [17] within the Many Species framework. We used the derived formulas to provide a three-flavor solution that is contingent upon the parameters characteristic of each of these specific theories.

As previously highlighted in [79] for the ADDM framework and [17] for the DR framework, both scenarios yield a common prediction: the non-conservation of neutrino number within the SM. This phenomenon arises from the mixing of SM active neutrinos with the tower of sterile partners. Consequently, this mixing leads to neutrino oscillations into hidden species and apparent violations of unitarity within the SM lepton sector.

In line with this, our calculations of these effects in the three-flavor scenario hold significant phenomenological implications in two key respects.

First, they provide insights into the deviations of neutrino oscillations from the predictions of the SM. Second, they offer a parameterization for quantifying the violation of unitarity in the PMNS matrix. These findings are valuable for enhancing our understanding of neutrino physics and its implications for BSM theories.

The structures of unitarity violation in the two distinct theories, namely the ADDM theory within the ADD framework [18, 79] and the DR theory within the Many Species framework [17], exhibit notable differences from each other. Therefore, our analyses possess the capability to discriminate between these two theories, offering a means to distinguish their predictions and implications in the context of neutrino physics.

In summary, the generation of small neutrino masses through mixing with a large number of extra species represents a fascinating and dynamic field with diverse phenomenological implications for low-energy neutrino physics. These effects can be searched for in both ongoing neutrino experiments, such as IceCube, and in planned experiments like JUNO [116]. Specifically, the violation of unitarity can be probed, and the results can be utilized to establish constraints on the parameters of these theories. This includes quantities such as the size of extra dimensions in the ADDM framework or the number of sterile neutrino species with which our neutrinos mix within the Many Species scenario. These experimental investigations play a pivotal role in shedding light on the nature of neutrino mass generation and the underlying theoretical frameworks.

Chapter 4

A Global Fit of Neutrino Data for Theories with Many Neutrino Copies

We set the stage for an experimental test of the proposed DR model. In the previous chapter, we worked out a realistic three-flavor scenario and in this chapter, I want to present our results of [22] where we performed a global fit of neutrino data to give the first experimental constraints on the DR model using neutrino experiments. After the introduction of the statistical framework, I will rely closely on our paper [22].

4.1 A Frequentist Analysis

Before we proceed to the actual analysis I introduce the theory necessary to understand the statistical analysis we performed in our work. For the theoretical background, I rely closely on [117] and personal communication.

4.1.1 Confidence Intervals

Different than a Bayesian analysis that we described in chapter 2 a frequentist analysis does not provide us with a posterior for the actual parameters of interest. The actual entity it is providing to make statistical statements is the so-called confidence interval. One of the most frequently used procedure to define a confidence interval is the so-called Feldman-Cousins Confidence Interval which I am going to discuss in the following.

For simplicity let us investigate a situation that can be described by the Poisson Distribution like an experiment that is counting events. If we define

ν as the expectation of signal events and λ as the number of background events, the Poisson distribution can be written as,

$$P(n|\nu,\lambda) = \frac{e^{-(\nu+\lambda)}(\nu+\lambda)^n}{n!}. \tag{4.1}$$

Now we can define a central interval. This can be constructed by defining a smallest member of the set of possible outcomes, n_1, and a largest member, n_2, such that

$$P(n < n_1) \leq \alpha/2\ , \quad P(n > n_2) \leq \alpha/2. \tag{4.2}$$

Then the central interval is defined as

$$\mathcal{O}^C_{1-\alpha} = \{n_1, n_1+1, ..., n_2\}. \tag{4.3}$$

With this knowledge, we can proceed and present the construction of the Feldman-Cousins Confidence Level. We have seen that for the construction of the central interval, the parameter $\mu = \nu + \lambda$ has to be known, but this is exactly the parameter of interest when I start conducting my experiment. Therefore, Feldman and Cousins defined a procedure how one can extract knowledge for μ in such a situation. The first step is to define the following quantity

$$r = \frac{P(n|\mu = \nu+\lambda)}{P(n|\hat{\mu})}, \tag{4.4}$$

where $\hat{\mu}$ is exactly that value that maximizes $P(n|\mu)$ for a specific n. It is noteworthy that due to the presence of the background, we have the restriction that $\mu \geq \lambda$ which then of course also holds for $\hat{\mu}$. Then one can rank every outcome n with the ratio value r and one can use the cumulative probability following this ranking to form an interval. For a concrete example, we set $\lambda = 3.0$ and $\nu = 1/3$. Then the situation for different n is shown in Tab. 4.1. Within this example, we see that the central interval under the condition $1 - \alpha \geq 0.9$ is $\mathcal{O}^C_{0.9} = \{1, ..., 7\}$ and the Feldman-Cousins interval is $\mathcal{O}^{FC}_{0.9} = \{1, ..., 6\}$.

How we can use this setup now to extract knowledge about our actual parameter of interest ν assuming that λ is known? The procedure for defining a Feldman-Cousins Confidence Interval goes as follows

- First, define α and r to be able to construct a Feldman-Cousins interval as in our example.
- The second step is to let the calculation for the Feldman-Cousins interval evolve over the whole range of ν. Then one can write down the result in a band plot like in Fig. 4.1.

n	P(n $\|\mu$)	$\hat{\mu}$	$P(n\|\hat{\mu})$	r	Rank	$F_R(n\|\mu)$
0	0.0357	3.0	0.050	0.717	5	0.7565
1	0.1189	3.0	0.149	0.796	4	0.7208
2	0.1982	3.0	0.224	0.885	3	0.6091
3	0.2202	3.0	0.224	0.983	1	0.2202
4	0.1835	4.0	0.195	0.941	2	0.4037
5	0.1223	5.0	0.175	0.699	6	0.8788
6	0.0680	6.0	0.161	0.422	7	0.9468
7	0.0324	7.0	0.149	0.217	8	0.9792
8	0.0135	8.0	0.140	0.096	9	0.9927
9	0.0050	9.0	0.132	0.038	10	0.9976
10	0.0017	10.0	0.125	0.014	11	0.9993
11	0.0005	11.0	0.119	0.004	12	0.9998
12	0.0001	12.0	0.114	0.001	13	1.0000

Table 4.1: Values of n, the probability to observe such a value given$\mu = \nu + \lambda = 3.3$, the value of μ that maximizes the probability of n given the constraint $\mu \geq \lambda$, the probability of n given $\hat{\mu}$, the ratio of the probabilities, the rank according to the probability ratio, and the cumulative probability according to rank [117].

- Now we perform an experiment and the result of counts is n_{exp}.
- Then we can compare our measured n_{exp} with Fig. 4.1 and find the corresponding range of ν.
- This range of ν is the so called $1 - \alpha$ Confidence Level interval for ν.

Note that the statistical statement such a Confidence Interval makes is different from a Bayesian Analysis. In frequentist analysis, one assumes that there exists a true parameter in our experiment we want to get a grasp on, ν_0. By defining our Confidence Interval with 90% we make the statement that the observed n_{exp} will be one of the members of $\mathcal{O}^C_{0.68}(\nu = \nu_0)$ in 90% the cases you would have performed this experiment. Therefore, within the extracted range of ν, ν_0 will be part of it in at least 90% of the experiments.

The construction of the Feldman-Cousins Confidence Interval can be generalized to a continuous probability distribution like the normal distribution. In principle, the procedure could also be generalized to a higher number of parameters of interest but it gets quickly very computationally expensive to calculate all the intervals in every possible scenario to then be able to draw a band plot like we have done in the one-dimensional case. To be able to

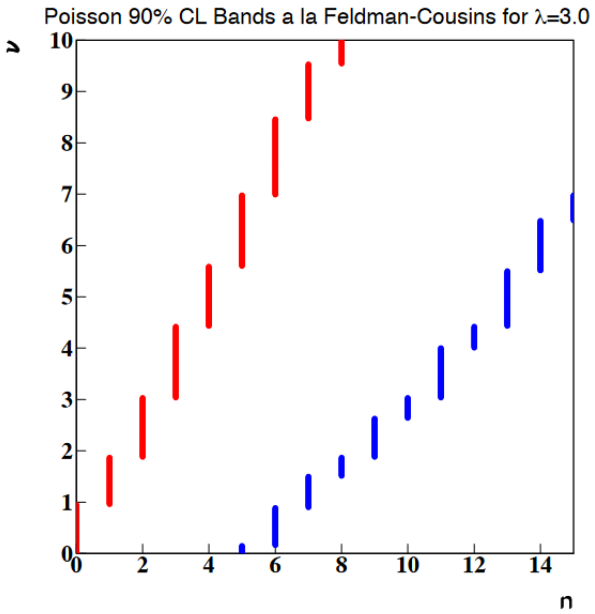

Figure 4.1: lower and upper limits on the values of n included in the Feldman-Cousins $1 - \alpha = 0.9$ set for different values of the signal expectation ν and for fixed background expectation $\lambda = 3.0$ [117].

perform a frequentist analysis also for a high dimensional setting one uses the concept of test statistics I am going to describe in the next section.

4.1.2 Test Statistic

A test statistic, T, is basically just a framework to bring a higher-dimensional problem back to the one-dimensional case. To this end, we define a test statistic being a scalar function of the data that does not loose information contained in the data. Whether a scalar function of the data is fulfilling the requirements of a test statistic depends on the model being tested and is a highly non-trivial question and a complete proof that the chosen test statistic is sufficient is often just possible in simple cases. Nevertheless, it is a widespread tool to perform a frequentist analysis. The procedure in a frequentist analysis goes as follows:

- Make a choice of your test statistic.
- Calculate the probability distribution for your test statistic for every possible choice of the parameters of the problem.

- Define the accepted set of values of the test statistic that contains the probability content $1 - \alpha$.
- Calculate the test statistic value of the observed data for different parameter values and find the set of parameters where the test statistic is within your accepted set. This is the range of the accepted set of parameters at a confidence level of $1 - \alpha$.

Usually, the difficult step is the second one. In principle, one would have to sum all probabilities of every possible data set for one possible parameter set to get the probability of T for this specific choice of parameters. To get the full solution this would have to be repeated for every possible set of parameters. This is in a realistic scenario not possible because of the lack of computing power. Instead one therefore, uses a generation of "toy experiments" to approximate $P(T|\{\tau\})$, where $\{\tau\}$ is the set of parameters. One does this in the following procedure

- Define a grid of $\{\tau\}$ values covering your parameter space.
- Fix one $\{\tau\}$.
- Sample a toy experiment with the outcome $\{n\}$.
- Calculate $T(\{n\};\{\tau\})$.
- Repeat the last two steps until you reach an accuracy that is sufficient and store all values of T.
- Next, depending on your test statistic if the maximal or minimal value of T describes the data best rank the values for T and define a set of a specific size $(68\%, 90\%, 95\%, etc.)$ which one accepts.
- Finally, calculate your T^{Data} and compare it with your accepted set. Is it within the accepted set, $\{\tau\}$ is accepted within a $1 - \alpha$ confidence interval.
- Repeat this for every $\{\tau\}$ in the grid.

This is the procedure how one can numerically calculate confidence intervals with the help of a test statistic.

A typical example of a test statistic is the so-called likelihood ratio defined as

$$\xi(\tau) = \frac{\mathcal{L}(\tau)}{\mathcal{L}(\tau^*)}, \tag{4.5}$$

where τ^* is the specific parameter that maximizes the likelihood. This Ansatz is similar to what we have seen in the definition of the Feldman-Cousins Confidence Interval and follows the logic that we rank our different parameter sets according to how well they fit the data. The reason why the likelihood ratio is a very popular test statistic is that when the sample size is large, the test statistic $\xi' = -2ln(\xi)$ will be χ^2 distributed according to Wilks´ theorem.

This allows us to draw approximate confidence intervals by using Wilks theorem. We can plot $\xi'^{\text{data}}(\tau)$ and use the cumulative of χ^2 to find the $1-\alpha$ confidence interval. How this works within the χ^2 framework is here not so important but one can show that depending on the number of parameters of the problem there exists a specific χ^2_{cut}. χ^2 values below χ^2_{cut} fall into a $1-\alpha$ confidence interval. For example in a one parameter scenario for a 68% confidence interval $\chi^2_{cut} = 1$ holds. A typical scenario with one parameter is depicted in Fig. 4.2 and the values below the red line correspond to a 68% confidence interval.

Equipped with this statistical knowledge we can now proceed to the setup of the data analysis of neutrino experiments in order to test the DR model.

4.2 Data Analysis of Neutrino Experiments

The effectiveness of the DR model's predictive capability, as discussed in 3, becomes apparent when contrasted with a generic approach involving the assumption of three additional sterile neutrinos, denoted as $n_s = 3$. In this alternative scenario, the count of independent physical mixing angles becomes $3(n_s+1) = 12$, and Dirac phases amount to $2n_s+1 = 7$. Additionally, three extra masses for the sterile neutrinos, namely m^s_1, m^s_2, m^s_3, are considered [118]. The overall count of independent parameters in a 3+3 framework is 22.

In contrast, the DR model introduces only two BSM parameters, namely N and μ. Given that μ establishes a connection between the masses of the SM neutrinos and the sterile neutrinos, another parameter of significance is the mass of the lightest neutrino, denoted as m_{lightest}. Consequently, the total number of parameters specifically relevant to neutrino oscillations is reduced to 9. Clearly, the DR model provides a more minimal framework for conducting a BSM neutrino fit compared to a general 3+3 neutrino fit.

Overall, our analysis has the following free parameters:

$$\{\delta_{CP}, \theta_{12}, \theta_{13}, \theta_{23}, \Delta m^2_{12}, \Delta m^2_{13}, m_{\text{lightest}}, N, \mu\}, \tag{4.6}$$

where $\delta_{CP}, \theta_{12}, \theta_{13}, \theta_{23}$ are the well known parameters of the PMNS matrix

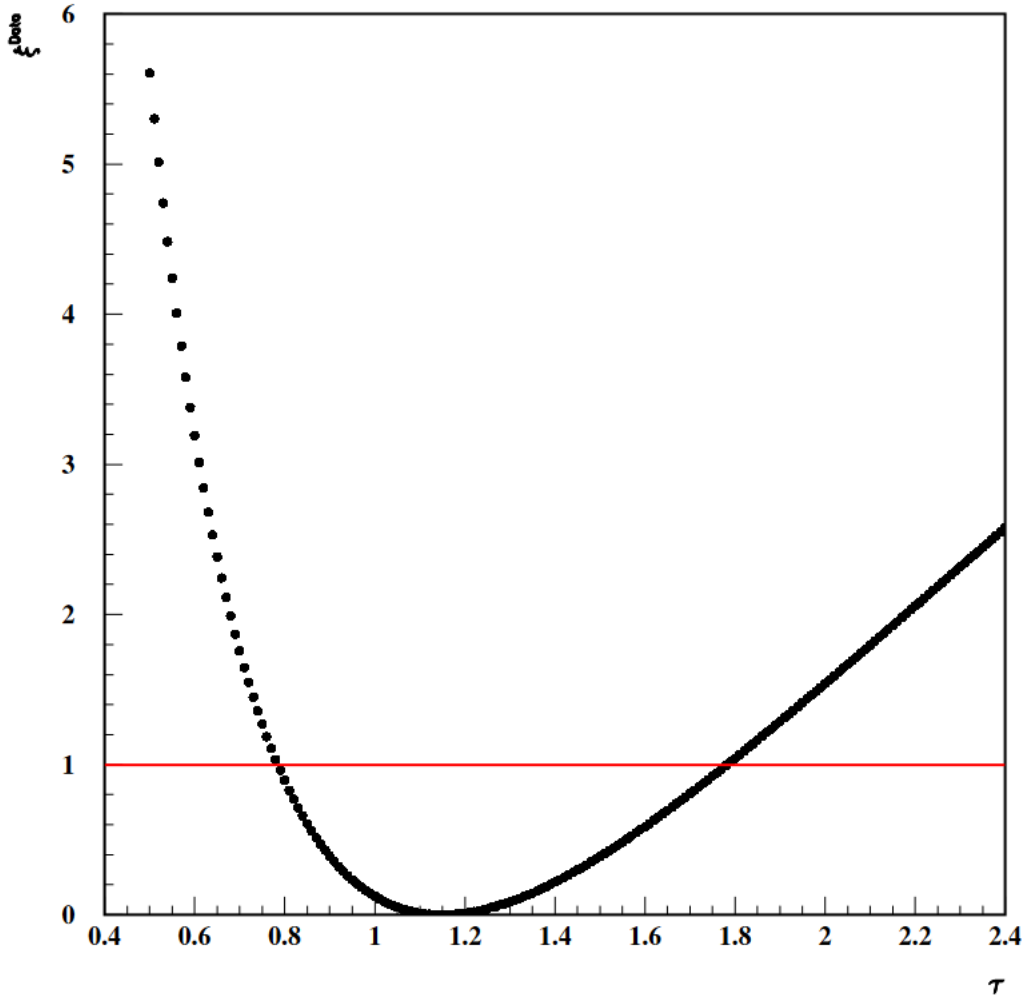

Figure 4.2: The distribution of the likelihood ratio of the data depending on τ. All values for τ who have a corresponding ξ value below the red line are part of the confidence interval [117].

and $\Delta m^2_{12}, \Delta m^2_{13}$ the differences of the mass eigenstates.

To ascertain the values of these parameters, we conduct a combined maximum likelihood fit. Given that we are exploring neutrino data within the DR regime for the first time, we lack prior knowledge of the parameters outlined in equation (4.6). Consequently, an independent analysis of the existing experimental data is necessary, and we cannot lean on previous SM global fits. Moreover, since every SM mixing angle undergoes corrections in this model and the additional mass splittings can potentially vary widely, our statistical analysis must encompass a fit for all nine free parameters.

The decision regarding which experiments to include in our analysis is grounded in the observation that neutrino oscillation experiments measure various combinations of the fraction $\frac{L}{E}$, where L represents the baseline lengths of the experiment and E denotes the energies of the neutrinos. This inclusive approach serves two primary purposes. Firstly, it enables us to select at least one experiment for each SM parameter, thereby imposing constraints on each of them. Secondly, the incorporation of a diverse array of experiments allows us to explore deviations in SM oscillations over a wide spectrum, encompassing very small to significantly large mass splittings between the SM mass eigenstates and the BSM ones.

Our selection of specific experiments is guided by the need to comprehensively understand how each contributes to the resulting exclusion limits of the BSM parameters. Let us point out here again that the BSM contribution to neutrino experiments scales with $1/N$. This means that for larger values of N we expect less influence and not more. Exactly this behavior makes neutrino experiments particularly interesting to study because in usual high-energy experiments like LHC larger values of N lead to stronger effects. This makes both approaches complementary as one gives lower bounds on N and the other one gives upper bounds.

Certainly, KATRIN [30] is an intuitively understandable experiment in our analysis. In the context of our model, the additional mass eigenstates contribute to the effective mass of the electron neutrino. The key model parameters governing this mass are m_{lightest} and μ. Unlike oscillation experiments, which are also sensitive to μ, KATRIN stands out as the sole experiment in our analysis capable of constraining m_{lightest}.

This distinction is significant because once m_{lightest} is fixed, the masses of the SM states are uniquely determined. Subsequently, μ serves as the parameter linking the SM masses to the BSM ones. In cases where μ has large values, the BSM masses become higher, exerting a more pronounced influence on the electron neutrino mass. Therefore, we anticipate that KATRIN will be most relevant in the regime characterized by large values of μ, where its capability to constrain m_{lightest} becomes crucial for refining our understanding

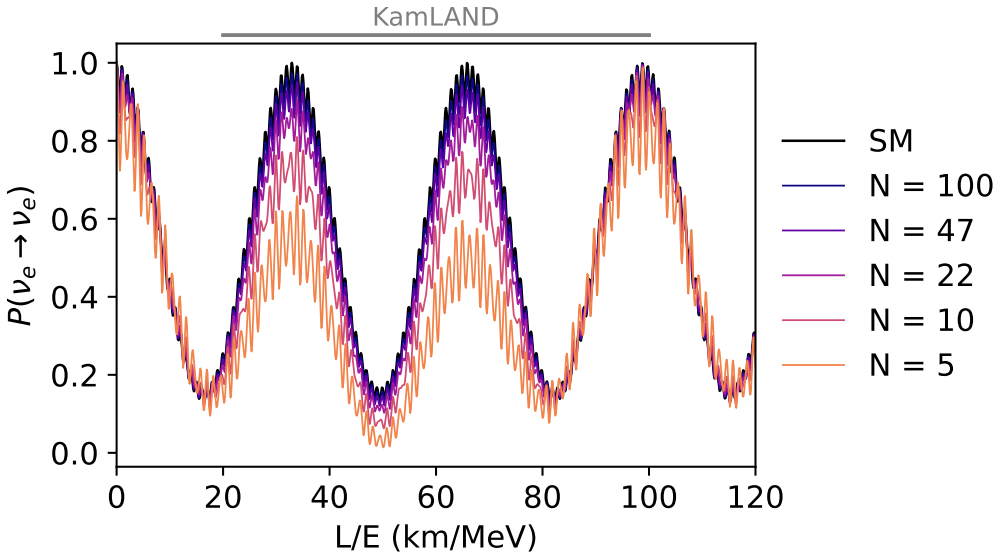

Figure 4.3: Example electron neutrino survival probabilities at an L/E around the solar mass splitting for various numbers of extra species N and massfactor $\mu = 5$.

of the model and its implications for neutrino masses.

In our analysis, the KamLAND experiment [119] plays a crucial role as it imposes constraints on SM parameters, specifically Δm^2_{12} and θ_{12}. By scrutinizing Fig. 4.3, we can estimate the expected sensitivity of KamLAND to BSM parameters. The figure illustrates that deviations from the SM oscillations become substantial when $N \leq 10$.

DayaBay [120, 121] on the other hand is much more sensitive to N as we see from Fig. 4.4. Together with the fact that this experiment provides us with very high statistics in its data, we expect that DayaBay will contribute significantly to our final exclusion limit for the BSM parameters. Additionally it is restricting θ_{13} and Δm^2_{13}.

MINOS and NOνA [122, 123] are complementary. Because NOνA is located exactly at the oscillation maximum it provides very good sensitivity for SM parameters θ_{23} and Δm^2_{13} but at the same time it is lacking sensitivity to the BSM parameters (see Fig. 4.5). MINOS on the other hand is located off maximum which is suited for searching for BSM contributions to the oscillation pattern.

Putting the pieces together we can define the following likelihood

$$\mathcal{L}_{\text{comb}} = \mathcal{L}_{\text{KATRIN}} \times \mathcal{L}_{\text{MINOS}} \times \mathcal{L}_{\text{KamLAND}} \times \mathcal{L}_{\text{DayaBay}} \times \mathcal{L}_{\text{NO}\nu\text{A}}, \tag{4.7}$$

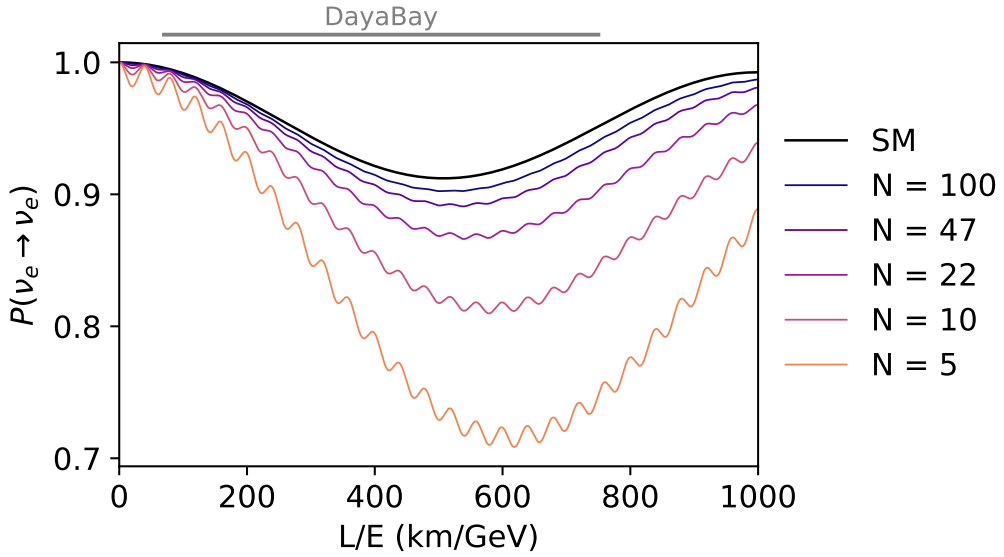

Figure 4.4: Example electron neutrino survival probabilities at an L/E around the atmospheric mass splitting for various numbers of extra species N and massfactor $\mu = 5$.

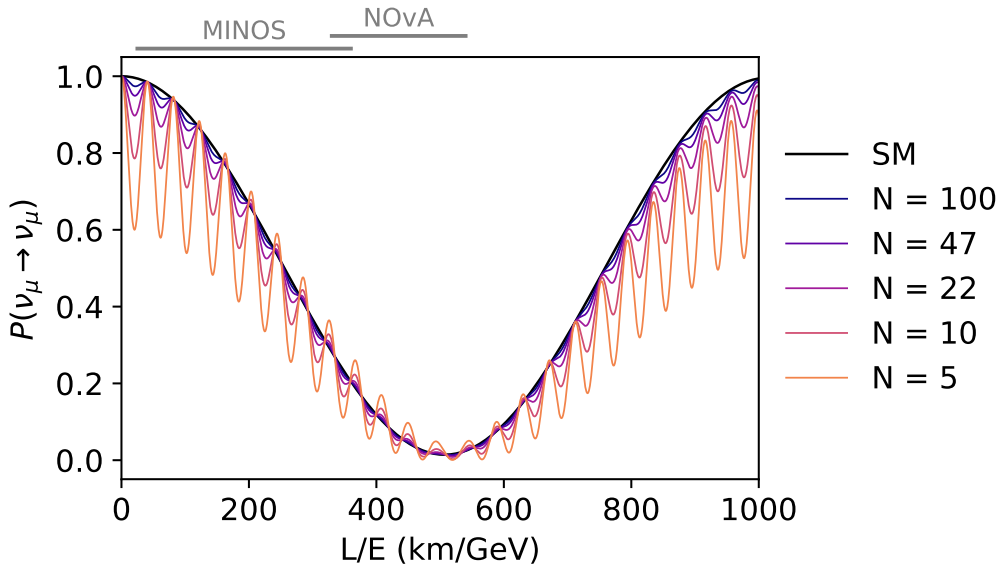

Figure 4.5: Example muon neutrino survival probabilities at an L/E around the atmospheric mass splitting for various numbers of extra species N and massfactor $\mu = 5$.

where we treated every data set independently which allows us to construct $\mathcal{L}_{\text{comb}}$ as a product of all the single likelihoods of the experiments. In our statistical analysis, we employ a likelihood ratio test statistic. Should the alternate hypothesis (DR model) demonstrate a preference over the null hypothesis (SM) with a significance exceeding 3σ it would warrant further investigation as a potential signal. Conversely, if the significance falls below this threshold, we would proceed to establish exclusion limits on the parameter N as a function of μ while simultaneously profiling over all other remaining parameters (meaning effectively maximizing the likelihood).

In conducting this analysis, publicly available data from the papers [119, 120, 121, 122, 123, 30] served as the foundational dataset. For each experiment, a fit of the SM was executed, and the results were cross-verified against the findings reported in the respective articles. We did the comparison among the reported SM parameters as well in checking if our predicted oscillated neutrino spectrum aligns with the ones of the papers. When this was the case we carried on and checked if the fit of the DR model represents the data as well. Because in the high N limit the DR model contains the SM oscillation behavior we expect that the DR model will at least result in an equally good fit of the data as the SM. This meticulous comparison was essential to ensure the reliability and validity of the subsequent analysis employing the proposed DR model.

A more detailed account of the specific methodologies employed for the analysis of each experiment is provided in the Appendix, offering a comprehensive overview of the procedures undertaken to assess the compatibility of the DR model with the observed data in the context of each individual experiment.

4.3 Results

The best-fitting DR hypothesis under the assumption of NO shows a log-likelihood advantage of 4.37 units over the Standard Model fit. In the case of the IO, this difference amounts to 2.49 log-likelihood units. These values, taking into account Wilks´ theorem and considering the three additional degrees of freedom $(N, \mu, m_{\text{lightest}})$, translate to significances of 1.8σ and 0.97σ for the NO and IO scenarios, respectively.

Given that neither of these significances surpasses the threshold of 3σ, we proceed to establish exclusion limits. This involves determining constraints on the parameter space, particularly for N, within which the proposed DR model is not favored by the observed data compared to the SM.

The resulting exclusion limits are depicted in Figure 4.6 for both NO

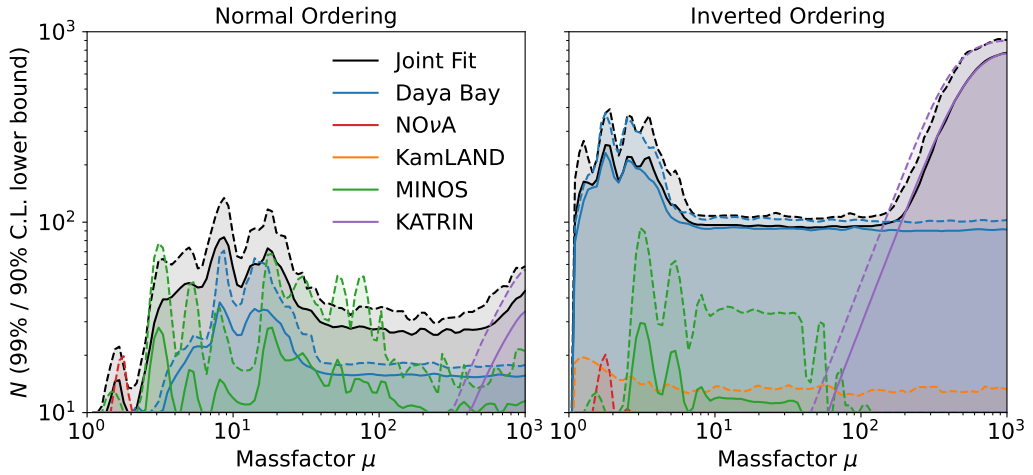

Figure 4.6: Lower bounds on the number of species N as a function of the massfactor μ for the normal and inverted neutrino mass ordering, respectively. The solid and dashed lines denote the 90% and 99% asymptotic confidence levels (CL), the shaded areas are excluded. The colorful lines represent fits of individual datasets, and the black lines result from a combined fit of all four datasets.

and IO. In the case of the IO, a consistent lower bound on N is established, exceeding $\mathcal{O}(10^2)$ across the range of μ. The exclusion limit for $\mu < 10^2$ is primarily set by oscillation experiments, while for $\mu > 10^2$, the exclusion is predominantly driven by KATRIN, aligning with expectations. As oscillation experiments measure the survival probability (3.167), they effectively test a beyond Standard Model contribution scaling in the first order as $\frac{1}{N}$. Consequently, for $N > \mathcal{O}(10^2)$, the corrections from the DR model are of the order of $< 1\%$, consistent with reported experimental measurements characterized by uncertainties around $1 - 5\%$.

In the case of NO, the situation is more intricate. Overall, the constraints on N are weaker compared to the IO scenario. The significance of KATRIN is diminished compared to the IO case, and its impact on the exclusion limit becomes noticeable for $\mu > 300$. However, for higher values of μ, KATRIN exhibits a similar behavior as in the IO case, albeit with reduced sensitivity.

In the parameter space where $\mu > 2$, a tentative lower bound on N can be established, indicating $N > 30$. However, for $\mu \leq 2$, it becomes evident that experiments start losing sensitivity to the DR model. This is attributed to the diminishing mass-splitting for the BSM states, rendering them too small to be effectively resolved by experiments operating in this regime.

If we compare our numerical results with what we would have expected

by the oscillograms as described in the previous section we see that our expectations agree with our results.

4.4 Conclusions

In this study, we conducted the inaugural experimental test of additional neutrino copies using available experimental data. Our findings lead us to the conclusion that contingent on the mass hierarchy realized in nature, we can establish a lower limit on the number of neutrino copies. Specifically, we find that $N > \mathcal{O}(30)$ for the case of NO and $N > \mathcal{O}(100)$ for the IO across a broad range of the parameter space.

The communication facilitated by the right-handed neutrino through the Dirac operator allows for the incorporation of cosmological considerations, enabling the derivation of lower bounds on the number of neutrino species [124]. It is noteworthy that, in comparison to these cosmologically derived bounds, our experimentally derived bounds are relatively weaker. However, the strength of our experimental results lies in their robustness, as they are not contingent on the details of the cosmological history beyond BBN.

Therefore our results show, that neutrino experiments are especially suited for testing models with additional neutrino species because compared to other physics we can give a lower bound on N meanwhile LHC [15, 16] and axion physics [3] give an upper bound on the number of species.

The complementary nature of neutrino experiments operating in the IR to UV experiments is quite exciting and future experiments like JUNO [125] and DUNE [126] are designed to improve our knowledge about the lepton mixing parameters by one order of magnitude which will give us the possibility to close the open window of the parameter space even further.

Together with theoretical considerations [3, 124], UV and IR experiments can help us to restrict the possible range of N_{sp} and reveal where we could expect the true scale of Quantum Gravity.

Chapter 5

Kaluza-Klein Spectroscopy from Neutron Oscillations into Hidden Dimensions

Next to the neutrino, another intriguing candidate emerges as a potential gateway to concealed realms – the neutron. Similar to the neutrino, the neutron lacks conserved gauge charges, opening the possibility of interaction with hidden degrees of freedom. Within this chapter, a novel mechanism is introduced, shedding light on this phenomenon. The outcomes of this research can be found in [4] which I follow closely in this chapter. The possibility of a neutron portal into hidden dimensions was first pointed out in [127]. As discussed in this work, neutron transitions into a hidden state are a generic feature of the brane-world scenario. This is due to the transportation of neutrons across the bulk by virtual brane bubbles, so-called "baby branes". In such a process, a neutron can tunnel across the bulk to a nearby parallel brane.

For an observer residing within the world-volume of our brane, the neutron's transition into a hidden particle can be effectively characterized. Originating from non-perturbative processes, this transition exhibits a probability that is exponentially suppressed, though never reaching zero, in accordance with all conservation laws. The naturally suppressed rate aligns well with the phenomenological constraints imposed on neutron disappearance.

Within this chapter, our exploration will delve into an alternative avenue of neutron transitions into extra dimensions, specifically through its interaction with a bulk fermion. The intrigue surrounding this process stems from several distinctive features. Primarily, the anticipated mixing between neutrons and bulk sterile fermions is deemed quite generic, given the absence of conserved SM gauge quantum numbers in either entity.

Secondly, a qualitative novelty arises in comparison to theories where the neutron engages in mixing with a partner of a fixed mass, as observed in scenarios like the neutron from a mirror SM [128] or multiple hidden copies of the SM [17]. In these theories, the presence of only one available partner introduces challenges in controlling resonance transitions, particularly evident in scenarios with a sole mirror copy. The inherent difficulty lies in the inevitable breakdown of mirror symmetry caused by environmental factors like the nuclear binding energy of the neutron or the presence of an ambient magnetic field. Consequently, the transition undergoes a suppression to the point of becoming unobservable, unless one posits specific coincidences or cancellations of external factors, as exemplified by the magnetic field within the hidden sector [129].

The transition of a neutron into extra dimensions paints a qualitatively distinct scenario, driven by the finely spaced tower of KK states in the ADD model. The heightened density of KK states allows neutrons across a broad spectrum of energy levels to encounter nearly degenerate bulk partners, enabling oscillations. As a consequence, a diverse array of bound or free neutrons can serve as gateways into extra space. This imposes stringent constraints on the theory's parameters while simultaneously presenting novel signatures for experimental investigations.

A notably intriguing signature arises from the repetitive resonant oscillations of a free neutron into the KK modes. These oscillations occur at special values of the magnetic field, forming a sequence of resonance events. In contrast to scenarios featuring a single oscillation partner with a fixed mass, the resonant transitions in the context of extra dimensions happen at quantized values of the magnetic field aligning with the KK spectrum. This unique behavior transforms the neutron into a magnetic imaging tool for the KK tower.

The described effects render the scenario susceptible to non-trivial constraints from ongoing experiments involving ultra-cold neutrons [130, 131]. By analyzing the results from these experiments, we establish constraints on the parameters associated with extra dimensions. Notably, these constraints are already delving into parameter regimes driven by the Hierarchy Problem. Additionally, we explore potential new signatures that could be uncovered through future, more refined measurements.

5.1 Neutron Oscillations into hidden dimensions

The main innovation introduced in this chapter lies in the prospect of neutron oscillations into extra dimensions. Analogous to the neutrino, the neutron lacks conserved gauge charge, allowing it to freely engage in mixing with bulk species. Our focus is on the oscillation of the neutron into KK modes of a bulk fermion. We denote this bulk fermion as Ψ. To start with, we assume that Ψ is massless.

The origin of Ψ will be maintained in a generic context. However, a particularly intriguing possibility arises if Ψ serves as the bulk partner of one of the SM neutrinos, generating its mass through the previously discussed mechanism. In this scenario, the neutron would mix with the same KK tower as the active neutrino. It is noteworthy that such mixing remains unaffected from the perspective of neutrino mass. Due to a significant mass separation between the neutrino and neutron, they primarily interact with highly distinct sectors of the KK spectrum. Consequently, they exert essentially zero influence on each other. This presents a notably economical scenario. Nonetheless, we will maintain a maximally general discussion throughout.

It is reasonable to assume that the mixing between the neutron and the bulk fermion originates from a more fundamental four-fermi interaction of the type,

$$\mathcal{S}_{\text{int}} = \int dx^4 \frac{1}{M_*^{2+N/2}} \overline{udd}\,\Psi \,+\, \text{h.c.}\,, \tag{5.1}$$

where M_* is a scale. We will refrain from specifying the origin of Ψ and treat it as a phenomenological parameter. In general, it is reasonable to anticipate that M_* is of the same order of magnitude as or higher than M_f.

In the effective low-energy theory below the scale of QCD confinement, the coupling given by (5.1) results in an effective mass term that induces mixing between the neutron and Ψ. This is expressed in the effective Lagrangian through the following replacement,

$$udd \to \Lambda_{\text{QCD}}^3\, n\,, \tag{5.2}$$

where n is the neutron field and Λ_{QCD} is of the order of the QCD scale.

As previously, we expand Ψ into the KK modes (3.24). Unlike the neutrino case, the neutron is a Dirac fermion. Consequently, both chiralities, n_L and n_R, are available for mixing with the corresponding components of the

KK tower:

$$\Psi_{\vec{k},R}(x) \equiv \frac{1}{\sqrt{\sum_{\bar{A}} |c_{\bar{A}}|^2}} \sum_{\bar{A}} c_{\bar{A}} \Psi^{(\bar{A})}_{\vec{k},R}(x)\,,$$
$$\Psi_{\vec{k},L}(x) \equiv \frac{1}{\sqrt{\sum_{A} |c_{A}|^2}} \sum_{A} c_{A} \Psi^{(A)}_{\vec{k},L}(x)\,. \tag{5.3}$$

We again make a simplified assumption that the combinations (5.3) with $A = \bar{A}$ are KK mass eigenstates. That is, modulo mixing with the neutron, at each KK level $\vec{k}$ they form a four-dimensional Dirac fermion $\Psi_{\vec{k}} \equiv \Psi_{\vec{k},L}(x) + \Psi_{\vec{k},R}(x)$ with mass $m_{\vec{k}}$. In such a case, the orthogonal combinations decouple and we get the following effective 4-dimensional Lagrangian describing the Dirac neutron, the KK tower of Dirac fermions $\Psi_{\vec{k}}$ and their mixing,

$$\mathcal{L} = \bar{n}\partial\!\!\!/ n - m_n \bar{n} n + \sum_k \left(\bar{\Psi}_k \partial\!\!\!/ \Psi_k - m_k \bar{\Psi}_k \Psi_k \right) + \alpha \sum_k \bar{n} \Psi_k + h.c., \tag{5.4}$$

where m_n is the SM mass of neutron and α is the mixing mass term,

$$\alpha \equiv \frac{\Lambda^3_{\rm QCD}}{M_*^{2+N/2}\sqrt{V_N}}\,. \tag{5.5}$$

We have absorbed the normalization factor $\sqrt{\sum_A |c_A|^2}$ into the rescaling of parameters.

It is important to note that α represents an extremely small mass scale. Specifically, considering that $M_* \geqslant M_f$ and taking into account the current experimental bound (3.36), we obtain the following upper bound on α,

$$\alpha \lesssim 10^{-24}\text{GeV}\,. \tag{5.6}$$

This quantity is significantly smaller than any other scale in the problem. This enables us to perturbatively study the oscillation picture in α.

The masses and mixings between the neutron and the bulk states are encapsulated by the following mass matrix,

$$\begin{pmatrix} m_n & \alpha & \alpha & \alpha \\ \alpha & 0 & 0 & 0 \\ \alpha & 0 & m_{\vec{k}} & 0 \\ \alpha & 0 & 0 & m_{\vec{k}'} \end{pmatrix}. \tag{5.7}$$

Notice that because of the bound (5.6), we have $\alpha/m_n \lesssim 10^{-24}$. In the leading approximation, each KK mixes with the neutron with an angle given by

$\tan\varphi_k = \frac{\alpha}{\Delta m_k}$, where $\Delta m_{\vec{k}} = |m_n - m_{\vec{k}}|$. Putting aside miraculous coincidences, the smallest value of $\Delta m_{\vec{k}}$ is set by the level splitting between the KK modes.

The scenario closely resembles what we encountered in the neutrino case, with two distinctions. First, the mass matrix is symmetric. Secondly, $\Delta m_{\vec{k}}$ reaches its minimum not at the lower end of the Kaluza-Klein spectrum but in the region closest to the energy of the neutron.

Due to the mixing with the Kaluza-Klein tower, the conventional neutron, being a Standard Model interaction eigenstate, does not constitute an exact mass eigenstate. Designating the mass eigenstates with primes, the Standard Model neutron is expressed as a superposition of mass eigenstates in the following form,

$$n \;=\; \frac{1}{\mathcal{N}}\Big(n' + \sum_{\vec{k}} \frac{\alpha}{\Delta m_{\vec{k}}}\Psi'_{\vec{k}}\Big), \tag{5.8}$$

where $\mathcal{N}^2 = 1 + \sum_k \frac{\alpha^2}{\Delta m_k^2} = 1 + \mathcal{O}(\alpha^2)$ is a normalization factor. This state evolves in time as,

$$n(t) = \frac{1}{\mathcal{N}}\Big(n' + \sum_{\vec{k}} \frac{\alpha}{\Delta m_{\vec{k}}} e^{i\phi_{\vec{k}}}\Psi'_{\vec{k}}\Big), \tag{5.9}$$

where $\phi_{\vec{k}} = |m_n - m_{\vec{k}}|t$. The corresponding survival probability of the neutron is,

$$P_{\text{surv}}(t) = |\langle n|n(t)\rangle|^2 = \frac{1}{\mathcal{N}^4}\Big|1 + \sum_{\vec{k}} \frac{\alpha^2}{\Delta m_{\vec{k}}^2} \exp\left(i\phi_{\vec{k}}\right)\Big|^2. \tag{5.10}$$

Parallel to the neutrino case, the oscillation unfolds across a series of modes. The "resonant" modes align with the Kaluza-Klein levels closest to the Standard Model energy of the neutron, m_n. The levels farther away oscillate with increasing frequencies and diminished amplitudes. Upon averaging over all modes except the one nearest to m_n, the probability of the neutron oscillating into Ψ is expressed as follows,

$$P_{n\to\Psi}(t) = \frac{Z}{\mathcal{N}^4}\frac{4\alpha^2}{\Delta m^2}\sin^2\left(\frac{\Delta m}{2}t\right). \tag{5.11}$$

where $\Delta m \equiv |m_n - m_{\vec{k}}|$ denotes the smallest mass splitting and the factor Z accounts for the corresponding degeneracy. For visualization, see Fig. 5.1.

For a single extra dimension of radius R, we have $Z = 2$ because the mass is degenerate for k and $-k$. Equivalently, the neutron mixes with the states $\Psi_k \equiv \frac{1}{\sqrt{2}}(\psi_k + \psi_{-k})$, whereas the orthogonal superpositions decouple. The corresponding survival probability is

$$P_{n\to\Psi}(t) = \frac{1}{\mathcal{N}^4}\frac{8\alpha^2}{\Delta m^2}\sin^2\left(\frac{\Delta m}{2}t\right), \tag{5.12}$$

where $\Delta m \leqslant 1/R$. Even though "accidentally" Δm could fall arbitrarily below this upper bound, a plausible natural value is $\Delta m \sim 1/R$.

In the case of a higher number of pertinent extra dimensions, the level-splitting becomes as small as $\Delta m \sim 1/(m_n R)^2$ (refer to the Appendix). The degeneracy count is as follows. For N_R relevant dimensions with equal radii R (again, N_R should not be confused with the total number N of large extra dimensions, where $N_R \leqslant N$), the general count Z of Kaluza-Klein states within a gap Δm is given by,

$$\frac{Z}{\Delta m} \sim \frac{1}{m_n}(m_n R)^{N_R} \,. \tag{5.13}$$

Taking this into account, the survival probability for N_R relevant dimensions of radius R can be presented in the following form

$$P_{n\to\Psi}(t) \;\sim\; \frac{m_n}{\Delta m}(m_n R)^{N_R}\left(\frac{\alpha}{m_n}\right)^2 \sin^2\left(\frac{\Delta m}{2}t\right). \tag{5.14}$$

The oscillation amplitude is the largest for the states with the smallest Δm. Equipped with these equations, we shall next discuss the effect of neutron disappearance.

5.2 Phenomenological bounds from neutron disappearance in nuclei

In the preceding section, we explored how, within the ADD framework, a neutron can undergo oscillations into particles propagating in extra dimensions. We will now seek phenomenological constraints on this process. Initially, we examine the scenario with a massless bulk partner. In this case, the most stringent constraints arise from the absence of observed neutron disappearance from nuclei.

Consider an atomic nucleus containing several neutrons. The previously derived formulas can be directly applied to these neutrons. In this context, the mass m_n should be interpreted as the energy level of a neutron within the given bound state. The neutron exhibits a finite probability of transitioning into the bulk KK modes. From the perspective of an observer within the SM, this process is perceived as the disappearance of the neutron. The vacated nucleus undergoes de-excitation, wherein a neutron from a higher level occupies the state vacated by the disappearing neutron. This de-excitation process is accompanied by the emission of a hard photon, i.e., a photon with nuclear energy.

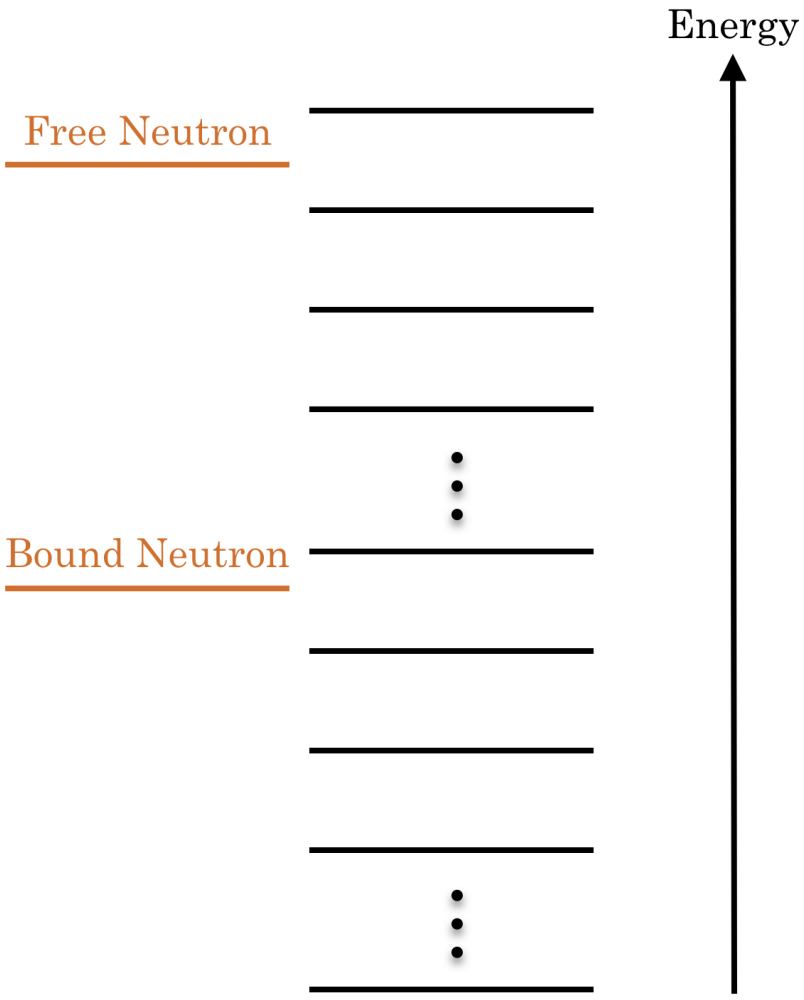

Figure 5.1: A schematic description of the matching of the energy levels of free and nuclear-bound neutrons with the KK spectrum of Ψ.

In scenarios involving large extra dimensions, the typical oscillation time, determined by the KK level splitting $\sim 1/\Delta m$, is significantly longer than the nuclear transition time. In such cases, after the de-excitation process, the return of the original neutron is no longer viable, as its position has been occupied. Consequently, this process would result in the decay of atoms into isotopes with fewer neutrons. This is not observed in nature and the experimental bound on the lifetime of neutrons within nuclei is [132]

$$\tau_n > 10^{30}\,\mathrm{y} \sim 10^{62}\,\mathrm{GeV}^{-1}\,. \tag{5.15}$$

This bound translates to a bound on the neutron disappearance rate in

our scenario. The rate can be derived from (5.12) as the average transition probability per unit time,

$$\lambda_n \;=\; \frac{2Z\alpha^2}{\Delta m} = \frac{2Z\Lambda_{QCD}^6}{\Delta m M_*^{4+N} V_N}, \tag{5.16}$$

where we plugged-in the parameter α from Eq. (5.5). Using the expression (5.14), it is also useful to present the rate as

$$\lambda_n \;\sim\; m_n \left(\frac{\alpha^2}{m_n^2}\right) (m_n R)^{N_R}\,. \tag{5.17}$$

Now, we demand that $\tau_n = 1/\lambda_n > 10^{30}$ y. This leads to the following constraint,

$$M_*^{4+N} > 10^{21} (\text{GeV}\; R)^{N_R} M_f^{2+N} \text{GeV}^2\,, \tag{5.18}$$

where we have expressed V_N through $M_P \sim 10^{19}$GeV and M_f and used the fact that $m_n \simeq$ GeV and $\Lambda_{QCD} \simeq 0.3$ GeV. We also used the neutron lifetime bound (5.15) in GeV units.

We aim to apply this bound to various cases distinguished by the number and size of relevant dimensions. To achieve this, let us quantify the concept of relevance. We have N_R relevant dimensions with a size of R and $N - N_R$ subdominant ones with radii $\tilde{R}$. Both categories contribute to (3.20). The key distinction lies in the fact that the contribution of the subdominant dimensions to the rate (5.17) is less. That is,

$$(m_n \tilde{R})^{N-N_R} \;\ll\; (m_n R)^{N_R}\,. \tag{5.19}$$

Then taking into account the relation (3.20) and the fact that $V_N = (R^{N_R} \tilde{R}^{N-N_R})$, we get

$$(m_n \tilde{R})^{N-N_R} \ll \frac{M_P}{M_f} \left(\frac{m_n}{M_f}\right)^{N/2}\,. \tag{5.20}$$

We can now apply the above considerations to specific cases. The first case involves $N_R = 1$, with just one relevant extra dimension of radius R. The parameters R and M_f are treated as free parameters. To obtain meaningful constraints, we set both to their current experimental bounds, as given by equations (3.37) and (3.36). The results for various total numbers N of extra dimensions are presented in Table 5.1.

Note that condition (5.20) implies that for $N_R = 1$ and the specified choice of R and M_f, we must have $N > 2$. In other words, with only two extra dimensions and $M_f \sim 10$ TeV, it is not feasible to have one dimension significantly shorter than the other without conflicting with observations.

N	M_*[GeV]
3	$> 3 \cdot 10^7$
4	$> 1 \cdot 10^7$
5	$> 5 \cdot 10^6$
6	$> 3 \cdot 10^6$

Table 5.1: Bound on M_* for one dominant R with $M_f = 10$ TeV and $R = 30\mu$m

The second example under consideration involves N equal-sized extra dimensions. In this case, $N_R = N$. Consequently, using (3.20),the right-hand side of (5.18) can be expressed in terms of $M_P \sim 10^{19}$ GeV, and the bound takes on a simple numerical form,

$$M_*^{4+N} > 10^{59}\text{GeV}^{4+N}\,. \tag{5.21}$$

The resulting bounds on M_* and corresponding values of R are listed in Table 5.2.

N	$R[\mu\text{m}]$	M_*[GeV]
2	1.1	$> 7 \cdot 10^9$
3	$1.6 \cdot 10^{-5}$	$> 3 \cdot 10^8$
4	$5.5 \cdot 10^{-8}$	$> 2 \cdot 10^7$
5	$2 \cdot 10^{-9}$	$> 4 \cdot 10^6$
6	$2.2 \cdot 10^{-10}$	$> 8 \cdot 10^5$

Table 5.2: Bound on M_* for equal size extra dimensions.

Another instructive choice is $M_* \sim M_f$. In this case, (5.18) becomes

$$M_f^2 > 10^{21}(\text{GeV}R)^{N_R}\text{GeV}^2\,. \tag{5.22}$$

Since $N_R \leqslant N$, from (3.20) we have $M_f \leqslant (M_P^2/(2\pi R)^{N_R})^{1/(N_R+2)}$. Together with this inequality, equation (5.22) becomes a bound on R. For example, for $N_R = 1$ we get

$$R \lesssim 10^2\text{GeV}^{-1} \sim 10^{-8}\mu\text{m}\,. \tag{5.23}$$

Equivalently, the bound on M_f is

$$M_f \gtrsim 10^{12}\text{GeV}\,. \tag{5.24}$$

5.3 Proton Decay

The prospect of neutron oscillations into a bulk fermion introduces the possibility of proton decay. If the high-dimensional mass of Ψ is smaller than the mass difference between the proton and the sum of the electron and neutrino masses, a tree-level decay process becomes feasible. Through a virtual neutron exchange, the proton can decay into a positron, the Standard Model neutrino, and Ψ,

$$p \to e^+ + \nu + \Psi. \tag{5.25}$$

The process is depicted in Fig. 5.2. The rate of the process is given by

$$\lambda_p \sim m_p \left(\frac{m_n}{v}\right)^4 \left(\frac{\alpha}{m_n}\right)^2 (m_p R)^{N_R}. \tag{5.26}$$

It is useful to compare this rate to the neutron disappearance rate (5.17). Taking into account that $m_n \simeq m_p$, we obtain that the proton decay rate is suppressed relative to the neutron rate by an additional factor $\left(\frac{m_n}{v}\right)^4 \sim 10^{-9}$ coming from the W-boson exchange,

$$\lambda_p \sim \lambda_n \left(\frac{m_n}{v}\right)^4 \sim \lambda_n 10^{-9}\,. \tag{5.27}$$

Simultaneously, the existing bound on the proton lifetime for this channel, $\tau_p > 10^{30}$ years [133], aligns with the bound on neutron disappearance (5.15). Consequently, as long as the bound on neutron disappearance is met, the bound on proton lifetime is automatically satisfied.

Due to this alignment, the bound on M_* inferred from the proton provides a less stringent constraint. For instance, assuming $M_f \sim 10$ TeV, the bound is,

$$M_*^{4+N} > 10^{12} (m_p R)^{N_R}\, M_f^{2+N} \mathrm{GeV}^2\,. \tag{5.28}$$

Therefore, the improved accuracy of neutron disappearance experiments would appear more promising for testing the discussed scenario.

5.4 Kaluza-Klein Spectroscopy from Free Neutron Oscillations

We now wish to discuss another experimentally-motivated domain of our framework. In this domain, the dominant effect is the oscillation of a free neutron into hidden dimensions. In this regime, the bulk partner of the neutron, Ψ, has a high-dimensional mass, μ. If the mass is above the energy

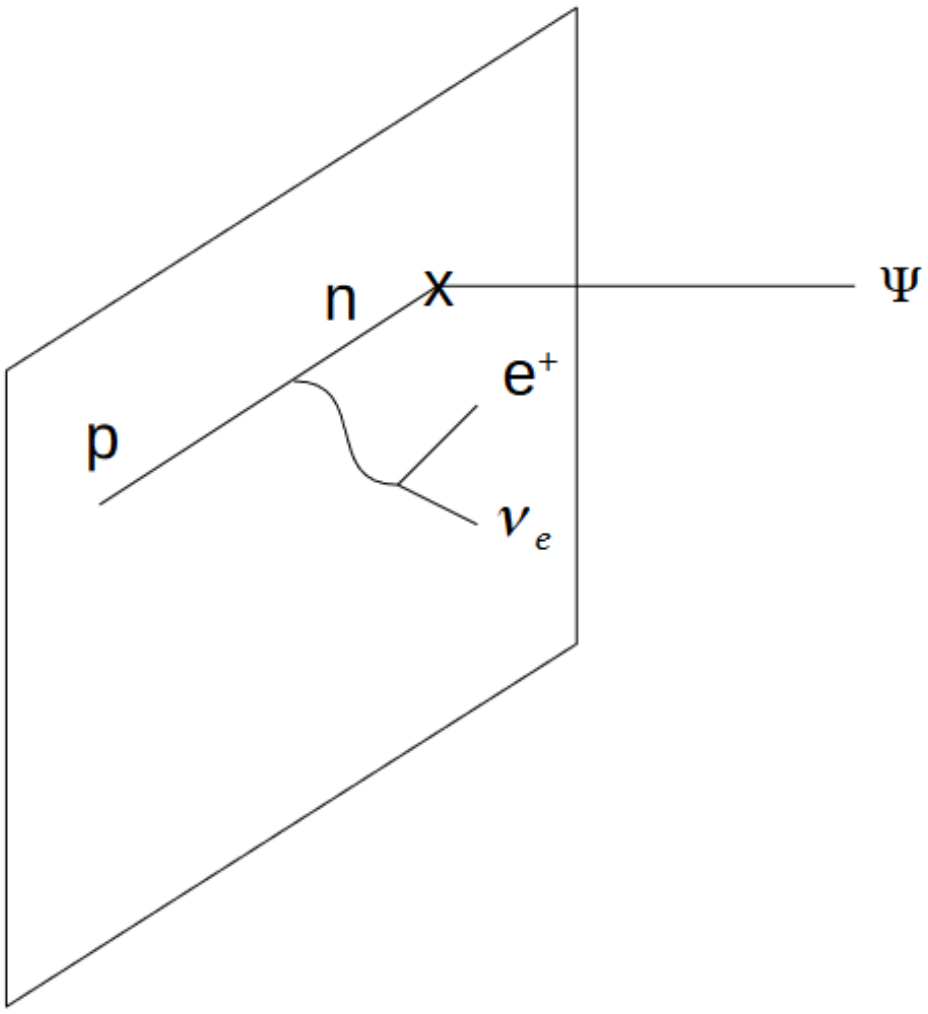

Figure 5.2: Proton Decay via virtual neutron exchange. The SM particles are confined to the brane, whereas the extra-dimensional particle, Ψ, propagates in the bulk.

levels of the nuclear neutron, the stability of nuclei is unaffected. Similarly, if μ is above the proton mass, there is no bound from proton decay. Thus, if μ is within a window, $\sim$ MeV below the mass of a free neutron, only the free neutron is experiencing oscillations into extra dimensions. The transition amplitude can correspondingly be much larger.

It is noteworthy that for dimensions satisfying $1/R \ll |m_n - \mu|$, the number and level-splitting of the available KK modes, to which the neutron can oscillate, are essentially the same as for $\mu = 0$.

In the case of $N_R = 2$, this level-splitting is sufficiently small to be probed by an external magnetic field available in current laboratory setups. This opens the possibility for potentially observable resonant $n - \Psi$ oscillations correlated with the features of the KK spectrum. Let us delve into a discussion of this effect.

The amplitude of the neutron oscillation into the bulk particle is suppressed by the minimal mass splitting between the neutron and the nearest KK mode, denoted as Δm. Simultaneously, the amplitude is enhanced by the KK multiplicity factor Z.

The oscillation of a free neutron is effectively mapped onto a 2×2 problem, in which the neutron mixes with a single state with the nearest mass,

$$\begin{pmatrix} m_n & \sqrt{Z}\alpha \\ \sqrt{Z}\alpha & m_n + \Delta m \end{pmatrix}. \tag{5.29}$$

In the absence of a parameter capable of scanning the neutron energy with a precision of Δm, the oscillation amplitude is suppressed as indicated by (5.14). However, an external magnetic field can function as a scanner. When a neutron is placed in a magnetic field $\vec{B}$, its magnetic moment $\vec{\mu}_n$ induces an additional energy level shift, denoted as ϵ, given by $\epsilon = \vec{\mu}_n \cdot \vec{B}$. Correspondingly, the mixing matrix becomes

$$\begin{pmatrix} m_n + \epsilon & \sqrt{Z}\alpha \\ \sqrt{Z}\alpha & m_n + \Delta m \end{pmatrix}. \tag{5.30}$$

It is crucial to note that, irrespective of the magnetic field strength, in the given mixing matrix, we must always consider $\epsilon \lesssim \Delta m$. If we increase the magnetic field to the extent that $\epsilon > \Delta m$, the entire problem will be shifted to the KK level closest to the shifted energy of the neutron $m_n + \epsilon$. Thus, an increase in the magnetic field above the resonance value,

$$B_r \equiv \Delta m / \mu_n, \tag{5.31}$$

results in the effective shift $m_n \to m_n + \epsilon$.

Due to this condition, within a range of magnetic field values, the neutron energy aligns with certain KK levels, leading to an enhanced oscillation amplitude.

For $N_R = 2$, the levels are not precisely equidistant. Consequently, the effect is not strictly periodic but exhibits a discernible repetitive pattern that fully mirrors the KK spectrum.

This characteristic sets our framework apart from theories where the neutron has a singular oscillation partner, such as dark neutrons from hidden

standard model copies. A more detailed comparison with such scenarios will be addressed later.

In the context of current experimental setups, ϵ is a very small quantity. For instance, with Earth's magnetic field, $|\vec{B}_e| \simeq 0.5$ G, we have $\epsilon_e \sim 10^{-12}$ eV. With the most powerful artificial magnets currently available, it can be increased by a few orders of magnitude.

This level of precision is adequate for scanning the KK spectrum for $N_R = 2$ within an interesting range of radii. For instance, considering the largest possible value for extra dimensions, $R = R_{\max}$, as constrained by the experimental bound (3.37), the splitting of closely spaced KK modes is $\Delta m \equiv 1/(2m_n R_{\max}^2) \simeq 2\times 10^{-14}$ eV. This value lies within the realm testable by currently available experimental setups.

For $\alpha < |\epsilon - \Delta m| < \Delta m$, the oscillation amplitude is

$$A \simeq \frac{\alpha^2}{|\epsilon - \Delta m|^2}\,, \tag{5.32}$$

and the oscillation frequency is given by $\omega = |\epsilon - \Delta m|$. In the resonance regime, $\alpha \leq |\epsilon - \Delta m|$, the amplitude becomes of the order of one, and the frequency is determined by $\omega \sim \alpha$.

Once again, it is crucial to note that for the regime $\epsilon \gg \Delta m$, we transition to a new KK level closest to $m_n + \epsilon$, and the excess of ϵ is effectively absorbed in the shift of m_n.

Now, we will compare the described dynamics with experimental data. To facilitate this comparison, we will express the amplitude (5.32) in a more user-friendly form. For this, we take into account that $\epsilon \simeq 6\times 10^{-14} B \frac{\text{eV}}{\mu\,\text{T}}$ [134] and that for $R = R_{max}$, we have $\Delta m \simeq 2 \times 10^{-14}$ eV. We can then write

$$A \sim \frac{10^{27}\,\alpha^2\,\text{eV}^{-2}}{|3\frac{B}{\mu\text{T}} - \frac{R_{max}^2}{R^2}|^2}\,. \tag{5.33}$$

Given that for resonant values of B, the crucial factor is the difference between the two terms in the denominator, we focus more precisely on these terms while examining the overall numerical coefficients less closely. We will employ this formula to interpret the two experimental results.

The first one [130], the ultra-cold neutron storage experiment, constrains the disappearance of a neutron for two separate values of the magnetic field: $B \simeq 10.20 \pm 0.02\mu$T and $B \simeq 20.39 \pm 0.04\mu$T.

Assuming $R = R_{\max}$, for the given magnetic field values, the first term in the denominator (5.33) is larger than the second one by factors of 30 and 60, respectively. This implies that the system will shift to a higher KK level,

absorbing the extra contribution from the magnetic energy into the mass of a new KK partner. Excluding miraculous coincidences or finer cancellations, the optimal KK level will satisfy:

$$|\epsilon - \Delta m| \sim \Delta m \,. \tag{5.34}$$

It is important to note that the error in $\delta\epsilon = \epsilon\delta B/B$, due to inaccuracy of the magnetic field (which is $|\delta B/B| \simeq 2 \times 10^{-3}$ in both cases), is not sufficient to further reduce the difference $|\epsilon - \Delta m|$.

Now, it is clear that the relation (5.34) will persist for $R < R_{\rm max}$. Specifically, for $\frac{R^2_{\rm max}}{R^2} \ll 3\frac{B}{\mu\rm T}$, the level will always get shifted to the one that satisfies (5.34). Simultaneously, for $\frac{R^2_{\rm max}}{R^2} > 3\frac{B}{\mu\rm T}$, the same condition is satisfied without any shift. Consequently, the relation (5.34) is satisfied for the entire parameter space probed by the experiment of [130]. Thus, for fitting the data, the equation (5.33) can be approximated as,

$$A \sim 10^{27}\,\alpha^2\,\frac{R^4}{R^4_{max}}\,\mathrm{eV}^{-2}\,. \tag{5.35}$$

Putting everything together, we get the following constraint on our parameters,

$$\alpha\,\frac{R^2}{R^2_{max}} \lesssim 10^{-16}\mathrm{eV}\,. \tag{5.36}$$

Expressing α in terms of M_* and M_f, we can write,

$$\frac{10\mathrm{TeV}}{M_f}\left(\frac{M_f}{M_*}\right)^{2+N/2}\,\frac{R^2}{R^2_{max}} \lesssim \frac{1}{3}\,. \tag{5.37}$$

It is intriguing that by setting M_f to its current experimental bound (3.36) of $M_f \sim 10$ TeV and simultaneously taking M_* at its theoretical limit, $M_* \sim M_f$, equation (5.37) corresponds to the current experimental constraint on R (3.37) imposed by tests of Newtonian gravity. Having a rigorous bound on the extra-dimensional setup from cold neutron experiments is indeed noteworthy.

Now, let us shift our focus to the second experiment [131], involving an ultra-cold neutron beam. The crucial insight from this measurement is that the authors scanned a broad range of magnetic fields within the interval between $B_{\rm min} \simeq 50, \mu\rm T$ and $B_{\rm max} \simeq 1100, \mu\rm T$, with a step of $\Delta B = 3\mu\rm T$. To translate the results of this experiment into bounds on our parameters, we need to consider various cases.

In the regime

$$\frac{R^2_{max}}{R^2} \gg 3\frac{|B_{max} - B_{min}|}{\mu\rm T} \simeq 3150\,, \tag{5.38}$$

or equivalently $\Delta m \gg \epsilon_{max} - \epsilon_{min}$, our transition amplitude is essentially the same as without the magnetic field, (5.35), and the bound is

$$\alpha \frac{R^2}{R^2_{max}} \lesssim 10^{-15}\text{eV}\,. \tag{5.39}$$

It has the same form as (5.36) but subject to (5.38).

In the opposite case,

$$\frac{R^2_{max}}{R^2} \;<\; 3\frac{|B_{max} - B_{min}|}{\mu\text{T}}\,, \tag{5.40}$$

the bound depends on the ratio between Δm and the scanning step $\Delta\epsilon$. In the denominator of expression (5.32) the smallest of the two will enter. Because of this, for $R^2_{max}/R^2 < 9$, the bound is again given by the expression (5.39).

For $R^2_{max}/R^2 > 9$, the situation is different since the Δm term in (5.32) can be compensated by the accuracy of $\Delta\epsilon$.

The magnetic term ϵ can be gradually cranked up in small increments $\Delta\epsilon$ all the way to Δm, sooner or later the resonant transition will take place with $|\epsilon - \Delta m| \simeq \Delta\epsilon$. In this case, the absolute value of Δm (and thus dependence on R) drops out from the transition amplitude and we have

$$A \;\sim\; \frac{\alpha^2}{|\Delta\epsilon|^2} \sim \alpha^2 10^{25}\,\text{eV}^{-2}\,. \tag{5.41}$$

This imposes the following R-independent constraint on α

$$\alpha \;\lesssim\; 10^{-14}\text{eV}. \tag{5.42}$$

In summary, the distinctive signature of neutron oscillations into extra dimensions, setting it apart from other proposals, is the recurrence of the resonance amplitude for multiple values of the magnetic field with steps $\Delta B, =, \frac{\Delta m}{\mu_n}$, where Δm is the mass splitting between the nearest KK levels. These recurrent resonance transitions are a characteristic prediction of the extra-dimensional scenario, as illustrated in Fig. 5.3 and Fig. 5.4.

The experiment [131] is effectively probing the interval

$$0.8\mu\text{m} < R < 10\mu\text{m} \tag{5.43}$$

and correspondingly impose the bound (5.42) on α.

Extensions of the upper and lower bounds of this interval can be achieved by increasing the range of the magnetic field and decreasing the step size,

respectively. For instance, reducing the step size to $1/3\mu$T would push the upper bound towards the level of (3.37), as determined by measurements of Newton's law. Conversely, expanding the range of the scanned magnetic field would enable the exploration of smaller sizes of extra dimensions.

The general trend is evident from the analysis above. Experiments with more refined scanning of broader ranges of the magnetic field can offer deeper insights into the physics of extra dimensions. Remarkably, the bounds (5.36), (5.39), and (5.42) suggest that these experiments are already delving into the domain motivated by the Hierarchy Problem.

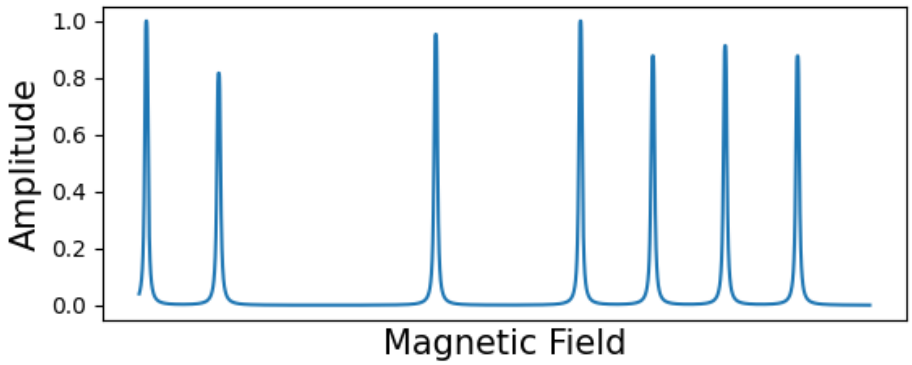

Figure 5.3: A qualitative sketch of the transition amplitude as a function of the magnetic field. The resonance transitions take place with steps $\Delta B = \Delta m/\mu_n$. The differences in the heights are due to different degeneracy factors of different KK levels. The repetitive but not strictly periodic behavior is due to the nonuniform population of KK levels.

5.5 Comparing with oscillations into hidden copies of the neutron

In this section, we aim to compare the presented scenario with the earlier proposal [17] where the neutron also interacts with multiple partners $n_i, i = 1, 2, ..., N$ from N hidden sectors (note that N here is not to be confused with the same notation for the number of dimensions in ADD). These partners represent neutron-like particles belonging to N copies of the Standard Model. The copies are connected by an exact permutation symmetry. Similar to the ADD model, this scenario was originally motivated by the Hierarchy Problem, as the existence of multiple SM copies lowers the cutoff of the theory[15, 16].

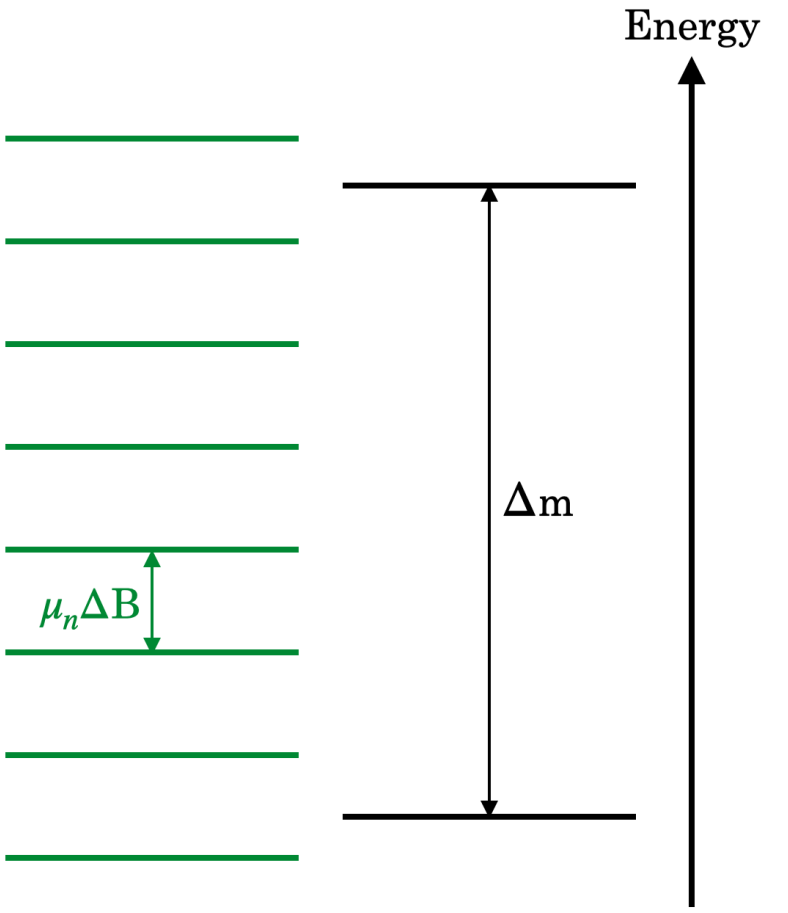

Figure 5.4: Scanning with the magnetic field between two KK-levels. A resonance occurs when the shifted energy level of the neutron comes close to a KK state with a precision of $\mu_n \Delta B$.

In a way, this scenario acts as a "Fourier transform" of the ADD solution, signifying that the dilution of gravity occurs in the space of species. Consequently, solutions to certain puzzles offered by ADD also find counterparts in this framework. For instance, a "dilution" of the neutrino mass in the space of species can be achieved [17, 2]. Additionally, the particles in the hidden copies of the Standard Model can serve as dark matter [21, 17] [1].

As discussed in [17], one of the phenomenological consequences of the scenario with N SM copies can be the oscillation of a neutron into the hidden partners, since the mixing $\alpha \sum_{i \neq j} \bar{n}_i n_j$ is permitted by the gauge symmetries

[1] This idea was originally proposed within the ADD framework, with the role of exact copies of the Standard Model played by the parallel folds of our brane [19]

of all sectors. The only constraint, $\alpha < m_n/N$, comes from unitarity.

This scenario exhibits some crucial differences from the present case. Because of the exact permutation symmetry, the mass matrix has the form,

$$\begin{pmatrix} 1 & 0 & 0 & 0 \\ 0 & 1 & 0 & 0 \\ 0 & 0 & 1 & 0 \\ 0 & 0 & 0 & 1 \end{pmatrix} (m_n - \alpha) + \begin{pmatrix} 1 & 1 & 1 & 1 \\ 1 & 1 & 1 & 1 \\ 1 & 1 & 1 & 1 \\ 1 & 1 & 1 & 1 \end{pmatrix} \alpha \,. \tag{5.44}$$

Due to this structure, the oscillation dynamics can be reduced to a 2×2 problem in which the neutron from our copy, n_1, mixes with the state $n_h \equiv \frac{1}{\sqrt{N-1}} \sum_{j \neq 1} n_j$, via the following mass matrix,

$$\begin{pmatrix} m_n & \alpha\sqrt{N-1} \\ \alpha\sqrt{N-1} & m_n + \alpha\sqrt{N-2} \end{pmatrix} . \tag{5.45}$$

The rest of the orthogonal $N-2$ states decouple.

The resulting disappearance probability is

$$P(t) \simeq \frac{4}{N} \sin^2 \left(\frac{N\alpha t}{2} \right) . \tag{5.46}$$

This scenario differs significantly from the case of a neutron mixing with the KK tower. The key distinction lies in the fact that the neutron has a single oscillation partner in the form of a state n_h. For neutrons in all possible energy states, this partner is unique and determined by the theory.

The phenomenology of free neutron oscillations is accordingly very different from the KK case, especially in terms of the magnetic field dependence of the resonant amplitude. In the case of an oscillation into a single hidden partner, the amplitude peaks around the resonant value of the magnetic field $B_r = \alpha\sqrt{N-2}/\mu_n$ and diminishes in both directions as a function of $|B - B_r|$.

This behavior sharply contrasts with the present scenario in which a neutron oscillates into the KK tower. As previously discussed, in this case, a neutron of arbitrary energy $m_n + \epsilon$ finds its oscillation partner among the KK states that are closest to it. Because of this effect, the amplitude is recurrent in B with steps of $\frac{\Delta m}{\mu_n}$.

This distinction holds for a scenario with an arbitrary number of Standard Model copies, including the special case of $N = 2$. This case is commonly referred to as the mirror Standard Model. The oscillation between neutrons of the two copies was previously studied in [128]. The additional challenge in this case is the exact degeneracy of the diagonal masses between n and its mirror partner n'. Due to this, the oscillations are suppressed by potentials

arising in our sector due to the environment, such as the Earth's magnetic field, which introduces a large level splitting.

Therefore, the transition can occur only if one assumes the presence of an analogous magnetic field in the hidden sector, which is beyond any experimental or theoretical control as it fully depends on the nature of the hidden sector. Regardless of this issue, assuming the proper conditions, the resonance can only occur for one specific value of the magnetic field that happens to match the hidden one. This is distinct from the extra-dimensional oscillations of neutrons, where the resonances occur for discrete values of the magnetic field synchronized with the Kaluza-Klein spectrum.

5.6 Neutron lifetime measurements

The possibility of free neutron oscillations into extra dimensions also emphasizes the need for more precise measurements of its lifetime. In fact, some authors have argued that existing measurements may indicate a discrepancy that supports the existence of new channels of neutron disappearance.

On the one hand, we have data from so-called ultra-cold neutron lifetime measurements, which account for the missing neutrons from a given number of free neutrons. The reported lifetime of the neutron is $\tau_1 = 878$ seconds [135, 136, 85]. On the other hand, we have data from beam experiments that look for the protons resulting from the ordinary decay of neutrons caused by the weak interaction. These experiments report a lifetime of $\tau_2 = 888$ seconds [137, 138, 85].

This difference between the reported neutron lifetimes has prompted some attempts to address it in the context of oscillations to mirror neutrons [128, 129, 139, 140], or decays of neutrons into other hypothetical particles [141]. For some cosmological implications, see [142]. However, doubts about the rigor of the discrepancy have also been raised [143].

Scrutinizing the validity of the puzzle is beyond the goal of the present paper. Regardless, the phenomenon of neutron oscillations into extra dimensions provides an additional motivation for improved precision measurements of the neutron lifetime.

5.7 Baryon and Lepton Numbers

Notice that the mixing of the SM neutrino with a bulk fermion (3.26) preserves lepton number symmetry since Ψ can be assigned one unit of lepton number. Likewise, the mixing of the neutron with the bulk fermion Ψ (5.1)

fixes the baryonic charge of Ψ as equal to one. In the case where the neutrino and neutron mix with the same Ψ, one combination of baryon and lepton number is preserved depending on whether both mix with Ψ or with their relative conjugates.

Mixing with the same Ψ leaves $B + L$ symmetry unbroken and breaks $B - L$. Mixing with the conjugates Ψ and Ψ^* has the opposite effect. Notice, as discussed in [14], the $B - L$ symmetry can be gauged in the bulk, resulting in gravity competing forces from the exchange of a $B - L$ gauge boson. If $B - L$ is gauged, one of the mixing operators must be suppressed by the vacuum expectation value of the field that Higgses it.

It is worth noting that the introduction of a Majorana mass term for the bulk particle Ψ of the form $\mu_M \Psi C \Psi$ would break the baryon number by two units. Consequently, the exchange of Ψ could lead to neutron-anti-neutron oscillations, which would correlate the neutron disappearance rate with the $n - \bar{n}$ oscillation. However, this particular case is not discussed further in this context.

5.8 Cosmology

We would like to briefly comment on some straightforward cosmological implications and constraints on the present scenario.

In the large extra-dimensional theory, there exists a standard list of constraints shared by the bulk species [14]. In particular, an important bound is coming from Big Bang Nucleosynthesis (BBN). In this consideration, the key control parameter is the "normalcy temperature". The point is that at BBN temperatures the production of bulk species must be sufficiently suppressed in order not to interfere with the standard evolution of the Universe. The bulk species must neither enter in thermal equilibrium with the SM particles nor be overproduced.

BBN provides stringent constraints on the presence and properties of additional particles, including bulk species in the large extra-dimensional theories. One crucial aspect is ensuring that these extra particles do not disrupt the standard evolution of the Universe during BBN. The "normalcy temperature" is the critical parameter. The point is that at BBN temperatures the production of bulk species must be sufficiently suppressed in order not to interfere with the standard evolution of the Universe. These constraints are essential for maintaining the successful predictions of light element abundances during the early stages of the Universe.

In the scenario involving a massless bulk fermion Ψ mixing with the neutrino, constraints related to BBN were examined in [127]. In the present case,

where the neutron mixes with the sector of the KK tower, these constraints are less stringent. This is because the KK tower is much heavier than the BBN temperature, resulting in a milder bound.

In particular, in the parameter regime relevant for free neutron oscillations into the bulk fermion, the thermal production of Ψ due to the rescattering of quarks via the four-fermi operator (5.1) is effectively shut off below the temperature of its mass $\mu \sim$ GeV.

In addition to constraints, cosmology offers compelling motivations for the existence of a neutron portal into extra dimensions, embodied by its bulk partner Ψ. One such motivation is the mechanism for baryogenesis introduced in [127]. The idea is that the excess of baryonic charge in our sector (i.e., particles inhabiting the SM brane) is generated by its loss into extra dimensions.

Although a neutron's transition into an extra dimension does not violate baryon number, baryogenesis can still occur, given that the other two Sakharov's conditions (CP-violation and an out-of-equilibrium state) are fulfilled. This is feasible because the bulk species can transport baryon number away from our SM sector, effectively "hiding" it in the KK states.

In our scenario, this process can manifest as an out-of-equilibrium conversion of our baryons into the fermions Ψ. Due to the extremely weak interaction of Ψ, the inverse decays are highly suppressed. The net result could be the generation of a baryon number asymmetry in our sector. While the exact amount of the missing baryonic charge is carried by the bulk species, it remains effectively inaccessible for our measurements, leading to an apparent asymmetry in baryon number in the Universe.

The second natural implication of the bulk particle Ψ is that its KK states can play the role of dark matter. The generic feature of bulk modes is that they interact with SM species with gravitational strength and, correspondingly, are extremely long-lived. This makes them viable candidates for dark matter. The possibility that KK gravitons of large extra dimensions can be dark matter was originally proposed in [14] (a more recent discussion of this idea can be found in [144]).

Similarly, in our scenario, Ψ can be a dark matter candidate. Of course, the construction of a fully viable and predictive scenario requires a more detailed cosmological investigation of the parameter space of our setup. This is beyond the goals of the present chapter.

5.9 Conclusions and outlook

In this chapter, we emphasized that neutron experiments offer a distinct spectroscopic insight into extra dimensions.

Neutrons assume a pivotal role in the investigation of particle species with ultra-feebly interacting behavior, akin to the strength of gravity. Theoretical frameworks that involve a multitude of such ultra-feebly interacting species are particularly intriguing. The motivation behind exploring these frameworks lies in their potential to address the Hierarchy Problem by reducing the theory's cutoff scale, as outlined in (3.38).

The ADD model of large extra dimensions [13, 14] and the framework featuring multiple exact copies of the SM[15, 16, 17] represent two extremes among theories that involve ultra-feebly interacting species. While neutron oscillations into hidden copies of the SM have been explored in the latter framework[17], investigations into neutron oscillations into large extra dimensions have, until now, remained unexplored. This paper aims to bridge this gap in our understanding.

In the ADD framework, we have examined the oscillations of a neutron into a fermion Ψ that propagates in large extra dimensions. Specifically, Ψ can be the same bulk fermion responsible for endowing the Standard Model neutrino with a naturally small mass, following the mechanism proposed in [18, 79]. This mechanism leads to the oscillation of the neutrino into the KK tower of the bulk sterile fermion [127].

In our current framework, the neutron undergoes a similar oscillation into the KK species of the bulk fermion. However, neutron oscillations exhibit distinctive features that make them particularly interesting for a variety of experiments and phenomenological constraints. An intriguing characteristic of a neutron mixing with a bulk species is that, due to the high density and degeneracy of the KK spectrum, neutrons in various energy states, whether free or within nuclei, encounter their respective oscillation partners. The threshold for these oscillations is determined by the mass of the bulk fermion Ψ, which is a parameter of the theory.

When the mass of the bulk fermion Ψ is below the energy of a nuclear neutron, the primary effect is the disappearance of neutrons from nuclei, leading to their de-excitation and the emission of a hard photon. This gives rise to various constraints on the parameters of the theory. The associated proton decay rate is further suppressed, making it a subdominant effect by nine orders of magnitude. Therefore, improving the precision of neutron disappearance experiments and expanding the diversity of samples become crucial avenues for tightening the constraints. The resonant energy levels, crucial for these experiments, depend on the specific features of the Kaluza-

Klein spectrum.

When the mass of the bulk fermion Ψ falls within a window between the energies of a bound and a free neutron, the stability of nuclei is unaffected. However, the resonant transition can still be observed for a free neutron. This scenario presents an exciting opportunity to map the Kaluza-Klein spectrum using a magnetic field as a scanner. In contrast to scenarios where the neutron has a single oscillation partner, in the extra-dimensional case, the resonance occurs recurrently as a function of the magnetic field. The resonant values of the magnetic field are quantized and correspond one-to-one with the KK spectrum.

The analysis of our findings was performed in the context of two recent experiments: the ultra-cold neutron storage experiment [130] and the experiment with an ultra-cold neutron beam [131]. Our results indicate that both experiments impose constraints on the parameters of extra dimensions. Notably, the bounds, such as (5.36), (5.39), and (5.42), already probe the domain motivated by the Hierarchy Problem.

Future experiments with enhanced accuracy and an extended range of the scanned magnetic field offer a unique opportunity to conduct precise Kaluza-Klein spectroscopy in neutron laboratories.

Chapter 6

Multiple Axions in Theories with Dark Yang-Mills Groups

6.1 The strong CP problem and the Axion Mechanism

In this section, I will give a short introduction to the so-called strong CP problem and how the axion mechanism gives a solution to it. For this, I will rely on the two reviews [7, 8]. Because of the several different aspects of this topic, I do not intend to give a complete overview but rather want to present one possible argumentation line. After the introduction of the theoretical setup I present our work published in [3] and rely closely on it in the following.

6.1.1 The role of the θ term

The story begins with the QCD Lagrangian

$$\mathcal{L}_{QCD} = \sum_q \bar{q}(i\not{D} - m_q e^{i\theta_q})\bar{q} - \frac{1}{4}G^{a\mu\nu}G^a_{\mu\nu} + \theta\frac{g_s^2}{32\pi^2}G^{a\mu\nu}\tilde{G}^a_{\mu\nu}. \tag{6.1}$$

In this equation, q stands for quark fields, m_q for their masses, and θ_p the phase of the quark masses. The other quantities in (6.1) are defined as

$$\begin{aligned} G^a_{\mu\nu} &= \partial_\mu A^a_\nu - \partial_\nu A^a_\mu + g_s f^{abc} A^b_\mu A^c_\nu, \\ \tilde{G}^a_{\mu\nu} &= \frac{1}{2}\epsilon_{\mu\nu\rho\sigma}G^{a\rho\sigma}, \\ \not{D} &= \gamma^\mu D_\mu = \gamma^\mu(\partial_\mu - ig_s T^a A^a_\mu), \end{aligned} \tag{6.2}$$

with $\epsilon^{0123} = -1$ and g_s being the strong coupling constant. We recognize that the last term in the Lagrangian is CP violating but due to the fact that it can be written in the form of a total derivative

$$G^{a\mu\nu}\tilde{G}^a_{\mu\nu} = \partial_\mu K^\mu = \partial_\mu \epsilon^{\mu\alpha\beta\gamma}\left(A^a_\alpha G^a_{\beta\gamma} - \frac{g_s}{3} f^{abc} A^a_\alpha A^b_\beta A^c_\gamma\right) \tag{6.3}$$

in terms of the Chern-Simons current, K^μ, it was originally thought that this term can be neglected in perturbation theory. In the following, we will show that this first intuition is wrong and that this term has physical meaning and must be included in a quantum theory.

Let us start with a pure Yang-Mills Lagrangian with the gauge group $SU(2)$ for simplicity.

$$\mathcal{L}(A) = -\frac{1}{4} G^a_{\mu\nu} G^{a\mu\nu} \tag{6.4}$$

The results we will obtain can be generalized to higher gauge groups and the baseline message is unaltered. Now we perform a Legendre transformation to go into the Hamiltonian formulation and the corresponding expression is

$$\mathcal{H} = \frac{1}{2}\int d^3x (E^a_i E^{ai} + B^a_i B^{ai}) \tag{6.5}$$

in the temporal gauge, $A_0 = 0$. If one searches now for the zero energy states we find

$$A_i(\vec{x})|_{vac} = \frac{i}{g} U(\vec{x}) \partial_i U^\dagger(\vec{x}), \tag{6.6}$$

where $U(\vec{x})$ is an element of SU(2). These configurations are called therefore "pure gauge". Because we are working in an undergauged setting the expression for A_i is not zero as one would naively expect but is built of pure gauge transformations. Now we demand that the corresponding action is finite and we impose the boundary condition

$$\lim_{\vec{x}\to\infty} U(\vec{x}) = const. \tag{6.7}$$

This boundary condition implies that the three-dimensional space is topologically equivalent to S^3. Because the group manifold of SU(2) is also S^3 the functions $U(\vec{x})$ realize a mapping $S^3 \to S^3$. These mappings can be characterized how often one sphere is wrapped around the other one. This means that the different $U(\vec{x})$ can be classified into different $U_n(\vec{x})$. The crucial point is that it is not possible to change n of a configuration by a continuous gauge transformation. If one wants to change n one passes through configurations that are not pure gauge and this means that there is an energy barrier between different field configurations of different n.

Now the situation is the following. Quantum mechanics teaches us that in a situation where two vacua configurations are separated by an energy barrier tunneling processes are possible. These processes can be described by non-perturbative field configurations called instantons. If one can show the existence of instantons in YM theories by finding solutions to the YM equations of motion with the appropriate boundary conditions one also showed that processes that change the winding number are possible.

The existence of these instantons can be shown and the action of these processes tunneling from n to m can be expressed as

$$S_E[A] = \frac{8\pi^2}{g_s^2}\nu, \tag{6.8}$$

where ν is

$$\nu = m - n = \frac{g^2}{32\pi^2}\int dx_E^4 G^a_{\mu\nu}\tilde{G}^{a\mu\nu}. \tag{6.9}$$

So far we have established the fact that we have degenerated vacua which are separated by an energy barrier and instantons describe the processes that allow tunneling from one vacuum to another one. This also means that the physical vacuum is not one specific one of the degenerated vacua but a superposition of all of them. In the framework of QFT every point has to perform this tunneling at the same time and therefore the action has to not vanish in the infinite volume limit. Generically one calculates the amplitude of tunneling via

$$\langle n|\, H\, |m\rangle = e^{-S_E}, \tag{6.10}$$

and therefore

$$\langle n|\, H\, |m\rangle = e^{-|\nu|\frac{g^2}{8\pi^2}}. \tag{6.11}$$

This shows that the action is independent of x and does not vanish in the infinite volume limit. Correspondingly the true vacuum is a superposition of all vacua like

$$|\theta\rangle = \sum_{n=-\infty}^{n=\infty} = e^{in\theta}\,|n\rangle\,. \tag{6.12}$$

This is known as the θ vacuum. The angular parameter θ characterizing this vacuum comes from the fact that one imposes on the wave function the periodic Bloch boundary condition $|n+1\rangle = e^{i\theta}\,|n\rangle$. This is a natural boundary condition for a periodic system like we have with our degenerated n vacua. The result of this definition of the true vacuum is that it is labeled by the angular parameter θ.

Now we show that the following relation holds

$$\langle\theta|\,\mathcal{O}\,|\theta'\rangle = 0, \tag{6.13}$$

where $\mathcal{O}$ is a gauge invariant operator. We start with

$$\langle\theta|\,\mathcal{O}\,|\theta'\rangle = \sum_{m,n} e^{i(n\theta - m\theta')}\,\langle m|\,\mathcal{O}\,|n\rangle = \sum_{m,n} e^{i(n\theta - m\theta')} F(\nu), \tag{6.14}$$

where we took into account that the matrix element will just depend on ν. Then we can rewrite it in the following way

$$\langle\theta|\,\mathcal{O}\,|\theta'\rangle = \sum_{n} e^{in(\theta-\theta')} \sum_{\nu} e^{i\frac{\nu}{2}(\theta+\theta')} F(\nu) = 2\pi\delta(\theta-\theta') \sum_{\nu} e^{i\nu\theta} F(\nu), \tag{6.15}$$

which proves the relation (6.13). This has the consequence that the Hilbert spaces are orthogonal which means that different θ correspond to different superselection sectors. Therefore we can take θ as a label for different physical vacua.

Now we will show how the θ term reappears in the Lagrangian if we take instantons into account even though we did not include it in (6.4). We start by calculating the expectation value of an local observable in a large Euclidean volume Ω in the path integral formalism as

$$\langle\mathcal{O}\rangle = \frac{\sum_\nu f(\nu) \int_\nu \mathcal{D}\phi e^{-S_\Omega[\phi]} \mathcal{O}[\phi]}{\sum_\nu f(\nu) \int_\nu \mathcal{D}\phi e^{-S_\Omega[\phi]}}. \tag{6.16}$$

In this equation ϕ stands for the fields of the theory, S_Ω is the integral of the Lagrangian restricted over the volume Ω and we have included the sum over all topological sectors ν, with a general weight factor $f(\nu)$. Now we split Ω in two volumes $\Omega = \Omega_1 + \Omega_2$ and localize $\mathcal{O}$ in Ω_1. This allows us to write (6.16) in

$$\langle\mathcal{O}\rangle = \frac{\sum_{\nu_1,\nu_2} f(\nu_1+\nu_2) \int_{\nu_1} \mathcal{D}\phi e^{-S_{\Omega_1}[\phi]} \mathcal{O}[\phi] \int_{\nu_2} \mathcal{D}\phi e^{-S_{\Omega_2}[\phi]}}{\sum_{\nu_1,\nu_2} f(\nu_1+\nu_2) \int_{\nu_1} \mathcal{D}\phi e^{-S_{\Omega_1}[\phi]} \int_{\nu_2} \mathcal{D}\phi e^{-S_{\Omega_2}[\phi]}} \tag{6.17}$$

Due to the requirement of cluster decomposition, we require that the Ω_2 dependence must cancel. This requirement needs

$$f(\nu_1+\nu_2) = f(\nu_1) f(\nu_2). \tag{6.18}$$

This is uniquely solved by

$$f(\nu) = e^{i\theta\nu}. \tag{6.19}$$

If we plug in the expression for ν form (6.9) we see the θ term reappearing

$$\mathcal{L}_\theta = \theta \frac{g^2}{32\pi^2} G^a_{\mu\nu} \tilde{G}^{a\mu\nu}. \tag{6.20}$$

This means that in a quantum theory of the YM Lagrangian this term cannot be neglected and must be included.

Now we want to list some direct physical consequences which result by the existence of this term. The first property we want to mention is the fact that the vacuum energy density, ρ, of QCD depends exactly on the θ parameter by the equation (see e.g. [145])

$$\rho(\theta) = -K\Lambda^4_{QCD} e^{-\frac{8\pi^2}{g_s^2(\Lambda_{QCD})}} \cos\theta. \tag{6.21}$$

Here K is a positive constant. Moreover, it was shown in the Vafa-Witten theorem [146] that the CP conserving vacuum $\theta = 0$ is a global minimum.

Another direct experimental consequence of the θ term is a contribution to the electric dipole moment of the neutron, d_n. The dependence is

$$|d_n| \approx \frac{1}{8\pi^2} \frac{m_q}{m_n} \frac{\bar{\theta} e}{m_n} \approx 10^{-4} \bar{\theta} e \, GeV^{-1}. \tag{6.22}$$

This experimental signature was hunted for and so far no signal was found. The current bound on $\bar{\theta}$ is

$$|\bar{\theta}| \leq 10^{-10}, \tag{6.23}$$

reported in [147]. This was a surprising result because as we argued the θ parameter is a parameter of the SM like others and there is no reason coming from first principles which would explain its smallness. This is the so called "strong CP problem". This raised the question if new physics could be the reason for the smallness of θ. A very famous mechanism that sets the value of θ dynamically to zero is the so called "axion mechanism" which is described in the next section.

6.1.2 The Axion Mechanism

To address the elimination of the θ-vacua, we can introduce an axion [148, 149]. This can be achieved through a conventional PQ formulation [150, 151], necessitating a spontaneously broken global $U(1)_{PQ}$ symmetry that is chiral, non-linearly realized, and anomalous with respect to the corresponding Yang-Mills (YM) group. In the low-energy effective theory the Lagrangian for the axion field $a(x)$ is described as

$$\mathcal{L} = \mathcal{L}_{\text{SM,axion}} + \frac{g_s}{32\pi^2} \left(\frac{a}{f^a} + \theta \right) G\tilde{G} \, , \tag{6.24}$$

where the f^a denotes the axion decay constant. At scales below confinement, this coupling undergoes a transformation into the axion potential. According to the Vafa-Witten theorem, the vacuum of the axion is situated at $\langle a \rangle = -f^a\theta$. Expanding around these vacua serves to eliminate the vacuum angle from the theory.

Incorporating the $U(1)_{PQ}$ with the necessary characteristics into the SM is typically accomplished through the KSVZ and DFSZ invisible axion models [152, 153, 154, 155]. The KSVZ model introduces an additional SM scalar singlet along with a heavy quark, whereas the DFSZ model utilizes a singlet and an extra Higgs doublet. In the former, the singlet Φ_1 acquires a vacuum expectation value f^{a_1} via a standard Mexican hat potential,

$$V_1(\Phi_1) = \lambda_1 \left(|\Phi_1|^2 - (f^a)^2 \right)^2 \tag{6.25}$$

which generates the spontaneous breaking of the $U(1)_{PQ}$. The axion can be identified as the angular degree of freedom of the singlet, conventionally normalized as $\theta(x) \equiv a(x)/f^a$. In the SM, introducing the singlet becomes essential to disentangle the electroweak scale from the PQ scale f^a, thereby avoiding constraints from star cooling and direct detection. Our focus here is on the minimal invisible axion models, although it is worth noting that a multitude of KSVZ- and DFSZ-type models exist, as cataloged in [156, 157] and [158], respectively, each offering potential realizations in our sector.

The resolution of the strong CP problem through a massless quark is indeed a manifestation of the PQ mechanism. When considering a massless quark, such as the up-quark in the SM, the $U(1)_{PQ}$ symmetry aligns with the QCD's $\mathrm{U}(1)_A$ symmetry, and the role of the axion is played by the η' meson [159]. Although this implementation is not observed in the SM due to the massiveness of all SM quarks, it can be achieved in a dark sector.

The axion mechanism can be alternatively implemented through an intrinsic gauge formulation, originally proposed in [159] and further explored in [160, 161, 162] (also refer to [163] for a consistency check). This formulation does not rely on any global $U(1)_{\mathrm{PQ}}$ symmetry. Instead, it is built upon the gauge redundancy inherent in the respective QCD-like theory. In this gauge formulation, the axion is introduced as a two-form $B^1_{\mu\nu}$ that serves as the longitudinal mode of the QCD Chern-Simons three-form $C^1_{\mu\nu\rho}$ (analogous to the scalar that becomes the longitudinal mode of the Maxwell field in the Stückelberg formulation of the Proca theory). This fixes the form of the theory, to the lowest order, as,

$$\mathcal{L}_{\mathrm{eff}} = -\frac{1}{2 \cdot 4!}(F^1_{\mu\nu\rho\sigma})^2 + \frac{m^2}{2 \cdot 3!}\left(C^1_{\mu\nu\rho} - \partial_{[\mu}B^1_{\nu\rho]}\right)^2 \ , \tag{6.26}$$

where $F^1_{\mu\nu\rho\sigma} \equiv \partial_{[\mu} C^1_{\nu\rho\sigma]}$ denotes the canonically normalized field strength tensor of the Chern-Simons three-form. In this configuration, the Chern-Simons theory enters the Higgs phase, rendering the vacuum angle effectively unphysical. A notable advantage of this implementation is its immunity to the so-called quality problem, ensuring that $\theta_1 = 0$ remains intact without being susceptible to explicit breaking, as no global symmetry is necessitated. Consequently, this mechanism exhibits stability under any gauge-invariant deformation of the theory. As discussed in [162], a notable consequence of this realization is that any measurement of a neutron electric dipole moment would signify new physics. This contrasts with the conventional PQ implementation, where a non-trivial θ_1 could arise from explicit breaking. Below f^{a_1}, the pseudo-scalar $a_1(x)$ and the two-form axion $B^1_{\mu\nu}$ are dual to each other, resulting in largely similar physics, with the main distinction being the potential explicit breaking in the ordinary PQ realization. However, above f^{a_1}, the formulations diverge significantly, and the gauge formulation likely necessitates direct UV-completion within quantum gravity. This implies a PQ scale of $f^{a_1} \sim M_P$ (or $f^{a_1} \sim M_*$ in the presence of a large number of species). Importantly, the gauge axion realization can be applied to arbitrary hidden sector gauge groups.

In dark sectors, the specific implementation of the $U(1)_{PQ}$ varies depending on the model. However, there is more flexibility in these scenarios, given the absence of stringent bounds. For exact SM copies, the KSVZ or DFSZ models, or the two-form implementation, could once again be employed. In pure YM sectors, the axion mechanism can be implemented using the KSVZ scenario, the gauge two-form formulation, or the massless quark solution.

In the early cosmologies of gauge and $U(1)_{PQ}$ axions, significant distinctions can arise, primarily stemming from fundamental differences in their UV completions above the scale f_a. Nevertheless, the initial conditions in the following render these potential differences unimportant. Consequently, we adopted an approach independent of any specific realization of the axion mechanism and treat f^{a_i} as free parameters. However, if needed, we will explore consequences that are specific to particular realizations.

6.1.3 The Need for the Axion

Attempts to measure the neutron electric dipole moment have shown no evidence of CP violation in the strong interaction. Given that QCD involves CP-violating processes proportional to a parameter θ, the absence of observation leads to the constraint $\theta < 10^{-10}$ [164]. This seemingly inexplicable smallness constitutes the strong CP problem. While it may initially appear to be a naturalness problem, this characterization is somewhat misleading. A

naturalness problem typically arises when fine-tuning is required to address unacceptably large quantum corrections, as seen, for example, in the case of the Higgs mass. However, for θ, the quantum corrections from the Standard Model are much smaller than the measured bound [165]. Thus, from the perspective of naturalness, it is more aptly described as a puzzle concerning the smallness of the value rather than a problem requiring fine-tuning.

The scenario undergoes a significant shift when considering the impact of quantum gravity [162]. Recent evidence suggests that quantum gravity is incompatible with (meta-)stable de Sitter vacua [166, 167], particularly in the context of the S-matrix formulation of quantum gravity, which is only consistent with asymptotically flat space-times [168]. This has profound implications for axion physics [169, 162].

Essentially, θ is not merely a parameter but a label for QCD vacua, which are non-degenerate. According to the Vafa-Witten theorem [146], the global minimum is the CP-conserving one at $\theta = 0$, with other vacua having higher energies. As argued in [169, 162], if all theta vacua were deemed physical, their non-degeneracy would imply the existence of de Sitter vacua among them. Furthermore [162], even with arbitrary fine-tuning, only one out of infinitely many vacua could be made viable for the S-matrix formulation, while others would lead to asymptotically non-flat cosmologies. Consequently, it was concluded in [169, 162] that θ vacua must be considered unphysical in the context of gravity.

Incorporating gravity transforms the strong CP problem into a consistency issue, necessitating the elimination of the non-degenerate vacuum structure to retain only the physically viable vacuum. Consequently, a mechanism for selecting the correct vacuum becomes imperative [169, 162]. Pioneered by Peccei and Quinn [150, 151], the solution involves introducing a non-linearly realized $U(1)_{\mathrm{PQ}}$ that is anomalous concerning QCD. This leads to the dynamic setting of the θ-parameter to zero by the pseudo-Goldstone boson of $U(1)_{\mathrm{PQ}}$, commonly known as the axion [148, 149].

From this perspective, the strong CP problem is not confined to QCD alone but extends to any YM group. Each YM group encompasses a vacuum angle that results in an undesirable de Sitter-type vacuum structure, necessitating its elimination [162].

Employing the PQ mechanism to address this issue necessitates having one axion per YM group. This is because a single axion is unable to simultaneously set multiple θ-parameters to zero. This holds true even when different YM sectors are connected by a discrete symmetry, such as an exact permutation symmetry among N SM copies [20, 159]. The topological susceptibilities in distinct YM sectors spontaneously break the discrete symmetry, preventing a single axion from nullifying all combinations of the vacuum angles. The

remaining combinations persist as physical and unconstrained, resulting in two problems.

Firstly, even without considering gravity, this implies that a single axion cannot effectively address the small θ puzzle for multiple YM groups [159, 20]. Secondly, allowing these vacuum angles to persist would inevitably introduce asymptotically non-flat vacua, conflicting with the requirement of an S-matrix formulation. As a consequence, one axion per YM group becomes a necessity [162].

6.2 Consequences of Multiple Axions in Theories with Dark Yang-Mills Groups

In this chapter, we consider theories in which dark matter includes one or more YM sectors and investigate the generic phenomenological consequences of the necessary axions. To our knowledge, axions have not been taken into account due to gravitational consistency reasons, which impose certain properties on them.

In precise terms, we examine models with N sectors denoted as $\mathcal{L}_i$, where each sector includes at least one YM subgroup. Without loss of generality, we designate our sector as the one labeled by $i = 1$. The remaining sectors collectively constitute the dark matter, referred to as hidden or dark sectors. Interactions between the sectors occur through gravity and additional non-gravitational forces, encapsulated in $\mathcal{L}_{\text{mix}}$. The associated Lagrangian can be written as

$$\mathcal{L} = \sum_{i=1}^{N} \mathcal{L}_i + \mathcal{L}_{\text{mix}} \ . \tag{6.27}$$

The potential models fall into two main categories. The first category involves a framework where the dark sector comprises N copies of the standard model, linked by an exact permutation symmetry [21, 17]. This scenario is highly restrictive due to the imposition of an exact symmetry. Motivations for large values of N stem from addressing the Hierarchy problem [15, 16], although we will also explore cases with smaller N. Instances of such models have been discussed in various contexts, including [170, 171].

The second category encompasses all other possibilities, where the dark sector is not necessarily related to the SM, allowing for a diverse range of gauge structures. These scenarios are anticipated to be more generic in the context of string theory compactifications [172, 173, 174, 175].

For specific illustrations, we will examine two simple models: one with a pure YM sector and another with N exact SM copies. The former has been

utilized to model dark matter, leveraging the dynamics of YM theories that may lead to a potential phase transition generating stochastic gravitational waves during the early universe [176, 177]. The latter was initially motivated by the many-species solution to the hierarchy problem [15, 16].

When dealing with extended dark sectors, one can distinguish between universal effects and model-dependent features characteristic of particular scenarios. A universal feature is the modification of black hole physics at scales below the species scale M_* (see, e.g., [101]). Additionally, there are model-dependent consequences. When applied to model dark matter [21], it gives rise to intriguing phenomena such as neutron and neutrino oscillations [17, 2], modified black hole physics [178], and compact dark matter objects [179]. Despite focusing on these two models in our calculations, we aim to keep our discussion as general as possible and highlight model-independent predictions.

It is noteworthy that in the scenario involving many dark sectors with their associated axions, we encounter a situation reminiscent of the axiverse inspired within string theory [180]. Intriguingly, the axions in our framework emerge from motivations that are entirely distinct from those in string theory. The phenomenology of multiple axions within the context of the axiverse has been studied, for instance, in [181, 182].

6.2.1 Cosmological Implications

Cosmological Framework

To initiate our exploration, let us elucidate the behavior of dark sectors within a cosmological context. For the time being, we will neglect interactions between sectors, except for gravity, by setting $\mathcal{L}_{\text{mix}} = 0$. Intersector interactions will be discussed separately in Sec. 6.2.2. This simplification does not impact the conclusions of this section.

For the cosmological viability of these models, the dark sectors should exhibit behavior akin to a cold and pressureless fluid, forming stable dark matter halos. Additionally, if the dark sectors encompass any massless fields, they must evade constraints on the number of massless particles during nucleosynthesis. Achieving these conditions may seem challenging, particularly in the presence of non-trivial interactions within the dark sectors. We will employ the solution proposed in [21] to address these challenges.

In the approach presented in [21], inflation was employed to populate and reheat the sectors differentially. A crucial aspect is that the reheating into the dark sectors is significantly less efficient than in the visible sector. The resulting low reheating temperature in the dark sectors is utilized to

sidestep the nucleosynthesis bound, suppress cooling processes leading to the collapse of dark matter halos, and generally induce distinct behaviors throughout cosmological history, despite potential similarities to the visible sector. In the case of large N, where each sector becomes so dilute that it is challenging to treat them as thermalized, the behavior as a pressureless fluid arises from kinematics, namely, the fact that particles from the same sector rarely interact with each other.

Even when starting with equal sectors, the cosmological evolution breaks the symmetry in a sense, leading to different energy densities and temperatures for each sector. Nonetheless, the field-theoretic parameters of each sector, such as masses and coupling constants, remain equal.

Misalignment: Exact SM Copies

In the case of a single axion, a stringent bound on the axion scale arises from the requirement that the misalignment mechanism should not produce more dark matter than observed [183, 184, 185]. A crucial factor in this bound is the initial misalignment angle $\theta^{\rm ini}$, which can be defined as the value in the latest epoch when the Hubble parameter falls below the axion mass. The most stringent bound typically results when $\theta^{\rm ini}$ is of order unity. However, as demonstrated in [186], this value is highly sensitive to the details of the previous evolution of the axion field, such as the value of the QCD scale during inflation. It can be made arbitrarily small via the early relaxation mechanism. Consequently, in our analysis, we treat $\theta^{\rm ini}$ in each gauge sector as independent free parameters. Under these circumstances, we will derive constraints on the parameter space for models with multiple axions.

For a clearer presentation, let us start with the case of N exact SM copies, where the equality between the sectors can be ensured by a discrete symmetry [15, 16]. Various phenomenological aspects of this framework were studied in [187, 17]. As explained previously [20], despite the exact permutation symmetry of the Lagrangian, solving the small θ puzzle requires the existence of N axions. The same demand arises from the S-matrix consistency of gravity [162], necessitating the existence of N axions. For alternative compositions of the dark sectors, we will only discuss the differences in the calculation and provide the final result.

In the standard axion scenario, the $U(1)_{PQ}$ symmetry is spontaneously broken at $T^{PQ} \sim f_a$. In our framework, this occurs in every sector at temperatures $T_i^{PQ} \sim f a_i \equiv f_a$. The axions $\theta_i(x)$ emerge as the corresponding Goldstone bosons and, as such, have flat potentials. Using the standard notation, we canonically normalize the Goldstone fields as $\theta_i(x) \equiv a_i(x)/f_a$.

The potential of each axion is flat only when the corresponding QCD is

in the Coulomb phase. In the confinement phase, each axion receives an effective potential from non-perturbative effects of its corresponding QCD, primarily contributed by instantons in the semi-classical approximation. In a cosmological context, these instantons are coupled to the thermal bath, causing the axion masses to depend on temperature. For example, in the dilute instanton gas approximation [188], the potential takes the form [189]

$$V_i(\theta_i) = m_a^2(T_i) f_a^2 \Big(1 - \cos(\theta_i)\Big) \,, \tag{6.28}$$

where the Temperature-dependent masses are given by

$$m_a(T_i) \equiv \frac{(\Lambda_{QCD}^3 m_u)^{\frac{1}{2}}}{f_a} \begin{cases} \beta \, \left(\frac{\Lambda_{QCD}}{T_i}\right)^4 & : T_i > \Lambda_{QCD} \,, \\ 1 & : T_i \lesssim \Lambda_{QCD} \,. \end{cases} \tag{6.29}$$

Here, m_u denotes the up-quark mass, while β encodes QCD and active quark physics at the temperature T_i. For the SM, a rough estimate for β is $\sim 10^{-2}$ [188].

In an FLRW background with $R(t)$ denoting the scale factor and $H(t)$ the Hubble parameter, the equation of motion for each axion takes the form

$$\ddot{\theta}_i + 3H(t)\dot{\theta}_i - \frac{1}{R^2(t)}\Delta\theta_i + \frac{V_i'(\theta_i)}{f_a^2} = 0 \,. \tag{6.30}$$

Let us utilize the potential (6.28) and introduce the following two simplifications. First, we consider only the leading order in θ_i in the potential. Second, we only take into account the zero mode of θ_i. With these simplifications, each equation of motion reduces to that of a damped harmonic oscillator,

$$\ddot{\theta}_i + 3H(t)\dot{\theta}_i + m_a^2\Big(T_i(t)\Big)\theta_i = 0 \,. \tag{6.31}$$

At $T_i >> \Lambda_{QCD}$ the potential is flat so that $\theta_i \approx$ const, i.e. the i-th axion is basically frozen out. At $T_i \sim \Lambda_{QCD}$ the corresponding axion potential gets significant but it is not until the Hubble friction is overcome before the axion starts performing coherent oscillations around the vacuum. We define this critical time via

$$m_a\Big(T_i(t_{osc})\Big) = 3H(t_{osc}) \,. \tag{6.32}$$

Following this transition, its equation of state no longer aligns with that of dark energy but rather with that of non-relativistic matter. Consequently, the corresponding axion starts contributing to the energy density of dark matter.

In our model, this implies that, owing to the very low temperature in the dark sectors, the axions there are essentially generated with their zero-temperature potential activated. In contrast, our axion is generated with a

flat potential. Consequently, given that the zero-temperature mass is greater than the high-temperature mass, the axion from our sector will commence oscillations later than the other axions. To quantify this, let us use our sector's temperature $T_1 \equiv T$ as a measure of time instead of the cosmic time t. In terms of T the Hubble parameter during radiation domination is given by

$$H(T) = \sqrt{\frac{\rho_{\text{tot}}}{3M_P^2}} \sim \frac{T^2}{M_P} \, . \tag{6.33}$$

Here, ρ_{tot} denotes the total energy density, which is dominated by our sector. Using (6.33) and the axion masses defined by (6.29), the condition (6.32) results in the oscillations commencing when

$$\begin{aligned} T_{\text{osc},1} &\sim \left[\frac{\beta M_P \Lambda_{QCD}^{\frac{11}{2}} m_u^{\frac{1}{2}}}{3f_a}\right]^{\frac{1}{6}} \\ &\sim 4 \times 10^{-1}\text{GeV} \left(\frac{10^{12}\text{GeV}}{f_a}\right)^{\frac{1}{6}} \, , \end{aligned} \tag{6.34}$$

in our sector and

$$\begin{aligned} T_{\text{osc},i} &\sim \left[\frac{M_P \Lambda_{QCD}^{\frac{3}{2}} m_u^{\frac{1}{2}}}{3f_a}\right]^{\frac{1}{2}} \\ &\sim 2 \times 10^{1}\text{GeV} \left(\frac{10^{12}\text{GeV}}{f_a}\right)^{\frac{1}{2}} \, , \end{aligned} \tag{6.35}$$

in the dark sectors with $i \neq 1$. Note that both moments in time are expressed in terms of our sector's temperature.

While we have treated f_a as a free parameter, there is a small caveat for $f_a \gtrsim 6 \times 10^{17}\text{GeV}$. In this range, our axion has also reached its zero-temperature mass before overcoming the Hubble friction [190]. Consequently, for these values of f_a, all axions start oscillating at the temperature dictated by (6.35).

The initial energy density of each oscillation is

$$\rho_{a_i}(T_{\text{osc},i}) = \frac{1}{2} f_a^2 m_{a_i}^2(T_{\text{osc},i}) \theta_i^2(T_{\text{osc},i}) \, , \tag{6.36}$$

where $\theta_i(T_{\text{osc},i}) \equiv \theta_i^{\text{ini}}$ is each sectors initial misalignment angle. Essentially, we define the initial misalignment angle θ_i^{ini} as the value when the axion mass crosses below the Hubble parameter in the most recent history. However, as

shown in [186], this quantity is highly sensitive to the pre-history and can be made arbitrarily small due to early relaxation mechanisms. Therefore, we shall treat $\theta_i^{\rm ini}$ as a free parameter.

Since Big Bang Nucleosynthesis took place during radiation domination, the dark axions must not dominate the energy density of the universe at $T_{{\rm osc},i}$. The energy density for relativistic degrees of freedom at that time is given by $\rho_{\rm rad}(T_{{\rm osc},i}) \sim g(T_{{\rm osc},i})(T_{{\rm osc},i})^4$, where the effective number of relativistic species is $g(T_{{\rm osc},i}) \sim 10^2$. The requirement $\sum_{i=2}^{N} \rho_{a_i}(T_{{\rm osc},i}) \ll \rho_{\rm rad}(T_{{\rm osc},i})$ results in the bound

$$N \lesssim \frac{g_*(T_{{\rm osc},i})T_{{\rm osc},i}^4}{\Lambda_{QCD}^3 m_{\rm u}(\theta_i^{\rm ini})^2} \sim 10^{12} \left(\frac{10^{12}{\rm GeV}}{f_a}\right)^2 \left(\frac{1}{\theta_i^{\rm ini}}\right)^2 . \tag{6.37}$$

As it turns out, a stronger bound on N can be found at today's temperature. Since the axions are decoupled, the number of zero modes per co-moving volume is conserved as long as the changes in mass are in the adiabatic regime. Assuming this to be the case in every sector, today's energy density per sector is

$$\rho_{a_i}(T_{\rm today}) = \rho_{a_i}(T_{{\rm osc},i}) \frac{m_{a_i}(T_{\rm today})}{m_{a_i}(T_{{\rm osc},i})} \left(\frac{T_{\rm today}}{T_{{\rm osc},i}}\right)^3 . \tag{6.38}$$

We normalize with respect to the critical energy density $\rho_{\rm cr} \sim M_P^2 H_{\rm today}^2$ to receive the corresponding axion fraction Ω_{a_i} in today's universe. By comparing Ω_{a_i} with the dark matter fraction $\Omega_{\rm DM}$ from the latest Planck mission [36], we find for our sector

$$\frac{\Omega_{a_1}}{\Omega_{\rm DM}} \sim 0.54 \left(\frac{\beta^{-\frac{1}{6}} m_u^{\frac{5}{12}} \Lambda_{QCD}^{\frac{7}{12}}}{10^{-2}{\rm GeV}}\right) \left(\frac{f_a}{10^{12}{\rm GeV}}\right)^{\frac{7}{6}} \left(\frac{\theta_1^{\rm ini}}{1}\right)^2 , \tag{6.39}$$

while for each dark sector, i.e. $i \neq 1$, we get

$$\frac{\Omega_{a_i}}{\Omega_{\rm DM}} \sim 0.01 \left(\frac{m_u^{\frac{1}{4}} \Lambda_{QCD}^{\frac{3}{4}}}{10^{-2}{\rm GeV}}\right) \left(\frac{f_a}{10^{12}{\rm GeV}}\right)^{\frac{3}{2}} \left(\frac{\theta_i^{\rm ini}}{1}\right)^2 . \tag{6.40}$$

In summary, variations in reheating temperatures lead to the commencement of axion oscillations at different times, resulting in varying axion densities despite identical field-theoretic parameters. While a single mirror sector has an insignificant cosmological influence due to lower axion density compared to our axion, larger numbers of mirror sectors result in the accumulation of densities, and their collective effect cannot be ignored. In the following,

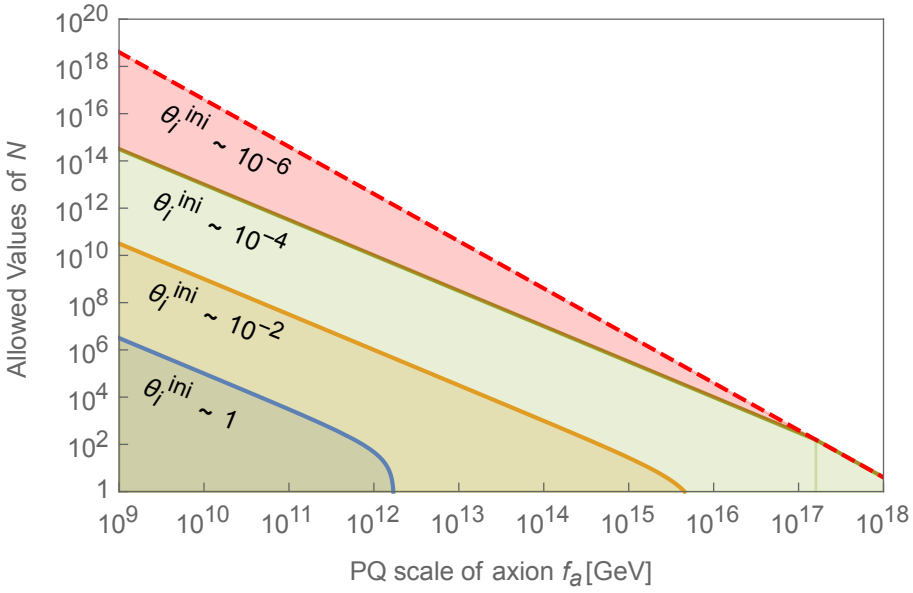

Figure 6.1: The allowed parameter space with different initial misalignment angles θ_i^{ini} according to (6.42). The values on the thick lines correspond to the case where the dark matter is entirely composed of axions. The dashed line presents the species bound, meaning that along this line the gravitational cutoff M_* and f_a coincide.

we will examine the parameter space and explore the consequences of this collective effect.

For our axion, a lower bound is imposed by astrophysics due to non-trivial couplings to matter [191]. These couplings result in contributions to the cooling of stars, yielding the bound $f_a \gtrsim 10^9$GeV. Although other axions are not directly coupled to our sector and, therefore, do not contribute to the cooling in stars, the PQ scale in all sectors must fulfill this bound due to the exact permutation symmetry between the sectors.

While our axion density matter is not allowed to exceed the observed dark matter density, leading to the known bound $f_a \lesssim 10^{12}$GeV, the total axion density must not exceed it as well, i.e.

$$\sum_{i=1}^{N} \frac{\Omega_{a_i}}{\Omega_{\text{DM}}} \lesssim 1 \,. \tag{6.41}$$

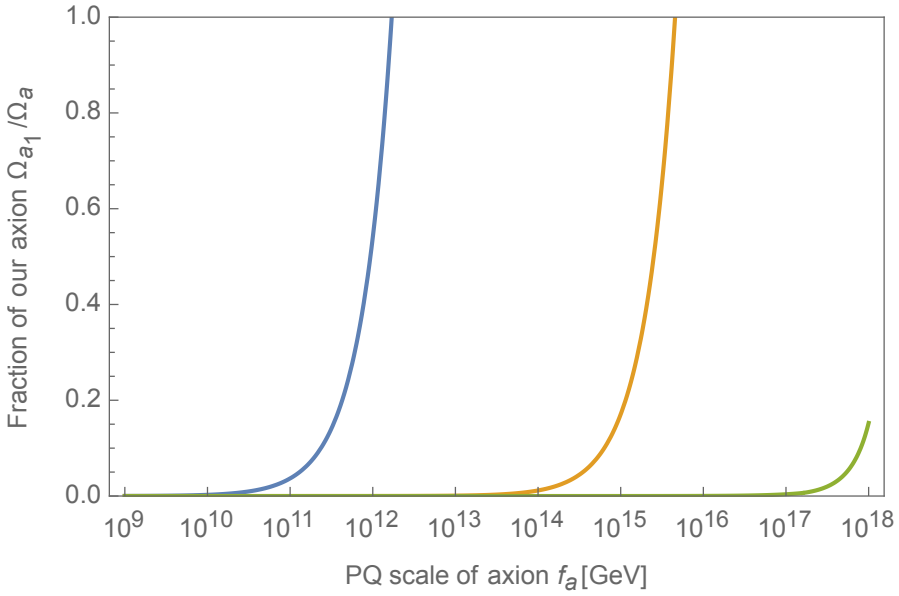

Figure 6.2: The fraction of our axion energy density with respect to the total axion energy density in the case when the axions make up all the dark matter. For larger f_a our axion is dominating, while for lower f_a the axions from dark sectors dominate.

This results in the following inequality for the viable parameter space,

$$N \lesssim 10^2 \left(\frac{10^{12}\text{GeV}}{f_a}\right)^{3/2} \left(\frac{1}{\theta_i^{\text{ini}}}\right)^2 \times \left[1 - 0.54 \left(\frac{f_a}{10^{12}\text{GeV}}\right)^{\frac{7}{6}} \left(\frac{\theta_1^{\text{ini}}}{1}\right)^2\right] . \tag{6.42}$$

We illustrate the viable regions in the N - f_a plane for different values of θ_i^{ini} in Figure 6.1. The thick lines indicate the combinations that result in the axions constituting all the dark matter, corresponding to the equality in (6.41). For example, along the blue line in the plot, the entire dark matter is composed of our axion when $f_a \sim 10^{12}$GeV, whereas for $f_a \sim 10^9$GeV essentially the $N \sim 10^6$ axions from the dark sectors make up the dark matter. A similar behavior is observed for the other depicted values of θ_i^{ini}.

We can quantify this by calculating the fraction of our axion along these lines, which we depict in Figure 6.2. There we also see that for a fixed θ_i^{ini}, lower f_a values result in a dominant contribution from dark sector axions, while larger f_a values lead to a dominant contribution from our axion.

Let us briefly explore the range of initial misalignment angles. The value of θ_i^{ini} hinges on whether the PQ symmetry undergoes a break either during or after inflation. If the break occurs post-inflation, all conceivable values of θ_i^{ini} manifest within today's Hubble patch for each sector. Consequently, averaging over this uniform distribution yields $\theta_i^{\text{ini}} = \pi/\sqrt{3}$ for all i.

When the PQ symmetry breaks during inflation, the initial misalignment angle becomes, in principle, an arbitrary condition. Opting for $\theta_i^{\text{ini}} \sim \mathcal{O}(1)$ appears reasonable in the absence of a specific explanation for special initial conditions. However, these conditions emerge naturally when QCD becomes robust during inflation, resulting in $\theta_i^{\text{ini}} \ll 1$ as demonstrated by Dvali [186] (also explored in [192, 193] for concrete implementations).

If such a phase or a comparable mechanism operates in each sector, the parameter space would extend to $f_a \gg 10^{12}$GeV and $N \gg 10^6$. It is crucial to note that for a given N, the PQ scale is upper-bounded by (6.42), depicted as a red dashed line in Figure 6.1.

The presence of such a phase in each sector could potentially permit $N > 10^6$, but the question arises as to whether this is sufficient to address the Hierarchy problem. As discussed earlier, having approximately $N \sim 10^{32}$ copies of the SM would offer a solution to the hierarchy problem. However, examining Figure 6.1 or equivalently considering (6.42), achieving this large number necessitates $f_a \ll 10^9$GeV along with an early phase of strong QCD.

This requirement clashes with the lower bound on the PQ scale derived from astrophysical considerations in our sector, specifically $f_a \gtrsim 10^9$GeV. At first glance, this seems to rule out a large number of exact SM copies as a viable solution for the hierarchy problem. Nevertheless, there are innovative proposals, such as the clockwork mechanism [194, 195], that enable the decoupling of the PQ scale from the suppression factor of the couplings. This potential separation would make the part of the parameter space addressing the hierarchy problem feasible.

Misalignment: Pure YM Dark Sector

To conclude, let us examine the scenario where each dark sector is grounded in a pure YM group $\text{SU}_i(N_C)$. The key distinction from the case with exact SM copies lies in the absence of light quarks. In the absence of light quarks, traditional chiral perturbation techniques become inapplicable for calculating the zero-temperature mass of the axion. Instead, alternative methods, such as large N_c methods, would need to be employed for determining the axion mass in this context.We use as an approximation for the axion mass the

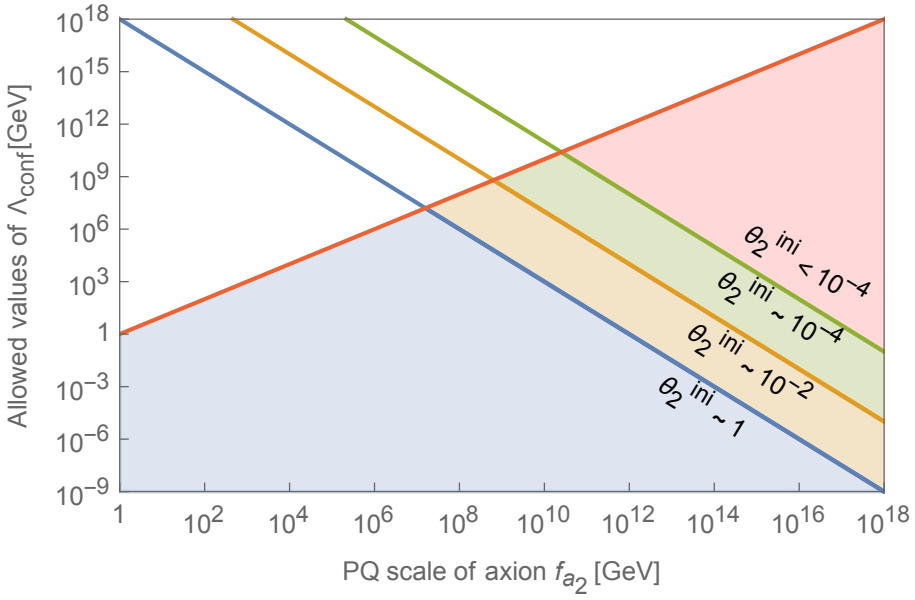

Figure 6.3: The allowed region for a single dark, pure YM sector with confinement scale Λ_{conf}, axion scale f_{a_2}, and no intersector interactions. Minimality favors $\theta_2^{\text{ini}} \sim 1$, since in this scenario there is no need for additional physics that results in a small misalignment angle. The red line represents the perturbative unitarity bound $\Lambda_{\text{conf}} \lesssim f_{a_2}$.

extrapolated result of the dilute instanton gas at finite temperatures [189],

$$m_{a_i}(T^i) \equiv \frac{(\Lambda^i_{\text{conf}})^2}{f_{a_i}} \begin{cases} \left(\frac{\Lambda^i_{\text{conf}}}{T^i}\right)^4 & : T^i > \Lambda^i_{\text{conf}} \,, \\ 1 & : T^i \lesssim \Lambda^i_{\text{conf}} \,, \end{cases} \tag{6.43}$$

where $\Lambda_{\text{conf},i}$ denotes the different confinement scales of the dark sectors and the factor of β was dropped due to the absence of light quarks. Unlike the scenario with exact Standard Model copies, the $\Lambda_{\text{conf},i}$ in this case are free parameters that, in principle, can be even smaller than the temperatures within the dark sectors. Consequently, the dark sector axion can potentially be generated with an essentially flat potential, albeit at the cost of requiring very low confining temperatures. In the subsequent discussion, we will exclusively focus on the scenario where the dark axions are created with their zero-temperature mass.

From there the calculation is vastly the same as in the exact SM case.

The oscillations in the dark sectors commence at

$$T_{\mathrm{osc},i} \sim \Lambda_{\mathrm{conf}}^{i} \left(\frac{M_P}{3 f_{a_i}}\right)^{\frac{1}{2}} ,$$

which results in the final dark sector density of

$$\frac{\Omega_{a_i}}{\Omega_{\mathrm{DM}}} \sim 10^{-18} \left(\frac{\Lambda_{\mathrm{conf}}^{i}}{\mathrm{GeV}}\right) \left(\frac{\theta_i^{\mathrm{ini}}}{1}\right)^2 \left(\frac{f_{a_i}}{\mathrm{GeV}}\right)^{\frac{3}{2}} . \tag{6.44}$$

Let us discuss the parameter space for the particularly interesting case of a single, pure YM sector, i.e. $N = 2$ with $i = 2$ being the dark sector. To simplify the notation, we define $\Lambda_{\mathrm{conf}}^{i=2} \equiv \Lambda_{\mathrm{conf}}$. For the dark sector axion to not result in an abundance of dark matter, we find

$$\Lambda_{\mathrm{conf}} \lesssim 10^{18}\mathrm{GeV} \left(\frac{1}{\theta_2^{\mathrm{ini}}}\right)^2 \left(\frac{\mathrm{GeV}}{f_{a_2}}\right)^{\frac{3}{2}} , \tag{6.45}$$

where the equality is valid when the dark axion makes up all the dark matter. Furthermore, to ensure perturbative unitarity in the dark sector, we must have

$$\Lambda_{\mathrm{conf}} \lesssim f_{a_2} . \tag{6.46}$$

This arises from the necessity for the axion's quartic self-interaction to remain in the weak coupling regime. The viable region is illustrated in Figure 6.3. If the dark sector axion is intended to constitute the dark matter, it becomes apparent that for Λ_{conf} to be below the Planck scale, the dark sector PQ scale must satisfy $f_{a_2} \gtrsim 1\mathrm{GeV}$. This requirement is further elevated for smaller values of θ_2^{ini}. Conversely, for f_{a_2} to be below the Planck scale, the dark confinement scale must satisfy $\Lambda_{\mathrm{conf}} \gtrsim 1\mathrm{eV}$. This minimum value also increases for smaller values of θ_2^{ini}.

It is important to note that the region where $\theta_2^{\mathrm{ini}} \sim 1$ is favored by minimality within the dark sector, as extremely small misalignment angles would necessitate the introduction of new physics [186, 193]. Without a discrete symmetry linking Λ_{conf} and f_{a_2} to their counterparts in our sector, there is no compelling reason to introduce new physics to achieve minuscule misalignment angles.

Remarkably, in the context of the two-form realization where a value of $f_{a_2} \sim M_P$ is strongly favored, this minimality argument leads to the dark confinement scale being $\Lambda_{\mathrm{conf}} \sim 1\mathrm{eV}$.

Isocurvature Perturbations

In scenarios where one of the PQ symmetries is broken during (or before) inflation and remains unbroken afterward, the associated axion field experiences quantum perturbations. Let us express the axion fields as $\theta_i = \langle\theta_i\rangle + \delta\theta_i$, where $\langle\theta_i\rangle = \theta_i^{\rm ini}$, and $\delta\theta_i$ represents the quantum perturbations. These fulfill $\langle\delta\theta_i\rangle = 0$ and have a standard deviation of

$$\sigma_{\theta_i} \sim \sqrt{\langle\delta\theta_i^2\rangle} \sim \frac{H}{2\pi f_{a_i}} \,. \tag{6.47}$$

Additionally, if none of the axions plays a role in driving inflation, the fluctuations associated with them will be of isocurvature type rather than adiabatic. As isocurvature perturbations leave a distinct signature in the temperature and polarization fluctuations of the CMB, they impose constraints on the parameter space of the axions.

There might be a concern that in the presence of multiple axions, the cumulative effect of isocurvature perturbations could significantly amplify the constraint, making it more stringent. However, it can be demonstrated that this is not necessarily the case, despite the additive nature of the contributions.

Assuming the perturbations to be normal distributed in the regime of small θ_i, where anharmonic corrections of the potentials can be ignored, the collective amplitude of the axions isocurvature fluctuations is given by [196]

$$\begin{aligned}\Delta_a(k_0) &= \frac{\delta\Omega_{\rm DM}}{\Omega_{\rm DM}} = \frac{\sum_i \Omega_{a_i}}{\Omega_{\rm DM}} \frac{\delta \ln \Omega_{a_i}}{\delta\theta_i^{\rm ini}} \sigma_{\theta_i} \\ &= \sum_i \frac{\Omega_{a_i}}{\Omega_{\rm DM}} \frac{H_{\rm I}}{\pi\theta_i^{\rm ini} f_{a_i}} \,,\end{aligned} \tag{6.48}$$

where $\theta_i^{\rm ini} \ll \sigma_{\theta_i}$ was used. The latest experimental bound on uncorrelated isocurvature perturbations by Planck is [36]

$$\beta(k_0) \equiv \frac{\Delta_a^2(k_0)}{\Delta_{\mathcal{R}}^2(k_0) + \Delta_a^2(k_0)} < 0.038 \quad \text{at } 95\% \text{ CL} \,, \tag{6.49}$$

where $k_0 = 0.050 \text{Mpc}^{-1}$. This can be translated to a constrain on $H_{\rm I}$,

$$H_{\rm I} \lesssim 10^7 \text{GeV} \sum_i \frac{\Omega_{\rm DM}}{\Omega_{a_i}} \left(\frac{f_{a_i}}{10^{12}\text{GeV}}\right) \left(\frac{\theta_i^{\rm ini}}{1}\right) \,. \tag{6.50}$$

For both models at hand, namely a single dark YM sector and N exact SM copies, the generated isocurvature perturbations are either dominated by our sector or the dark sector(s).

For the former, if the dark matter is dominated by the axion from the dark sector, we can express the bound on $H_{\rm I}$ in terms of the dark confinement scale by using the equality of (6.45) to eliminate $\theta_2^{\rm ini}$. This results in

$$H_{\rm I} \lesssim 10^7 {\rm GeV} \left(\frac{f_{a_i}}{10^{12}{\rm GeV}}\right)^{\frac{1}{4}} \left(\frac{1{\rm GeV}}{\Lambda_{\rm conf}}\right)^{\frac{1}{2}} . \tag{6.51}$$

For a two-form axion originating from a dark sector, specifically with $f_{a_2} \sim M_{\rm P}$ and the minimal conceivable dark confinement scale $\Lambda_{\rm conf} \sim$ eV, the constraint is alleviated to $H_{\rm I} \lesssim 10^{13}$GeV. This implies that such an axion is essentially unaffected by an isocurvature constraint.

For N exact SM copies, when the dark matter is collectively composed by the axions from the copies, i.e. $\sum_i \Omega_{a_i} \sim \Omega_{\rm DM}$, using (6.42) to eliminate the initial misalignment angles in (6.50) yields

$$H_{\rm I} \lesssim 10^7 {\rm GeV} \left(\frac{f_{a_i}}{10^{12}{\rm GeV}}\right)^{\frac{1}{4}} \left(\frac{10}{\sqrt{N}}\right) . \tag{6.52}$$

We observe that for moderate values of $N \sim 10^2$, the bound remains relatively unaffected. Conversely, for values necessary to address the Hierarchy problem, namely $N \sim 10^{32}$ and $f_a \sim$ TeV, the bound seemingly tightens to $H_{\rm I} \lesssim 10^{-10}$GeV. However, in this scenario, both the dark confinement scale and the axion mass surpass the inflationary Gibbons-Hawking temperature $T_{\rm I} \sim H_{\rm I}$.

This signifies that the dark Yang-Mills sector becomes strongly coupled during inflation. Consequently, the axion acquires a significant mass, rendering the conditions necessary for the development of isocurvature perturbations no longer satisfied. Of course, this requires avoiding the astrophysical bounds on f_a by a mechanism such as clockworking (see discussion at the end of Section 6.2.1).

6.2.2 Kinetic Mixing between Axions

Kinetic Mixing as Intersector Interaction

In this section, we delve into non-gravitational interactions between sectors by reintroducing $\mathcal{L}_{\rm mix}$ in (6.27). For now, we specifically center our attention on the case of N exact Standard Model copies. In the absence of additional axions, the conceivable renormalizable interactions in this model, aligning with gauge-, Lorentz-, and the underlying discrete symmetry, encompass photon kinetic mixing, a Higgs portal coupling, and neutrino mass mixing.

Additionally, at the non-renormalizable level, other interactions such as neutron oscillations become feasible. Extensive discussions on the implications of these interactions can be found in the literature (see [197] for a review). As our primary focus lies elsewhere, we refrain from delving further into the intricacies of these interactions in this discussion. Instead, we focus on axion kinetic mixing, which in the model under consideration is described by

$$\mathcal{L}_{\text{mix}} = \epsilon \sum_{i \neq j} \partial_\mu a^i \partial^\mu a^j \ , \tag{6.53}$$

where ϵ parametrizes the kinetic mixing strength. A crucial implication of kinetic mixing between our visible and hidden sectors is the potential establishment of thermal equilibrium between the sectors. To avoid inconsistencies with nucleosynthesis or an excessive amount of dark matter particles, thermal equilibrium must not be achieved before BBN. This typically imposes a constraint on the strength of the kinetic mixing.

It is noteworthy that the axions produced by misalignment are non-thermal, meaning they cannot transfer heat between the sectors via axion-axion interactions to thermally equilibrate any of the sectors. However, this does not hold true for other types of interactions, which may lead to a constraint on the kinetic mixing parameter ϵ to prevent reheating of the dark sectors before nucleosynthesis. Conducting a thorough analysis of such scenarios, which may require additional assumptions, extends beyond the scope of this paper. Therefore, we treat ϵ as a phenomenologically free parameter in the subsequent discussions.

The way in which axion kinetic mixing can emerge in the low energy effective theory depends on the specific implementation of the axion. In the standard implementation of the axion via the KSVZ model a singlet Higgs is added to make the axion invisible. Denoting this singlet in each sector as Φ_i allows for the following dimension six Higgs portal couplings between the sectors

$$\mathcal{L}^{\text{UV}}_{\text{mix}} = \frac{1}{M^2} \sum_{i \neq j} (\Phi_i^\dagger \partial_\mu \Phi_i)(\Phi_j \partial^\mu \Phi_j^\dagger) + \text{h.c.} \ , \tag{6.54}$$

where M is some cut-off scale. The singlets acquire the VEVs $f_{a_i} \equiv f_a$ via a proper scalar potential that spontaneously breaks the $\text{U}(1)_{\text{PQ}}$ symmetries. This results in the kinetic mixing described in (6.53) with

$$\epsilon \equiv \frac{f_a^2}{2M^2} \ . \tag{6.55}$$

A diagram stemming from such an operator is illustrated in Figure 6.4. Analogous operators that lead to axion kinetic mixing are also conceivable in

DFSZ-type models, which necessitate extra Higgs doublets in addition to the singlet.

Although we currently neglect the phenomenological constraint on ϵ arising from the imperative avoidance of dark sector thermalization before BBN, it is crucial to recognize that ϵ is still subject to consistency limitations stemming from unitarity.The operators in (6.54) already at tree-level put a unitarity constraint:

$$\epsilon \lesssim \frac{1}{\sqrt{N}} \,. \tag{6.56}$$

However, the bound on ϵ is much more severe. Since it describes an intersector interaction coupling at momentum transfer $q \sim f_a$ among all species, it has to fulfill the bound

$$N_s < \frac{1}{\alpha(q)}, \tag{6.57}$$

where N_s is the number of inter-coupled species and α a coupling constant evaluated at q which was shown in [198, 199]. This gives

$$\epsilon \lesssim \frac{1}{N} \,. \tag{6.58}$$

In the alternative two-form implementation of the axion, axion kinetic mixing appears via non-diagonal mass terms of three-form action,

$$\mathcal{L}_{\text{mix}} \sim \sum_{i \neq j} \left(C^i_{\mu\nu\rho} - \partial_{[\mu} B^i_{\nu\rho]}\right) \left(C^j_{\mu\nu\rho} - \partial_{[\mu} B^j_{\nu\rho]}\right) \,. \tag{6.59}$$

Mixing of this kind is not prohibited by gauge symmetries and can have diverse origins, one of which is virtual black hole exchange [20]. However, there could be alternative mechanisms leading to such operators. Notably, the appearance of these operators is only feasible for $i \neq j$ if they are suppressed by powers of M_{P}^{-1}. This suppression arises from the fact that micro-black holes cannot be universally coupled, mandating gravitational suppression of inter-sector transitions at the fundamental level.

In the remainder of this section, we will study the consequences of the axion kinetic mixings in the pseudo-scalar formulation. We will stay agnostic of their origin, but use the unitarity bound described by (6.58).

Modification of Axion Physics for SM Copies

The introduction of the additional term in the Lagrangian requires a change of basis to express it in a canonical form. Consequently, a mismatch arises

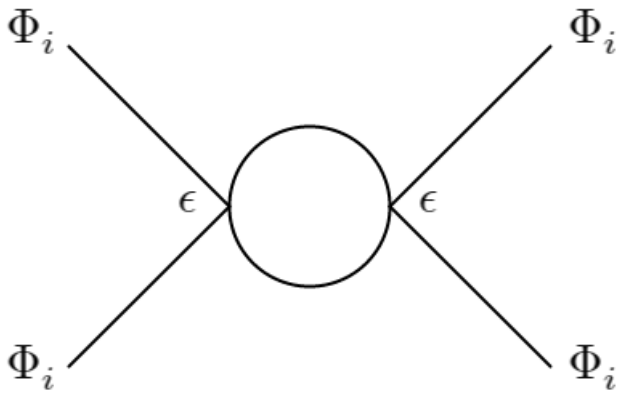

Figure 6.4: Loop induced by the operators in (6.54). Each vertex contributes the effective coupling $\Delta p^2/M^2$, but for maximum momentum transfers of order f_a the effective coupling becomes ϵ.

between the "sector basis", corresponding to the labels of the species, and the "canonical kinetic basis", where the propagator is in canonical form. The objective is to establish the relationship between these two bases.

It is worth noting that a similar scenario unfolds in the SM's neutrino sector. There, the interaction terms are diagonal in the flavor basis. However, in this basis, the mass matrix of neutrinos becomes off-diagonal, leading to phenomena such as neutrino oscillations. In our case, the mismatch emerges between the canonical kinetic basis and the sector basis.

The first step is to express the kinetic part in (6.53) as

$$\mathcal{L} \supset \begin{pmatrix} \partial_\mu a_1 \\ \vdots \\ \vdots \\ \partial_\mu a_N \end{pmatrix}^T \begin{pmatrix} 1 & \epsilon & \dots & \epsilon \\ \epsilon & 1 & \ddots & \vdots \\ \vdots & \ddots & \ddots & \epsilon \\ \epsilon & \dots & \epsilon & 1 \end{pmatrix} \begin{pmatrix} \partial_\mu a_1 \\ \vdots \\ \vdots \\ \partial_\mu a_N \end{pmatrix} . \tag{6.60}$$

This matrix appears due to the permutation symmetry among the copies also in other cases, which have been studied in [17]. We can rewrite the matrix, which we shall call K from now on, in the following way,

$$K = \begin{pmatrix} 1-\epsilon & 0 & \dots & 0 \\ 0 & 1-\epsilon & \ddots & \vdots \\ \vdots & \ddots & \ddots & 0 \\ 0 & \dots & 0 & 1-\epsilon \end{pmatrix} + \epsilon \begin{pmatrix} 1 & \dots & 1 \\ \vdots & \ddots & \vdots \\ 1 & \dots & 1 \end{pmatrix} . \tag{6.61}$$

The problem reduces then to the diagonalization of a matrix of just ones. The transformation matrix S that diagonalizes K is

$$S = \begin{pmatrix} 1 & 1 & 1 & \dots & 1 \\ 1 & -1 & 0 & \dots & 0 \\ 1 & 0 & -1 & \ddots & \vdots \\ \vdots & \vdots & \ddots & \ddots & \vdots \\ 1 & 0 & \cdots & 0 & -1 \end{pmatrix} . \tag{6.62}$$

The first row gives rise to the eigenstate of the form,

$$\tilde{a}_L = \frac{1}{\sqrt{N}} a_1 + \sqrt{\frac{N-1}{N}} a_h \ , \tag{6.63}$$

where we have introduced the notation

$$a_h = \frac{1}{\sqrt{N-1}} \sum_{i=2} a_i \ , \tag{6.64}$$

due to later convenience. The eigenstate $\tilde{a}_H$ corresponds to the eigenvalue of $1 + (N-1)\epsilon$. Because the matrix S is not a unitary matrix we still have to find a convenient basis.

From all other rows, we see that we have $N-1$ degenerate eigenstates v_i of the eigenvalue $1-\epsilon$. These v_i´s are the columns of S. Due to this degeneracy, we can reduce the $N \times N$ problem to a 2×2 problem by defining a superposition of these degenerate eigenstates. This looks like

$$\tilde{a}_H = \frac{1}{N-1} \sum_i v_i = a_1 - \frac{1}{\sqrt{N-1}} a_h \ , \tag{6.65}$$

and again has the eigenvalue $1-\epsilon$. After normalization this becomes

$$\tilde{a}_H = \sqrt{\frac{N-1}{N}} a_1 - \frac{1}{\sqrt{N}} a_h \ . \tag{6.66}$$

We see that $\tilde{a}_H$ is a collective expression made out of all former a_i´s. Using expressions (6.66) and (6.63), we find a_1 expressed in the canonical kinetic basis

$$a_1 = \sqrt{\frac{N-1}{N}} \tilde{a}_H + \frac{1}{\sqrt{N}} \tilde{a}_L \ . \tag{6.67}$$

It is important to note that the designation of what we define as species one is entirely arbitrary, and this holds true for every $i = 1, ..., N$. This stems from the fact that the parameter ϵ is the same across all sectors. Consequently,

the 2×2 matrix connecting a_1 and a_h with $\tilde{a}_H$ and $\tilde{a}_L$ becomes a unitary matrix.

Expressing (6.60) in terms of $\tilde{a}_L$ and $\tilde{a}_H$, the mixing vanishes, and each term is now multiplied by the corresponding eigenvalue. In order to have canonical kinetic terms, the states $\tilde{a}_L$ and $\tilde{a}_H$ need to be redefined by

$$\tilde{a}_H \to \frac{1}{\sqrt{1-\epsilon}}\tilde{a}_H \ , \quad \tilde{a}_L \to \frac{1}{\sqrt{1+(N-1)\epsilon}}\tilde{a}_L \ . \tag{6.68}$$

One effect of this redefinition is that the mass part in the Lagrangian is changed to

$$\mathcal{L}_{\text{mass}} \sim \begin{pmatrix} \tilde{a}_H \\ \tilde{a}_L \end{pmatrix}^T \begin{pmatrix} \frac{m_a^2}{1-\epsilon} & 0 \\ 0 & \frac{m_a^2}{1+(N-1)\epsilon} \end{pmatrix} \begin{pmatrix} \tilde{a}_H \\ \tilde{a}_L \end{pmatrix} \ . \tag{6.69}$$

with m_a being the mass induced by the PQ-mechanism. The introduction of kinetic mixing results in a mass splitting among the axions. Specifically, $N-1$ axions become degenerate, while one light axion emerges with its mass suppressed by the number of copies. In essence, the kinetic mixing of multiple axion copies gives rise to two distinct detectable axion states characterized by different masses. The relation between these masses is

$$\frac{m_L}{m_H} = \sqrt{\frac{1-\epsilon}{1+(N-1)\epsilon}} \sim \frac{1}{\sqrt{2}} \ , \tag{6.70}$$

where for the approximation we assumed natural values of ϵ with respect to the unitarity bound, i.e. $\epsilon \sim 1/N$, and $N \gg 1$.

With the relation between the species basis and the canonical kinetic basis, we can turn to the phenomenological implications of this model. Due to the Goldstone nature of the axion, its lowest order couplings to fermions and gauge bosons have the generic form

$$g_{ao} a_1 \mathcal{O} \ , \tag{6.71}$$

where the whole UV dependency is encoded in g_{ao}. After the diagonalization and field redefinition of (6.68), the coupling becomes,

$$g_{ao}\left(\sqrt{\frac{N-1}{N}}\frac{1}{\sqrt{1-\epsilon}}\tilde{a}_H + \frac{1}{\sqrt{N}}\frac{1}{\sqrt{1+(N-1)\epsilon}}\tilde{a}_L\right)\mathcal{O} \ . \tag{6.72}$$

We observe that by having N kinetically mixed axions, our sector couples to N axions instead of one. These N axions come in two categories: $N-1$

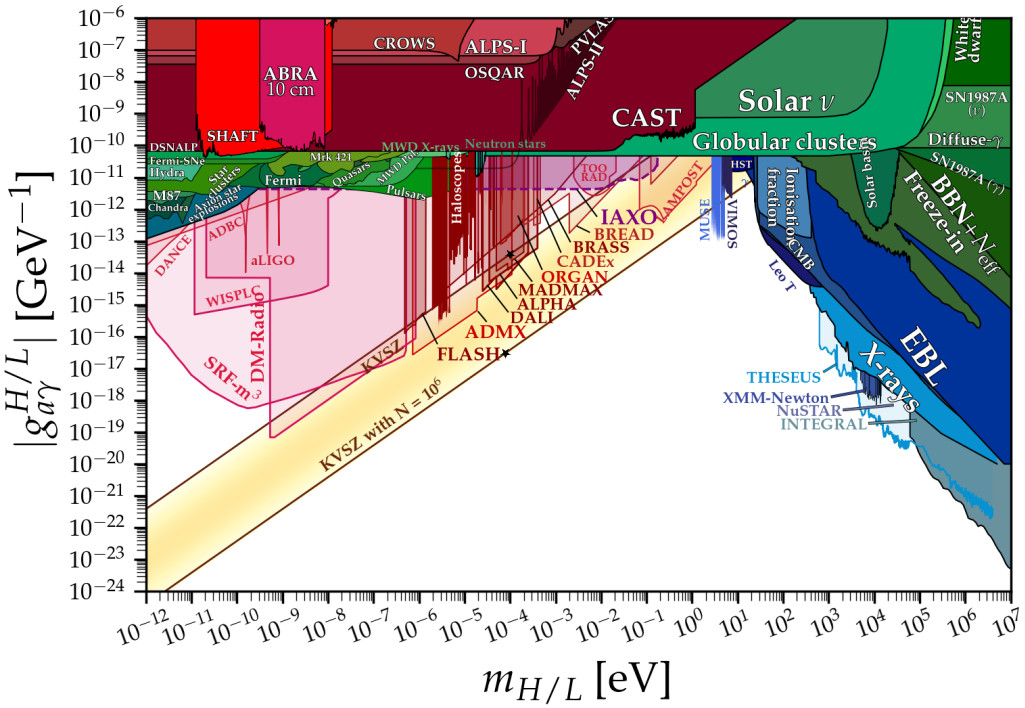

Figure 6.5: Viable axion-photon couplings for the light axion state (yellow band), which arises from equal kinetic mixing of axions from N sectors. Current bounds and predicted sensitivities of future experiments are depicted in different colors. The parameter space for $N \lesssim 10$ will be probed by future experiments. The yellow band is not to be confused with the bands from [158], which include the set of DFSZ-type or KSVZ-type models. The two stars represent a situation when future experiments measure one axion (the upper star) and where we expect the second axion (the lower star). This plot was created with the help of the software [200].

axions ($\tilde{a}_H$) that behave exactly the same, and one special axion ($\tilde{a}_L$). The single axion coupling g_{ao} gets modified by one of the following factors,

$$f_H(N,\epsilon) \equiv \sqrt{\frac{N-1}{N}}\frac{1}{\sqrt{1-\epsilon}} \sim 1\,, \tag{6.73}$$

$$f_L(N,\epsilon) \equiv \frac{1}{\sqrt{N}}\frac{1}{\sqrt{1+(N-1)\epsilon}} \sim \frac{1}{\sqrt{2N}}\,, \tag{6.74}$$

where for the approximation we again used the natural value of ϵ and $N \gg 1$. We observe that the coupling of $\tilde{a}_H$ remains approximately constant compared to the single axion case, while $\tilde{a}_L$ experiences a suppression. In summary, in addition to the previously mentioned mass splitting into two distinct

physical states, these states also exhibit differing couplings characterized by the factors f_H and f_L.

For the axion-photon coupling, this modification results in

$$\begin{aligned} g_{a\gamma}^{H/L} &= \frac{\alpha}{2\pi f_a}\left(\frac{\mathcal{E}}{\mathcal{N}} - 1.92\right) f_{H/L}(N,\epsilon) \\ &= \frac{\alpha}{2\pi f_a} C_{a\gamma} f_{H/L}(N,\epsilon)\ , \end{aligned} \tag{6.75}$$

where $\mathcal{E}$ and $\mathcal{N}$ are the electromagnetic and QCD anomaly coefficients, respectively, and α is the electromagnetic fine-structure constant. In the second line, we defined the model dependent factor $C_{a\gamma}$ for compactness. In order to bring this to a more useful form, we express f_a in terms of the physical mass states from (6.69), i.e.

$$m_a = \frac{\sqrt{\Lambda_{\rm QCD}^3 m_u}}{f_a} = \begin{cases} \sqrt{1-\epsilon}\ m_H & : \text{for } \tilde{a}_H\ , \\ \sqrt{1+(N-1)\epsilon}\ m_L & : \text{for } \tilde{a}_L. \end{cases} \tag{6.76}$$

After plugging in (6.73) and (6.74), this results in

$$g_{a\gamma}^H = \frac{\alpha}{2\pi}\frac{C_{a\gamma}}{\sqrt{\Lambda_{\rm QCD}^3 m_u}}\sqrt{\frac{N-1}{N}}\ m_H \tag{6.77}$$

$$g_{a\gamma}^L = \frac{\alpha}{2\pi}\frac{C_{a\gamma}}{\sqrt{\Lambda_{\rm QCD}^3 m_u}}\sqrt{\frac{1}{N}}\ m_L\ . \tag{6.78}$$

For a specific case, let us examine the axion-photon couplings in the context of KSVZ axions. Figure 6.5 illustrates the potential couplings for $N < 10^6$. Although the projected sensitivities of future experiments extend into the predicted band, it is evident that a significant portion of the parameter space may not be covered in the near future. Nonetheless, it is crucial to consider that the heavy axion, which couples in a manner similar to a scenario with just one axion (with a maximal enhancement of approximately ~ 1.3), has a realistic chance of being discovered soon.

In the context of multiple axions, the next step following the discovery of the ordinary axion would be to search for a second light weakly coupled state. Despite the apparent challenge posed by the large available parameter space, it is important to recognize that there exists a clear functional dependence among the couplings and masses between the heavy and light states. For instance, suppose an axion has been discovered, leading to known values for m_H and $g_{a\gamma}^H$. In the expression for the coupling of the light axion (6.78), we can replace m_L with m_H using (6.70). We can then eliminate N by plugging

in the expression for the heavy axion (6.77), yielding an expression for $g^L_{a\gamma}$ in terms of experimentally known parameters,

$$g^L_{a\gamma} \sim \frac{\alpha C_{a\gamma} m_H}{2\pi\sqrt{\Lambda^3_{\mathrm{QCD}} m_u}} \sqrt{1 - \left(\frac{2\pi g^H_{a\gamma}\sqrt{\Lambda^3_{\mathrm{QCD}} m_u}}{\alpha C_{a\gamma} m_H}\right)^2} \,, \tag{6.79}$$

This means that after measuring the coupling and the mass of the first axion, the properties of the second are uniquely determined.

Modification of Axion Physics for one YM Sector

Another interesting case for kinetic mixing is the scenario of a single YM sector with PQ scale f_{a_2} and confinements scale Λ_{conf}, as discussed in Section 6.2.1. The procedure of analyzing the kinetic mixing remains unchanged and $N = 2$ in this case.

The coupling to our photons after the step of choosing the proper kinetic basis reads as

$$g^{L/H}_{a\gamma} = \frac{\alpha}{2\pi f_a} C_{a\gamma} \frac{1}{\sqrt{2}} \frac{1}{\sqrt{1 \pm \epsilon}} \,. \tag{6.80}$$

Since Λ_{conf} and f_{a_2} differ from the analog quantities in our sectors, the axion masses differ as well. This leads to a non-diagonal mass matrix,

$$\begin{aligned} \mathcal{L}_{\mathrm{mass}} &\sim m^2_{a_1} a_1 a_1 + m^2_{a_2} a_2 a_2 \\ &\sim \begin{pmatrix} \tilde{a}_H \\ \tilde{a}_L \end{pmatrix}^T \begin{pmatrix} \frac{m^2_{a_1}+m^2_{a_2}}{1-\epsilon} & \frac{m^2_{a_1}-m^2_{a_2}}{\sqrt{1-\epsilon}\sqrt{1+\epsilon}} \\ \frac{m^2_{a_1}-m^2_{a_2}}{\sqrt{1-\epsilon}\sqrt{1+\epsilon}} & \frac{m^2_{a_1}+m^2_{a_2}}{1+\epsilon} \end{pmatrix} \begin{pmatrix} \tilde{a}_H \\ \tilde{a}_L \end{pmatrix} . \end{aligned} \tag{6.81}$$

As usual, this mass term must be diagonalized by an orthogonal matrix with the mixing angle

$$\theta = \frac{1}{2} \arctan\left(\frac{m^2_{a_1} - m^2_{a_2}}{m^2_{a_1} + m^2_{a_2}} \frac{\sqrt{1-\epsilon^2}}{\epsilon}\right) \,, \tag{6.82}$$

leading to the eigenvalues,

$$m_{H/L} = \frac{m^2_{a_1} + m^2_{a_2} \pm (m^2_{a_1} - m^2_{a_2}) \sqrt{1 + \frac{4\epsilon^2}{\left(\frac{m_{a_1}}{m_{a_2}} - \frac{m_{a_2}}{m_{a_1}}\right)^2}}}{1 - \epsilon^2} \,. \tag{6.83}$$

Expressing a_H and a_L in terms of the final eigenstates A_H and A_L, the axion-photon coupling from (6.80) becomes

$$\begin{aligned} g^{H/L}_{A\gamma} &= \frac{\alpha}{4\pi f_{a_1}} C_{a\gamma} \left(\frac{\cos\theta}{\sqrt{1+\epsilon}} \pm \frac{\sin\theta}{\sqrt{1-\epsilon}}\right) \\ &\equiv \frac{\alpha}{4\pi f_{a_1}} C_{a\gamma} \kappa_{H/L} \,. \end{aligned} \tag{6.84}$$

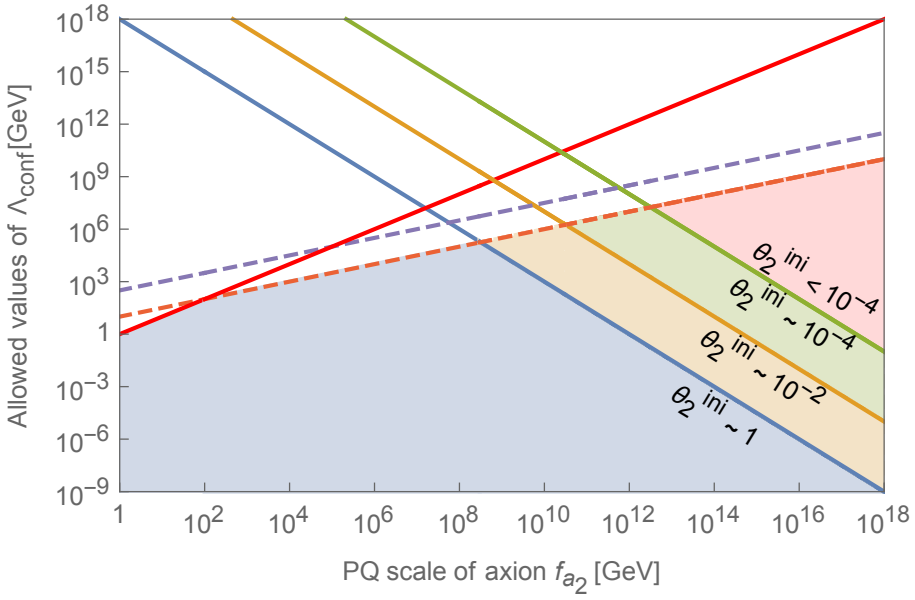

Figure 6.6: Same as Figure. 6.3 but with axion kinetic mixing. The mixing results in both axion states being able to decay into our photons. Requiring the stability of the heavy axion state results in the viable region to lie below the dashed orange line ($f_a \sim 10^{12}$GeV) or below the dashed purple line ($f_a \sim M_{\rm P}$).

Using this coupling and the masses, given in (6.83), the lifetime of the axions is given by

$$\tau(A_{H/L} \to 2\gamma) = \frac{2^6\pi}{\left(g_{A\gamma}^{H/L}\right)^2 m_{H/L}} = \frac{2^{10}\pi^3}{\alpha^2 C_{a\gamma}^2}\frac{f_{a_1}^2}{\kappa_{H/L}^2 m_{H/L}^3} \,. \tag{6.85}$$

For the axion to serve as a component of dark matter, the lifetime (τ) of $A_{H/L} \to 2\gamma$ must exceed the age of the universe. This condition is reflected in the viable region depicted in Figure 6.6. It is noteworthy that the chosen value of $\epsilon \sim 1/2$ in this figure does not significantly impact the viable region; it remains essentially independent of ϵ.

The interpretation of this viable region is vastly unchanged from the discussion in Section 6.2.1. With kinetic mixing an additional upper bound of the dark confinement scale emerges. Consequently, if the dark sector axion makes up the dark matter, the confinement scale of the dark YM sector must be in the range

$$1\text{eV} \lesssim \Lambda_{\rm conf} \lesssim 10^{12}\text{GeV} \,. \tag{6.86}$$

6.3 Conclusions

In this chapter, we delved into the phenomenological implications of introducing axions to dark YM sectors. These axions are mandated by quantum gravitational arguments that elevate the strong CP problem to a consistency problem. Consequently, axions become essential components not only in QCD but also in every YM group [169, 162]. Our focus was on two models: N exact copies of the SM [15, 16] and a single pure YM sector.

Our initial requirement involved ensuring that the total axion density, considering contributions from all sectors, does not surpass the observed dark matter density. For N exact copies of the SM, utilizing the misalignment mechanism across all sectors results in a constrained range of viable N for a given PQ scale. Remarkably, the applicability of the misalignment mechanism remains intact even for very large values of N when the sectors are exceedingly dilute, as the mechanism is independent of the thermalization of the dark sectors.

In the case of a single pure YM sector, we established a relationship between the dark confinement scale and the PQ scale. Specifically, when requiring the dark sector axion to constitute the dark matter, the PQ scale does not surpass the Planck scale, provided the dark confinement scale satisfies $\Lambda_{\text{conf}} \gtrsim 1\text{eV}$ in the scenario with maximal misalignment. This minimal value increases for smaller initial misalignment angles.

Additionally, we demonstrated that the inclusion of extra axions does not necessarily impose a more stringent constraint on H_{I} concerning isocurvature fluctuations. Interestingly, both models reveal regions in the parameter space where the bound is essentially evaded. In the case of N exact Standard Model copies, the viable parameter space necessitates either a moderate number of copies, around $N \sim 10^2$, or a mechanism enabling smaller PQ scales.

Finally, we explored non-gravitational interactions between the dark sectors arising from axion kinetic mixing. We revealed the emergence of a mass splitting, resulting in $N-1$ degenerate states and one lighter state. Interestingly, the lighter state is approximately $1/\sqrt{2}$ times lighter and has couplings weaker by a factor of $1/\sqrt{N}$ compared to the heavier axion states. For N exact copies of the Standard Model, this enables the complete prediction of the light axion once the heavier one is discovered. In the case of a single Yang-Mills sector, the axion masses differ, potentially leading to the decay of the dark sector axion into photons. To ensure the stability of the axion as a dark matter candidate, an upper bound on the dark confinement scale emerges, requiring $\Lambda_{\text{conf}} \lesssim 10^{12}\text{GeV}$. This bound, in most parts of the parameter space, is stronger than the bound $\Lambda_{\text{conf}} \lesssim f_{a_2}$ derived from perturbative unitarity.

This work provides certain insights into the potential consequences of multiple axions. As mentioned earlier, the situation with multiple axions closely resembles the axiverse proposed by string theory [180]. However, in our case, the axions arise from quantum gravitational consistency in theories with numerous hidden YM groups. Given that hidden YM groups and multiple axions are predictions of string theory, exploring this connection further is a valuable pursuit. This connection can in principle also be applied to dark energy. If the dark energy is realized by quintessence [201, 202], it would suggest the existence of a non-trivial vacuum structure that needs to be eliminated by this scalar field. All in all, it seems that axions could play a more significant role in nature than initially anticipated.

Chapter 7

Summary and Outlook

In this work, I investigated how infrared signatures can arise from UV physics and could be testable in infrared experimental setups. We started with a well-known signature of that type namely $0\nu\beta\beta$ decay and examined the discovery probability of the next-generation experimental setups in different scenarios of cosmological probes of the neutrino mass sum. We concluded that the prospect of discovery for these experiments are heavily influenced by future results of cosmological experiments.

Then we adapted the same philosophy of $0\nu\beta\beta$ searches and asked if gravity could give rise to signatures in the infrared that could be testable by current experiments. We identified two candidate models namely ADD and the DR model. We discussed in chapter 3 that both models have an intrinsic mechanism that could explain the smallness of neutrino masses by using the fact that the right-handed mixing partner of the neutrino is uncharged under the SM gauge group and could therefore be spread out into an extra space may this be a physical space (extra dimensions) or an abstract space (many species).

Even though the mechanism for small neutrino masses is the same the concrete structure of the neutrino mass matrix is of course different in both theories. The extra-dimensional scenario has been discussed in depth by previous analyses both in theory and in experimental physics and is still an ongoing endeavor. The situation in the DR model on the other hand has not been discussed so far and with this work, my collaborators and I aimed to fill this gap.

First in chapter 3 I generalized the original one flavor analysis to a realistic 3 flavor scenario and gave a description how the DR model would manifest itself in neutrino oscillations and in violating unitarity of the PMNS matrix.

In chapter 4 I described how my collaborators and I put the DR model under an experimental test by performing a global fit of neutrino oscillation

and neutrino mass data. We gave the very first experimental constraints on the number of additional neutrino species which are of order $\mathcal{O}(100)$ for the IO hierarchy and $\mathcal{O}(30)$ for the NO hierarchy over a wide range of the second parameter of interest μ.

Another candidate for experiencing the influence of the extra space is the neutron. Like the neutrino does the neutron not carry a conserved charge of the SM. Therefore, the neutron like the neutrino can mix with hidden degrees of freedom. The situation in the literature between the ADD and DR model was inversed to the neutrino case. Even though discussed in the DR model, the possibility that the neutron could mix with an extra-dimensional fermion has not been discussed so far. We found out (chapter 5) that the effective operator for mixing with the KK tower of a fermion with a mass below the mass of the bounded neutron has to be at least suppressed by a scale of order 10^7GeV. This bound results from the neutron disappearance lifetime from matter. If the fermion is heavier than the bounded but not the free neutron the stability of matter is ensured and the operators are much less restricted. We found that ultra-cold neutron experiments that search for neutron oscillations are currently probing the parameter space motivated by the Hierarchy Problem. Due to the unique feature of the repetitive appearance of KK states one can hit oscillation resonances if one varies an external B field.

In chapter 6 we ask the question of how the introduction of multiple Yang-Mills groups as in the DR model can influence the phenomenology of the axions one has to introduce with every additional Yang-Mills group. We found that axion production via the misalignment mechanism gives us an upper bound on the number of possible additional Yang-Mills groups of $N < \mathcal{O}(10^6)$ in the most severe scenario. Simultaneously by allowing kinetic mixing among the additional axions, we found that two axion states arise that could be potentially measured. Their masses and mixing are modified compared to the one axion case and this allows us to outline how a potential measurement of one axion can pin down the position of the second axion in the parameterspace. A measurement of the second axion can be used to cross-check a multiple-axion scenario.

The take-home message of this work is that the nature of gravity can lead to new phenomena that manifest themselves even in low-energy experiments and not just at M_P which one would naively expect. Combining theoretical consideration with perusing the experimental tests of these theories can guide us to where to expect the true scale of Quantum Gravity.

Appendix A

Supporting Material to Kaluza-Klein Spectroscopy from Neutron Oscillations into Hidden Dimensions

A.1 Mass Splitting in KK Tower for Equal Size Extra Dimensions

In this appendix I follow closely the discussion of [4]. We show that for $N \geq 2$ with all radii equal to R, the mass splitting of the KK tower (around the neutron mass) is proportional to

$$\delta m \sim \frac{1}{R^2 m_n}. \tag{A.1}$$

This is correct for both the KK tower originating from a massless or a massive extra-dimensional fermion.

We estimate δm by calculating the mass difference between two special states $(k+1, \ldots, k+1)$ and $(k, \ldots, k)$ with masses $m_{k+1} \equiv \sqrt{N}(k+1)/R$ and $m_k \equiv \sqrt{N}k/R$, respectively and then dividing their mass difference by the number of states in between the two.

The mass difference between the two special states is

$$m_{k+1} - m_k = \frac{\sqrt{N}}{R}. \tag{A.2}$$

Now, we estimate the number of different levels in between them (i.e., ignoring the level degeneracies). That is, we want to find the number of

levels that fulfill

$$m_k < m_{k_1,\ldots,k_N} < m_{k+1}. \tag{A.3}$$

Using the expression (3.13) for the mass levels in the KK tower, this reduces to

$$Nk^2 < k_1^2 + \cdots + k_N^2 < N(k+1)^2. \tag{A.4}$$

For $N > 3$, we can express every integer as a sum of integer squares (This is actually a theorem: Lagrange theorem, see, e.g., [203].) This is also very accurate for $N = 3$, where we can express almost every integer as a sum of squares, as well as for $N = 2$ up to a log-factor [204]. Therefore, in all cases of our interest, the number of levels is essentially given by the number of integers in between the mass states

$$\#\text{mass} - \text{levels} = N(k+1)^2 - Nk^2 \approx 2Nk. \tag{A.5}$$

Thus, the mass splitting of the KK tower is

$$\delta m = \frac{m_{k+1} - m_k}{\#\text{mass} - \text{levels}} \approx \frac{1}{2\sqrt{N}Rk} = \frac{1}{2R^2 m_k}. \tag{A.6}$$

Now set $m_k \approx m_n$ and we get

$$\delta m \approx \frac{1}{2R^2 m_n}. \tag{A.7}$$

For $N \leq 3$, the above is essentially exact. For $N = 2$ the level spacing is less uniform but is an excellent approximation for averaged splitting.

Indeed, for $N = 2$, the number of states in between m_{k+1} and m_k is lower, because we cannot express every integer as a sum of two integer squares. The number of integers between 0 and x that can be expressed as a sum of two integer squares goes as $x/\sqrt{\log x}$ [204]. Hence, the number of integers we are looking for between x_1 and x_2 is proportional to

$$\frac{x_1}{\sqrt{\log x_1}} - \frac{x_2}{\sqrt{\log x_2}}. \tag{A.8}$$

For $x_1 = Nk^2$ and $x_2 = N(k+1)^2$ and $k \sim 10^{11}$ (remember $k \sim m_n R/\sqrt{2}$), this number is $0.42k \approx k/2$.

Thus, for $N = 2$, the mass splitting of the tower around $m_k \approx m_n$ is

$$\delta m \approx \frac{4}{R^2 m_n}. \tag{A.9}$$

For a massive bulk fermion with mass μ, we repeat the calculation with,

$$m_k^2 = \mu^2 + \frac{k_1^2}{R_1^2} + \cdots + \frac{k_N^2}{R_N^2}. \tag{A.10}$$

The mass-splitting between the two special states is

$$m_{k+1} - m_k \approx \frac{Nk}{R^2 m_k}\,. \tag{A.11}$$

For $N \geq 3$, the number of states in between the two special states is the same as in the massless case, #states $\approx 2Nk$. Correspondingly, so is the level-splitting,

$$\delta m \approx \frac{1}{2R^2 m_n}. \tag{A.12}$$

For $N = 2$, the number of states is slightly different due to a smaller gap $k^2 \sim (m_n^2 - \mu^2)R^2/2 \approx$ MeV GeV$R^2/2$, which limits the maximal k, approximately by $k \sim 10^9$ instead of $k \sim 10^{11}$ of the massless case. This however is a small difference. Using again Eq. (A.8), #mass-levels $\approx 0.46k \approx k/2$, we also get approximately the same result as in the massless case, (A.9).

A.2 Degeneracy of States

Using the expression of KK masses,

$$(mR)^2 = k_1^2 + \cdots + k_N^2, \tag{A.13}$$

we map the degeneracy count onto a problem in number theory of counting the number of different possibilities, $r_N(n)$, of integers $k_1, \ldots, k_N$ that satisfy $n = k_1^2 + \cdots + k_N^2$, with $n = (mR)^2$. The averaged number of possibilities $r_N(n)$, will give us the degeneracy of states Z.

There is a "cheap" way of getting the answer by making a continuum approximation. That is, for $R \to \infty$, the number of states $n(m)$ with mass $\leq m$ is

$$n(m) = v_N (mR)^N\,, \tag{A.14}$$

where v_N is a volume of an unit N-ball. The number of states within the interval of masses between $m + \Delta m$ and m then is

$$Z(m) = N v_N \Delta m\, m^{N-1} R^N\,, \tag{A.15}$$

which for $\Delta m = 1/(2mR^2)$ taken from (A.7) gives,

$$Z(m) \approx \frac{N}{2}\, v_N (mR)^{N-2}\,. \tag{A.16}$$

For an alternative count, we start by estimating all possibilities to solve the equation $k_1^2 + \cdots + k_N^2 \leq x$. This can be solved geometrically, as it is just the volume of a ball,

$$\sum_{n=0}^{x} r_N(n) = v_N x^{\frac{N}{2}}. \tag{A.17}$$

To estimate the average of r_N at some number x, we average the a nearest values of r_N

$$Z = \frac{1}{a}(r_N(x-a+1) + \cdots + r_N(x)) \tag{A.18}$$
$$= \frac{v_N}{a}(x^{\frac{N}{2}} - (x-a)^{\frac{N}{2}}) \tag{A.19}$$
$$\approx \frac{N}{2} v_N x^{\frac{N}{2}-1}. \tag{A.20}$$

In our case, we replace $x = (mR)^2$ and find for the degeneracy of states given by (A.16).

Appendix B

Supporting Material to A Global Fit of Neutrino Data for Theories with Many Neutrino Copies

In the appendix, we describe in more detail how the different experiments have been analyzed. We follow closely the discussion in [22].

DayaBay was a reactor neutrino experiment located in China to measure the parameters θ_{13} and Δm^2_{32}. Together with [120] the collaboration released their data set of 26 data points which we analyzed in this work. Because DayaBay's neutrino flux is sourced by several nuclear reactors which have different baselengths to the experimental halls the detectors are placed in, we calculated the contribution of every reactor to the overall flux at the experimental site. DayaBay consists of experimental halls close to the reactor to determine the predicted flux in the far experimental hall. The data of the far experimental hall (EH3) was used in this analysis. The geometric averaged baseline to EH3 is around 1663 m. In order to incorporate the systematical uncertainties of the experiment we took the covariance matrix published in [121] and scaled the general covariance matrix accordingly to the data which is analyzed here. Performing a fit for standard mixing parameters, we find that our values are well consistent with those reported by the collaboration.

KamLAND was a reactor experiment based in Japan designed to measure θ_{12} and Δm^2_{12}. We averaged the survival probability of the neutrino flux over all baselines of the reactors placed in Japan while neglecting the contribution from South Korea which is around 5% and the world contribution which is around 1%. Our analysis is based on the publication [119] that also in-

cludes a non-oscillated spectrum of the neutrino flux at the experiment. The necessary information was extracted from Fig. 1 in this publication. Due to lacking public information, we could not include a full covariance matrix and resorted to using a diagonal covariance matrix which we constructed by using the uncertainties of the measured events per bin. In our final analysis, we incorporated 17 data points. The energy resolution was approximated by the bin width. Our fit results are well consistent with those reported by the collaboration.

MINOS was an accelerator muon neutrino experiment located at Fermilab in the U.S. that operates slightly off maximum of the atmospheric mass splitting regime (see Fig. 4.5). In principle, it can be used to determine θ_{23} and Δm^2_{13} even though due to the energy range it is not optimal, but provides excellent data for searching for BSM signals in the oscillation pattern. This makes this experiment of particular interest for our analysis. We use the far detector (FD) CC and NC data from MINOS and MINOS+. The simulation templates, smearing matrices, covariance matrices, as well as the observed counts are provided in the data release accompanying the publication [122]. We implement our analysis by replicating the provided reference implementation. Our fit results are well consistent with those reported by the collaboration.

Also, NOνA uses the same muon neutrino beam as MINOS but this experiment is located off-axis, resulting in maximum mixing if the atmospheric mass splitting regime (see Fig. 4.5). Therefore, it is optimized to restrict the SM parameters θ_{23} and Δm^2_{13}. We use the muon disappearance data from [205]. Forward and reversed horn current data is included in our analysis. A detector response is implemented via a smearing function defined according to the resolution specified in Table 2 in [205]. Our fit results are well consistent with those reported by the collaboration.

Another relevant type of experiment is the direct measurement of the neutrino mass. The leading experiment for this is KATRIN which analyzes the spectrum of beta decays. In [30] the collaboration also performed a Bayesian analysis and reported a posterior on the mass of the electron neutrino. Because a flat prior on the m_{lightest} was used to calculate this result, we can easily interpret this posterior as our likelihood. We approximated the posterior distribution with a truncated normal distribution and calculated the predicted neutrino mass of the DR model with (3.168). In this analysis, we just evaluated the likelihood as described above and did not take into account the change in the shape of the energy distribution which would be caused by additional mass states in the expression for the flavor states. This is usually done in sterile neutrino searches with KATRIN and could still be improved in our analysis.

Bibliography

[1] M. Ettengruber, M. Agostini, A. Caldwell, P. Eller, and O. Schulz, "Discovering neutrinoless double-beta decay in the era of precision neutrino cosmology," *Phys. Rev. D* **106** no. 7, (2022) 073004, arXiv:2208.09954 [hep-ph].

[2] M. Ettengruber, "Neutrino physics in TeV scale gravity theories," *Phys. Rev. D* **106** no. 5, (2022) 055028, arXiv:2206.00034 [hep-ph].

[3] M. Ettengruber and E. Koutsangelas, "Consequences of Multiple Axions in Theories with Dark Yang-Mills Groups," arXiv:2307.10298 [hep-ph].

[4] G. Dvali, M. Ettengruber, and A. Stuhlfauth, "Kaluza-Klein Spectroscopy from Neutron Oscillations into Hidden Dimensions," arXiv:2312.13278 [hep-ph].

[5] A. Arbey and F. Mahmoudi, "Dark matter and the early Universe: a review," *Prog. Part. Nucl. Phys.* **119** (2021) 103865, arXiv:2104.11488 [hep-ph].

[6] G. Senjanovic, "Neutrino mass," in *International Europhysics Conference on High-energy Physics*. 2, 1994. arXiv:hep-ph/9402359.

[7] L. Di Luzio, M. Giannotti, E. Nardi, and L. Visinelli, "The landscape of QCD axion models," *Phys. Rept.* **870** (2020) 1–117, arXiv:2003.01100 [hep-ph].

[8] E. Koutsangelas, *How the axion paves the way beyond the standard model*. PhD thesis, Munich U., 2023.

[9] G. Dvali, "Strong coupling and classicalization," in *The future of our physics including new frontiers: Proceedings of the International School of Subnuclear Physics*, pp. 189–200. World Scientific, 2017.

[10] G. Senjanovic, "Is left–right symmetry the key?," *Mod. Phys. Lett. A* **32** no. 04, (2017) 1730004, arXiv:1610.04209 [hep-ph].

[11] S. P. Martin, "A Supersymmetry primer," *Adv. Ser. Direct. High Energy Phys.* **18** (1998) 1–98, arXiv:hep-ph/9709356.

[12] W. de Boer, "Grand unified theories and supersymmetry in particle physics and cosmology," *Prog. Part. Nucl. Phys.* **33** (1994) 201–302, arXiv:hep-ph/9402266.

[13] N. Arkani-Hamed, S. Dimopoulos, and G. R. Dvali, "The Hierarchy problem and new dimensions at a millimeter," *Phys. Lett. B* **429** (1998) 263–272, arXiv:hep-ph/9803315.

[14] N. Arkani-Hamed, S. Dimopoulos, and G. R. Dvali, "Phenomenology, astrophysics and cosmology of theories with submillimeter dimensions and TeV scale quantum gravity," *Phys. Rev. D* **59** (1999) 086004, arXiv:hep-ph/9807344.

[15] G. Dvali, "Black Holes and Large N Species Solution to the Hierarchy Problem," *Fortsch. Phys.* **58** (2010) 528–536, arXiv:0706.2050 [hep-th].

[16] G. Dvali and M. Redi, "Black Hole Bound on the Number of Species and Quantum Gravity at LHC," *Phys. Rev. D* **77** (2008) 045027, arXiv:0710.4344 [hep-th].

[17] G. Dvali and M. Redi, "Phenomenology of 10^{32} Dark Sectors," *Phys. Rev. D* **80** (2009) 055001, arXiv:0905.1709 [hep-ph].

[18] N. Arkani-Hamed, S. Dimopoulos, G. R. Dvali, and J. March-Russell, "Neutrino masses from large extra dimensions," *Phys. Rev. D* **65** (2001) 024032, arXiv:hep-ph/9811448.

[19] N. Arkani-Hamed, S. Dimopoulos, G. R. Dvali, and N. Kaloper, "Many fold universe," *JHEP* **12** (2000) 010, arXiv:hep-ph/9911386.

[20] G. Dvali and G. R. Farrar, "Strong CP Problem with 10**32 Standard Model Copies," *Phys. Rev. Lett.* **101** (2008) 011801, arXiv:0712.3170 [hep-th].

[21] G. Dvali, I. Sawicki, and A. Vikman, "Dark Matter via Many Copies of the Standard Model," *JCAP* **0908** (2009) 009, arXiv:0903.0660 [hep-th].

[22] M. Ettengruber, A. Zander, and P. Eller, "Testing the Number of Neutrino Species with a Global Fit of Neutrino Data," arXiv:2402.00490 [hep-ph].

[23] E. Majorana, "Teoria simmetrica dell'elettrone e del positrone," *Nuovo Cim.* **14** (1937) 171–184.

[24] B. T. Cleveland, T. Daily, R. Davis, Jr., J. R. Distel, K. Lande, C. K. Lee, P. S. Wildenhain, and J. Ullman, "Measurement of the solar electron neutrino flux with the Homestake chlorine detector," *Astrophys. J.* **496** (1998) 505–526.

[25] B. Pontecorvo, "Mesonium and anti-mesonium," *Sov. Phys. JETP* **6** (1957) 429.

[26] B. Pontecorvo, "Inverse beta processes and nonconservation of lepton charge," *Zh. Eksp. Teor. Fiz.* **34** (1957) 247.

[27] M. C. Gonzalez-Garcia and M. Maltoni, "Phenomenology with Massive Neutrinos," *Phys. Rept.* **460** (2008) 1–129, arXiv:0704.1800 [hep-ph].

[28] J. Engel and J. Menéndez, "Status and Future of Nuclear Matrix Elements for Neutrinoless Double-Beta Decay: A Review," *Rept. Prog. Phys.* **80** no. 4, (2017) 046301, arXiv:1610.06548 [nucl-th].

[29] **Particle Data Group** Collaboration, P. A. Zyla *et al.*, "Review of Particle Physics," *PTEP* **2020** no. 8, (2020) 083C01. and 2021 update.

[30] **KATRIN** Collaboration, M. Aker *et al.*, "Direct neutrino-mass measurement with sub-electronvolt sensitivity," *Nature Phys.* **18** no. 2, (2022) 160–166, arXiv:2105.08533 [hep-ex].

[31] M. Fukugita and T. Yanagida, "Baryogenesis Without Grand Unification," *Phys. Lett. B* **174** (1986) 45–47.

[32] M. J. Dolinski, A. W. P. Poon, and W. Rodejohann, "Neutrinoless Double-Beta Decay: Status and Prospects," *Ann. Rev. Nucl. Part. Sci.* **69** (2019) 219–251, arXiv:1902.04097 [nucl-ex].

[33] U. von Toussaint, "Bayesian inference in physics," *Rev. Mod. Phys.* **83** (Sep, 2011) 943–999.

[34] A. Caldwell, M. Ettengruber, A. Merle, O. Schulz, and M. Totzauer, "Global Bayesian analysis of neutrino mass data," *Phys. Rev. D* **96** no. 7, (2017) 073001, arXiv:1705.01945 [hep-ph].

[35] M. Lattanzi and M. Gerbino, "Status of neutrino properties and future prospects - Cosmological and astrophysical constraints," *Front. in Phys.* **5** (2018) 70, arXiv:1712.07109 [astro-ph.CO].

[36] **Planck** Collaboration, N. Aghanim *et al.*, "Planck 2018 results. VI. Cosmological parameters," *Astron. Astrophys.* **641** (2020) A6. [Erratum: Astron.Astrophys. 652, C4 (2021)].

[37] A. Font-Ribera, P. McDonald, N. Mostek, B. A. Reid, H.-J. Seo, and A. Slosar, "DESI and other dark energy experiments in the era of neutrino mass measurements," *JCAP* **05** (2014) 023, arXiv:1308.4164 [astro-ph.CO].

[38] **Euclid** Collaboration, S. Ilić *et al.*, "Euclid preparation - XV. Forecasting cosmological constraints for the Euclid and CMB joint analysis," *Astron. Astrophys.* **657** (2022) A91, arXiv:2106.08346 [astro-ph.CO].

[39] M. Agostini, G. Benato, J. A. Detwiler, J. Menéndez, and F. Vissani, "Toward the discovery of matter creation with neutrinoless $\beta\beta$ decay," *Rev. Mod. Phys.* **95** no. 2, (2023) 025002, arXiv:2202.01787 [hep-ex].

[40] I. Esteban, M. C. Gonzalez-Garcia, M. Maltoni, T. Schwetz, and A. Zhou, "The fate of hints: updated global analysis of three-flavor neutrino oscillations," *JHEP* **09** (2020) 178, arXiv:2007.14792 [hep-ph].

[41] R. Jimenez, C. Pena-Garay, K. Short, F. Simpson, and L. Verde, "Neutrino masses and mass hierarchy: evidence for the normal hierarchy," *JCAP* **09** (2022) 006, arXiv:2203.14247 [hep-ph].

[42] S. Gariazzo *et al.*, "Neutrino mass and mass ordering: no conclusive evidence for normal ordering," *JCAP* **10** (2022) 010, arXiv:2205.02195 [hep-ph].

[43] M. Agostini, G. Benato, J. A. Detwiler, J. Menéndez, and F. Vissani, "Testing the inverted neutrino mass ordering with neutrinoless double-β decay," *Phys. Rev. C* **104** no. 4, (2021) L042501, arXiv:2107.09104 [hep-ph].

[44] F. Feruglio, A. Strumia, and F. Vissani, "Neutrino oscillations and signals in beta and 0nu2beta experiments," *Nucl. Phys. B* **637** (2002) 345–377, arXiv:hep-ph/0201291. [Addendum: Nucl.Phys.B 659, 359–362 (2003)].

[45] G. Benato, "Effective Majorana Mass and Neutrinoless Double Beta Decay," *Eur. Phys. J. C* **75** no. 11, (2015) 563, arXiv:1510.01089 [hep-ph].

[46] **CUPID** Collaboration, W. R. Armstrong *et al.*, "CUPID pre-CDR," arXiv:1907.09376 [physics.ins-det].

[47] **LEGEND** Collaboration, N. Abgrall *et al.*, "The Large Enriched Germanium Experiment for Neutrinoless $\beta\beta$ Decay: LEGEND-1000 Preconceptual Design Report," arXiv:2107.11462 [physics.ins-det].

[48] **nEXO** Collaboration, S. A. Kharusi *et al.*, "nEXO Pre-Conceptual Design Report," arXiv:1805.11142 [physics.ins-det].

[49] E. Lisi and A. Marrone, "Majorana neutrino mass constraints in the landscape of nuclear matrix elements," *Phys. Rev. D* **106** no. 1, (2022) 013009, arXiv:2204.09569 [hep-ph].

[50] L. Gráf, M. Lindner, and O. Scholer, "Unraveling the $0\nu\beta\beta$ decay mechanisms," *Phys. Rev. D* **106** no. 3, (2022) 035022, arXiv:2204.10845 [hep-ph].

[51] M. Agostini, G. Benato, and J. Detwiler, "Discovery probability of next-generation neutrinoless double- β decay experiments," *Phys. Rev. D* **96** no. 5, (2017) 053001, arXiv:1705.02996 [hep-ex].

[52] S. Dell'Oro, S. Marcocci, and F. Vissani, "Empirical Inference on the Majorana Mass of the Ordinary Neutrinos," *Phys. Rev. D* **100** no. 7, (2019) 073003, arXiv:1909.05381 [hep-ph].

[53] M. Agostini, G. Benato, S. Dell'Oro, S. Pirro, and F. Vissani, "Discovery probabilities of Majorana neutrinos based on cosmological data," *Phys. Rev. D* **103** no. 3, (2021) 033008, arXiv:2012.13938 [hep-ph].

[54] **CUORE** Collaboration, D. Q. Adams *et al.*, "Search for Majorana neutrinos exploiting millikelvin cryogenics with CUORE," *Nature* **604** no. 7904, (2022) 53–58, arXiv:2104.06906 [nucl-ex].

[55] **EXO-200** Collaboration, G. Anton *et al.*, "Search for Neutrinoless Double-β Decay with the Complete EXO-200 Dataset," *Phys. Rev. Lett.* **123** no. 16, (2019) 161802, arXiv:1906.02723 [hep-ex].

[56] **GERDA** Collaboration, M. Agostini *et al.*, "Final Results of GERDA on the Search for Neutrinoless Double-β Decay," *Phys. Rev. Lett.* **125** no. 25, (2020) 252502, arXiv:2009.06079 [nucl-ex].

[57] **KamLAND-Zen** Collaboration, S. Abe *et al.*, "Search for the Majorana Nature of Neutrinos in the Inverted Mass Ordering Region with KamLAND-Zen," *Phys. Rev. Lett.* **130** no. 5, (2023) 051801, arXiv:2203.02139 [hep-ex].

[58] A. Caldwell and K. Kroninger, "Signal discovery in sparse spectra: A Bayesian analysis," *Phys. Rev. D* **74** (2006) 092003, arXiv:physics/0608249.

[59] O. Schulz, F. Beaujean, A. Caldwell, C. Grunwald, V. Hafych, K. Kröninger, S. La Cagnina, L. Röhrig, and L. Shtembari, "BAT.jl: A Julia-Based Tool for Bayesian Inference," *SN Comput. Sci.* **2** no. 3, (2021) 1–17, arXiv:2008.03132 [stat.CO].

[60] J. Hyvärinen and J. Suhonen, "Nuclear matrix elements for $0\nu\beta\beta$ decays with light or heavy Majorana-neutrino exchange," *Phys. Rev. C* **91** no. 2, (2015) 024613.

[61] F. Šimkovic, A. Smetana, and P. Vogel, "$0\nu\beta\beta$ nuclear matrix elements, neutrino potentials and SU(4) symmetry," *Phys. Rev. C* **98** no. 6, (2018) 064325, arXiv:1808.05016 [nucl-th].

[62] T. R. Rodriguez and G. Martinez-Pinedo, "Energy density functional study of nuclear matrix elements for neutrinoless $\beta\beta$ decay," *Phys. Rev. Lett.* **105** (2010) 252503, arXiv:1008.5260 [nucl-th].

[63] N. López Vaquero, T. R. Rodríguez, and J. L. Egido, "Shape and pairing fluctuations effects on neutrinoless double beta decay nuclear matrix elements," *Phys. Rev. Lett.* **111** no. 14, (2013) 142501, arXiv:1401.0650 [nucl-th].

[64] L. S. Song, J. M. Yao, P. Ring, and J. Meng, "Nuclear matrix element of neutrinoless double-β decay: Relativity and short-range correlations," *Phys. Rev. C* **95** no. 2, (2017) 024305, arXiv:1702.02448 [nucl-th].

[65] J. Barea, J. Kotila, and F. Iachello, "$0\nu\beta\beta$ and $2\nu\beta\beta$ nuclear matrix elements in the interacting boson model with isospin restoration," *Phys. Rev. C* **91** no. 3, (2015) 034304, arXiv:1506.08530 [nucl-th].

[66] F. F. Deppisch, L. Graf, F. Iachello, and J. Kotila, "Analysis of light neutrino exchange and short-range mechanisms in $0\nu\beta\beta$ decay," *Phys. Rev. D* **102** no. 9, (2020) 095016, arXiv:2009.10119 [hep-ph].

[67] A. Faessler, G. L. Fogli, E. Lisi, A. M. Rotunno, and F. Simkovic, "Multi-Isotope Degeneracy of Neutrinoless Double Beta Decay Mechanisms in the Quasi-Particle Random Phase Approximation," *Phys. Rev. D* **83** (2011) 113015, arXiv:1103.2504 [hep-ph].

[68] V. Cirigliano, W. Dekens, J. De Vries, M. L. Graesser, E. Mereghetti, S. Pastore, M. Piarulli, U. Van Kolck, and R. B. Wiringa, "Renormalized approach to neutrinoless double- β decay," *Phys. Rev. C* **100** no. 5, (2019) 055504, arXiv:1907.11254 [nucl-th].

[69] F. Simpson, R. Jimenez, C. Pena-Garay, and L. Verde, "Strong Bayesian Evidence for the Normal Neutrino Hierarchy," *JCAP* **06** (2017) 029, arXiv:1703.03425 [astro-ph.CO].

[70] J. Alvey, M. Escudero, N. Sabti, and T. Schwetz, "Cosmic neutrino background detection in large-neutrino-mass cosmologies," *Phys. Rev. D* **105** no. 6, (2022) 063501, arXiv:2111.14870 [hep-ph].

[71] P. Gysbers *et al.*, "Discrepancy between experimental and theoretical β-decay rates resolved from first principles," *Nature Phys.* **15** no. 5, (2019) 428–431, arXiv:1903.00047 [nucl-th].

[72] A. Belley, C. G. Payne, S. R. Stroberg, T. Miyagi, and J. D. Holt, "*AbInitio* Neutrinoless Double-Beta Decay Matrix Elements for ^{48}Ca , ^{76}Ge , and ^{82}Se," *Phys. Rev. Lett.* **126** no. 4, (2021) 042502, arXiv:2008.06588 [nucl-th].

[73] V. Cirigliano, W. Dekens, J. De Vries, M. L. Graesser, E. Mereghetti, S. Pastore, and U. Van Kolck, "New Leading Contribution to Neutrinoless Double-β Decay," *Phys. Rev. Lett.* **120** no. 20, (2018) 202001, arXiv:1802.10097 [hep-ph].

[74] M. D. Schwartz, *Quantum Field Theory and the Standard Model*. Cambridge University Press, 3, 2014.

[75] G. Dvali, "Strong Coupling and Classicalization," *Subnucl. Ser.* **53** (2017) 189–200, arXiv:1607.07422 [hep-th].

[76] I. Antoniadis, N. Arkani-Hamed, S. Dimopoulos, and G. R. Dvali, "New dimensions at a millimeter to a Fermi and superstrings at a TeV," *Phys. Lett. B* **436** (1998) 257–263, arXiv:hep-ph/9804398.

[77] M. Shifman, "Large Extra Dimensions: Becoming acquainted with an alternative paradigm," *Int. J. Mod. Phys. A* **25** (2010) 199–225, arXiv:0907.3074 [hep-ph].

[78] G. R. Dvali and M. A. Shifman, "Domain walls in strongly coupled theories," *Phys. Lett. B* **396** (1997) 64–69, arXiv:hep-th/9612128. [Erratum: Phys.Lett.B 407, 452 (1997)].

[79] G. R. Dvali and A. Y. Smirnov, "Probing large extra dimensions with neutrinos," *Nucl. Phys. B* **563** (1999) 63–81, arXiv:hep-ph/9904211.

[80] F. Wilczek and A. Zee, "Families from Spinors," *Phys. Rev. D* **25** (1982) 553.

[81] P. A. N. Machado, H. Nunokawa, and R. Zukanovich Funchal, "Testing for Large Extra Dimensions with Neutrino Oscillations," *Phys. Rev. D* **84** (2011) 013003, arXiv:1101.0003 [hep-ph].

[82] D. V. Forero, C. Giunti, C. A. Ternes, and O. Tyagi, "Large extra dimensions and neutrino experiments," *Phys. Rev. D* **106** no. 3, (2022) 035027, arXiv:2207.02790 [hep-ph].

[83] **ATLAS** Collaboration, G. Aad *et al.*, "Search for new phenomena in events with an energetic jet and missing transverse momentum in pp collisions at $\sqrt{s}$ =13 TeV with the ATLAS detector," *Phys. Rev. D* **103** no. 11, (2021) 112006, arXiv:2102.10874 [hep-ex].

[84] **CMS** Collaboration, A. Tumasyan *et al.*, "Search for new particles in events with energetic jets and large missing transverse momentum in proton-proton collisions at $\sqrt{s} = 13$ TeV," *JHEP* **11** (2021) 153, arXiv:2107.13021 [hep-ex].

[85] **Particle Data Group** Collaboration, R. L. Workman *et al.*, "Review of Particle Physics," *PTEP* **2022** (2022) 083C01.

[86] J. G. Lee, E. G. Adelberger, T. S. Cook, S. M. Fleischer, and B. R. Heckel, "New Test of the Gravitational $1/r^2$ Law at Separations down

to 52 μm," *Phys. Rev. Lett.* **124** no. 10, (2020) 101101, arXiv:2002.11761 [hep-ex].

[87] E. G. Adelberger, J. H. Gundlach, B. R. Heckel, S. Hoedl, and S. Schlamminger, "Torsion balance experiments: A low-energy frontier of particle physics," *Prog. Part. Nucl. Phys.* **62** (2009) 102–134.

[88] W.-H. Tan, S.-Q. Yang, C.-G. Shao, J. Li, A.-B. Du, B.-F. Zhan, Q.-L. Wang, P.-S. Luo, L.-C. Tu, and J. Luo, "New Test of the Gravitational Inverse-Square Law at the Submillimeter Range with Dual Modulation and Compensation," *Phys. Rev. Lett.* **116** no. 13, (2016) 131101.

[89] S. R. Coleman, J. Preskill, and F. Wilczek, "Growing hair on black holes," *Phys. Rev. Lett.* **67** (1991) 1975–1978.

[90] L. M. Krauss and F. Wilczek, "Discrete Gauge Symmetry in Continuum Theories," *Phys. Rev. Lett.* **62** (1989) 1221.

[91] J. Preskill and L. M. Krauss, "Local Discrete Symmetry and Quantum Mechanical Hair," *Nucl. Phys. B* **341** (1990) 50–100.

[92] M. G. Alford and F. Wilczek, "Aharonov-Bohm Interaction of Cosmic Strings with Matter," *Phys. Rev. Lett.* **62** (1989) 1071.

[93] G. Dvali and C. Gomez, "Quantum Information and Gravity Cutoff in Theories with Species," *Phys. Lett. B* **674** (2009) 303–307, arXiv:0812.1940 [hep-th].

[94] G. Dvali and D. Lust, "Evaporation of Microscopic Black Holes in String Theory and the Bound on Species," *Fortsch. Phys.* **58** (2010) 505–527, arXiv:0912.3167 [hep-th].

[95] G. Dvali and C. Gomez, "Species and Strings," arXiv:1004.3744 [hep-th].

[96] G. Dvali and L. Funcke, "Small neutrino masses from gravitational θ-term," *Phys. Rev. D* **93** no. 11, (2016) 113002, arXiv:1602.03191 [hep-ph].

[97] G. Fantini, A. Gallo Rosso, F. Vissani, and V. Zema, "Introduction to the Formalism of Neutrino Oscillations," *Adv. Ser. Direct. High Energy Phys.* **28** (2018) 37–119, arXiv:1802.05781 [hep-ph].

[98] E. Akhmedov, "Quantum mechanics aspects and subtleties of neutrino oscillations," in *International Conference on History of the Neutrino: 1930-2018*. 1, 2019. arXiv:1901.05232 [hep-ph].

[99] B. Kayser, "On the quantum mechanics of neutrino oscillation," *Phys. Rev. D* **24** (Jul, 1981) 110–116. https://link.aps.org/doi/10.1103/PhysRevD.24.110.

[100] S. Nussinov, "Solar Neutrinos and Neutrino Mixing," *Phys. Lett. B* **63** (1976) 201–203.

[101] G. Dvali, "Nature of Microscopic Black Holes and Gravity in Theories with Particle Species," *Int. J. Mod. Phys. A* **25** (2010) 602–615, arXiv:0806.3801 [hep-th].

[102] I. Esteban, M. C. Gonzalez-Garcia, M. Maltoni, T. Schwetz, and A. Zhou, "The fate of hints: updated global analysis of three-flavor neutrino oscillations," *JHEP* **09** (2020) 178, arXiv:2007.14792 [hep-ph].

[103] P. A. N. Machado, H. Nunokawa, F. A. P. dos Santos, and R. Z. Funchal, "Bulk Neutrinos as an Alternative Cause of the Gallium and Reactor Anti-neutrino Anomalies," *Phys. Rev. D* **85** (2012) 073012, arXiv:1107.2400 [hep-ph].

[104] V. S. Basto-Gonzalez, A. Esmaili, and O. L. G. Peres, "Kinematical Test of Large Extra Dimension in Beta Decay Experiments," *Phys. Lett. B* **718** (2013) 1020–1023, arXiv:1205.6212 [hep-ph].

[105] I. Girardi and D. Meloni, "Constraining new physics scenarios in neutrino oscillations from Daya Bay data," *Phys. Rev. D* **90** no. 7, (2014) 073011, arXiv:1403.5507 [hep-ph].

[106] W. Rodejohann and H. Zhang, "Signatures of Extra Dimensional Sterile Neutrinos," *Phys. Lett. B* **737** (2014) 81–89, arXiv:1407.2739 [hep-ph].

[107] J. M. Berryman, A. de Gouvêa, K. J. Kelly, O. L. G. Peres, and Z. Tabrizi, "Large, Extra Dimensions at the Deep Underground Neutrino Experiment," *Phys. Rev. D* **94** no. 3, (2016) 033006, arXiv:1603.00018 [hep-ph].

[108] M. Carena, Y.-Y. Li, C. S. Machado, P. A. N. Machado, and C. E. M. Wagner, "Neutrinos in Large Extra Dimensions and Short-Baseline ν_e

Appearance," *Phys. Rev. D* **96** no. 9, (2017) 095014, arXiv:1708.09548 [hep-ph].

[109] G. V. Stenico, D. V. Forero, and O. L. G. Peres, "A Short Travel for Neutrinos in Large Extra Dimensions," *JHEP* **11** (2018) 155, arXiv:1808.05450 [hep-ph].

[110] C. A. Argüelles *et al.*, "New opportunities at the next-generation neutrino experiments I: BSM neutrino physics and dark matter," *Rept. Prog. Phys.* **83** no. 12, (2020) 124201, arXiv:1907.08311 [hep-ph].

[111] **DUNE** Collaboration, B. Abi *et al.*, "Prospects for beyond the Standard Model physics searches at the Deep Underground Neutrino Experiment," *Eur. Phys. J. C* **81** no. 4, (2021) 322, arXiv:2008.12769 [hep-ex].

[112] V. S. Basto-Gonzalez, D. V. Forero, C. Giunti, A. A. Quiroga, and C. A. Ternes, "Short-baseline oscillation scenarios at JUNO and TAO," *Phys. Rev. D* **105** no. 7, (2022) 075023, arXiv:2112.00379 [hep-ph].

[113] C. A. Argüelles *et al.*, "Snowmass White Paper: Beyond the Standard Model effects on Neutrino Flavor," in *2022 Snowmass Summer Study*. 3, 2022. arXiv:2203.10811 [hep-ph].

[114] **Particle Data Group** Collaboration, P. A. Zyla *et al.*, "Review of Particle Physics," *PTEP* **2020** no. 8, (2020) 083C01.

[115] M. Ahlers, K. Helbing, and C. Pérez de los Heros, "Probing Particle Physics with IceCube," *Eur. Phys. J. C* **78** no. 11, (2018) 924, arXiv:1806.05696 [astro-ph.HE].

[116] **JUNO** Collaboration, F. An *et al.*, "Neutrino Physics with JUNO," *J. Phys. G* **43** no. 3, (2016) 030401, arXiv:1507.05613 [physics.ins-det].

[117] A. Caldwell, "Aspects of frequentism," *Annalen der Physik* **531** no. 3, (2019) 1700457.

[118] J. Barry, W. Rodejohann, and H. Zhang, "Light Sterile Neutrinos: Models and Phenomenology," *JHEP* **07** (2011) 091, arXiv:1105.3911 [hep-ph].

[119] **KamLAND** Collaboration, A. Gando *et al.*, "Constraints on θ_{13} from A Three-Flavor Oscillation Analysis of Reactor Antineutrinos at KamLAND," *Phys. Rev. D* **83** (2011) 052002, arXiv:1009.4771 [hep-ex].

[120] **Daya Bay** Collaboration, D. Adey *et al.*, "Measurement of the Electron Antineutrino Oscillation with 1958 Days of Operation at Daya Bay," *Phys. Rev. Lett.* **121** no. 24, (2018) 241805, arXiv:1809.02261 [hep-ex].

[121] **Daya Bay** Collaboration, F. P. An *et al.*, "Improved Measurement of the Reactor Antineutrino Flux and Spectrum at Daya Bay," *Chin. Phys. C* **41** no. 1, (2017) 013002, arXiv:1607.05378 [hep-ex].

[122] **MINOS+** Collaboration, P. Adamson *et al.*, "Search for sterile neutrinos in MINOS and MINOS+ using a two-detector fit," *Phys. Rev. Lett.* **122** no. 9, (2019) 091803, arXiv:1710.06488 [hep-ex].

[123] **NOvA** Collaboration, M. A. Acero *et al.*, "New constraints on oscillation parameters from ν_e appearance and ν_μ disappearance in the NOvA experiment," *Phys. Rev. D* **98** (2018) 032012, arXiv:1806.00096 [hep-ex].

[124] A. Zander, M. Ettengruber, and P. Eller, "How Many Dark Neutrino Sectors Does Cosmology Allow?," arXiv:2308.00798 [hep-ph].

[125] **JUNO** Collaboration, Z. Djurcic *et al.*, "JUNO Conceptual Design Report," arXiv:1508.07166 [physics.ins-det].

[126] **DUNE** Collaboration, B. Abi *et al.*, "Deep Underground Neutrino Experiment (DUNE), Far Detector Technical Design Report, Volume I Introduction to DUNE," *JINST* **15** no. 08, (2020) T08008, arXiv:2002.02967 [physics.ins-det].

[127] G. Dvali and G. Gabadadze, "Nonconservation of global charges in the brane universe and baryogenesis," *Phys. Lett. B* **460** (1999) 47–57, arXiv:hep-ph/9904221.

[128] Z. Berezhiani and L. Bento, "Neutron - mirror neutron oscillations: How fast might they be?," *Phys. Rev. Lett.* **96** (2006) 081801, arXiv:hep-ph/0507031.

[129] Z. Berezhiani, "More about neutron - mirror neutron oscillation," *Eur. Phys. J. C* **64** (2009) 421–431, arXiv:0804.2088 [hep-ph].

[130] **nEDM** Collaboration, C. Abel *et al.*, "A search for neutron to mirror-neutron oscillations using the nEDM apparatus at PSI," *Phys. Lett. B* **812** (2021) 135993, arXiv:2009.11046 [hep-ph].

[131] G. Ban *et al.*, "Search for Neutron-to-Hidden-Neutron Oscillations in an Ultracold Neutron Beam," *Phys. Rev. Lett.* **131** no. 19, (2023) 191801, arXiv:2303.10507 [hep-ph].

[132] **KamLAND** Collaboration, T. Araki *et al.*, "Search for the invisible decay of neutrons with KamLAND," *Phys. Rev. Lett.* **96** (2006) 101802, arXiv:hep-ex/0512059.

[133] J. Learned, F. Reines, and A. Soni, "Limits on Nonconservation of Baryon Number," *Phys. Rev. Lett.* **43** (1979) 907. [Erratum: Phys.Rev.Lett. 43, 1626 (1979)].

[134] E. Tiesinga, P. J. Mohr, D. B. Newell, and B. N. Taylor, "CODATA recommended values of the fundamental physical constants: 2018*," *Rev. Mod. Phys.* **93** no. 2, (2021) 025010.

[135] **UCNτ** Collaboration, F. M. Gonzalez *et al.*, "Improved neutron lifetime measurement with UCNτ," *Phys. Rev. Lett.* **127** no. 16, (2021) 162501, arXiv:2106.10375 [nucl-ex].

[136] V. F. Ezhov *et al.*, "Measurement of the neutron lifetime with ultra-cold neutrons stored in a magneto-gravitational trap," *JETP Lett.* **107** no. 11, (2018) 671–675, arXiv:1412.7434 [nucl-ex].

[137] A. T. Yue, M. S. Dewey, D. M. Gilliam, G. L. Greene, A. B. Laptev, J. S. Nico, W. M. Snow, and F. E. Wietfeldt, "Improved Determination of the Neutron Lifetime," *Phys. Rev. Lett.* **111** no. 22, (2013) 222501, arXiv:1309.2623 [nucl-ex].

[138] J. S. Nico *et al.*, "Measurement of the neutron lifetime by counting trapped protons in a cold neutron beam," *Phys. Rev. C* **71** (2005) 055502, arXiv:nucl-ex/0411041.

[139] Z. Berezhiani, "Neutron lifetime puzzle and neutron–mirror neutron oscillation," *Eur. Phys. J. C* **79** no. 6, (2019) 484, arXiv:1807.07906 [hep-ph].

[140] W. Tan, "Neutron oscillations for solving neutron lifetime and dark matter puzzles," *Phys. Lett. B* **797** (2019) 134921, arXiv:1902.01837 [physics.gen-ph].

[141] B. Fornal and B. Grinstein, "Dark Matter Interpretation of the Neutron Decay Anomaly," *Phys. Rev. Lett.* **120** no. 19, (2018) 191801, arXiv:1801.01124 [hep-ph]. [Erratum: Phys.Rev.Lett. 124, 219901 (2020)].

[142] G. K. Karananas and A. Kassiteridis, "Small-scale structure from neutron dark decay," *JCAP* **09** (2018) 036, arXiv:1805.03656 [hep-ph].

[143] A. Czarnecki, W. J. Marciano, and A. Sirlin, "Neutron Lifetime and Axial Coupling Connection," *Phys. Rev. Lett.* **120** no. 20, (2018) 202002, arXiv:1802.01804 [hep-ph].

[144] E. Gonzalo, M. Montero, G. Obied, and C. Vafa, "Dark dimension gravitons as dark matter," *JHEP* **11** (2023) 109, arXiv:2209.09249 [hep-ph].

[145] S. Coleman, *Aspects of Symmetry: Selected Erice Lectures*. Cambridge University Press, Cambridge, U.K., 1985.

[146] C. Vafa and E. Witten, "Parity Conservation in QCD," *Phys. Rev. Lett.* **53** (1984) 535.

[147] M. Pospelov and A. Ritz, "Theta vacua, QCD sum rules, and the neutron electric dipole moment," *Nucl. Phys. B* **573** (2000) 177–200, arXiv:hep-ph/9908508.

[148] S. Weinberg, "A New Light Boson?," *Phys. Rev. Lett.* **40** (1978) 223–226.

[149] F. Wilczek, "Problem of Strong P and T Invariance in the Presence of Instantons," *Phys. Rev. Lett.* **40** (1978) 279–282.

[150] R. D. Peccei and H. R. Quinn, "Constraints Imposed by CP Conservation in the Presence of Instantons," *Phys. Rev. D* **16** (1977) 1791–1797.

[151] R. D. Peccei and H. R. Quinn, "Constraints imposed by CP conservation in the presence of pseudoparticles," *Phys. Rev. D* **16** (Sep, 1977) 1791–1797.

[152] A. R. Zhitnitsky, "On Possible Suppression of the Axion Hadron Interactions. (In Russian)," *Sov. J. Nucl. Phys.* **31** (1980) 260.

[153] M. Dine, W. Fischler, and M. Srednicki, "A Simple Solution to the Strong CP Problem with a Harmless Axion," *Phys. Lett. B* **104** (1981) 199–202.

[154] J. E. Kim, "Weak Interaction Singlet and Strong CP Invariance," *Phys. Rev. Lett.* **43** (1979) 103.

[155] M. A. Shifman, A. I. Vainshtein, and V. I. Zakharov, "Can Confinement Ensure Natural CP Invariance of Strong Interactions?," *Nucl. Phys. B* **166** (1980) 493–506.

[156] L. Di Luzio, F. Mescia, and E. Nardi, "Window for preferred axion models," *Phys. Rev. D* **96** no. 7, (2017) 075003, arXiv:1705.05370 [hep-ph].

[157] V. Plakkot and S. Hoof, "Anomaly ratio distributions of hadronic axion models with multiple heavy quarks," *Phys. Rev. D* **104** no. 7, (2021) 075017, arXiv:2107.12378 [hep-ph].

[158] J. Diehl and E. Koutsangelas, "Dine-Fischler-Srednicki-Zhitnitsky-type axions and where to find them," *Phys. Rev. D* **107** no. 9, (2023) 095020, arXiv:2302.04667 [hep-ph].

[159] G. Dvali, "Three-form gauging of axion symmetries and gravity," arXiv:hep-th/0507215.

[160] G. Dvali, R. Jackiw, and S.-Y. Pi, "Topological mass generation in four dimensions," *Phys. Rev. Lett.* **96** (2006) 081602, arXiv:hep-th/0511175.

[161] G. Dvali, "Topological Origin of Chiral Symmetry Breaking in QCD and in Gravity," arXiv:1705.06317 [hep-th].

[162] G. Dvali, "Strong-CP with and without gravity," arXiv:2209.14219 [hep-ph].

[163] O. Sakhelashvili, "Consistency of the dual formulation of axion solutions to the strong CP problem," *Phys. Rev. D* **105** no. 8, (2022) 085020, arXiv:2110.03386 [hep-th].

[164] J. M. Pendlebury *et al.*, "Revised experimental upper limit on the electric dipole moment of the neutron," *Phys. Rev. D* **92** no. 9, (2015) 092003, arXiv:1509.04411 [hep-ex].

[165] J. R. Ellis and M. K. Gaillard, "Strong and Weak CP Violation," *Nucl. Phys. B* **150** (1979) 141–162.

[166] G. Dvali and C. Gomez, "Quantum Compositeness of Gravity: Black Holes, AdS and Inflation," *JCAP* **01** (2014) 023, arXiv:1312.4795 [hep-th].

[167] G. Dvali, C. Gomez, and S. Zell, "Quantum Breaking Bound on de Sitter and Swampland," *Fortsch. Phys.* **67** no. 1-2, (2019) 1800094, arXiv:1810.11002 [hep-th].

[168] G. Dvali, "S-Matrix and Anomaly of de Sitter," *Symmetry* **13** no. 1, (2020) 3, arXiv:2012.02133 [hep-th].

[169] G. Dvali, C. Gomez, and S. Zell, "A Proof of the Axion?," arXiv:1811.03079 [hep-th].

[170] S. I. Blinnikov and M. Y. Khlopov, "ON POSSIBLE EFFECTS OF 'MIRROR' PARTICLES," *Sov. J. Nucl. Phys.* **36** (1982) 472.

[171] E. W. Kolb, D. Seckel, and M. S. Turner, "The Shadow World," *Nature* **314** (1985) 415–419.

[172] D. J. Gross, J. A. Harvey, E. J. Martinec, and R. Rohm, "The Heterotic String," *Phys. Rev. Lett.* **54** (1985) 502–505.

[173] L. J. Dixon, J. A. Harvey, C. Vafa, and E. Witten, "Strings on Orbifolds," *Nucl. Phys. B* **261** (1985) 678–686.

[174] O. Lebedev, H. P. Nilles, S. Raby, S. Ramos-Sanchez, M. Ratz, P. K. S. Vaudrevange, and A. Wingerter, "A Mini-landscape of exact MSSM spectra in heterotic orbifolds," *Phys. Lett. B* **645** (2007) 88–94, arXiv:hep-th/0611095.

[175] V. Braun, Y.-H. He, B. A. Ovrut, and T. Pantev, "A Heterotic standard model," *Phys. Lett. B* **618** (2005) 252–258, arXiv:hep-th/0501070.

[176] J. Halverson, C. Long, A. Maiti, B. Nelson, and G. Salinas, "Gravitational waves from dark Yang-Mills sectors," *JHEP* **05** (2021) 154, arXiv:2012.04071 [hep-ph].

[177] W.-C. Huang, M. Reichert, F. Sannino, and Z.-W. Wang, "Testing the dark SU(N) Yang-Mills theory confined landscape: From the lattice to gravitational waves," *Phys. Rev. D* **104** no. 3, (2021) 035005, arXiv:2012.11614 [hep-ph].

[178] G. Dvali and O. Pujolas, "Micro Black Holes and the Democratic Transition," *Phys. Rev. D* **79** (2009) 064032, arXiv:0812.3442 [hep-th].

[179] G. Dvali, E. Koutsangelas, and F. Kuhnel, "Compact Dark Matter Objects via N Dark Sectors," *Phys. Rev. D* **101** (2020) 083533, arXiv:1911.13281 [astro-ph.CO].

[180] A. Arvanitaki, S. Dimopoulos, S. Dubovsky, N. Kaloper, and J. March-Russell, "String Axiverse," *Phys. Rev. D* **81** (2010) 123530, arXiv:0905.4720 [hep-th].

[181] K. J. Mack and P. J. Steinhardt, "Cosmological Problems with Multiple Axion-like Fields," *JCAP* **05** (2011) 001, arXiv:0911.0418 [astro-ph.CO].

[182] J. W. Foster, S. Kumar, B. R. Safdi, and Y. Soreq, "Dark Grand Unification in the axiverse: decaying axion dark matter and spontaneous baryogenesis," *JHEP* **12** (2022) 119, arXiv:2208.10504 [hep-ph].

[183] J. Preskill, M. B. Wise, and F. Wilczek, "Cosmology of the Invisible Axion," *Phys. Lett. B* **120** (1983) 127–132.

[184] M. Dine and W. Fischler, "The Not So Harmless Axion," *Phys. Lett. B* **120** (1983) 137–141.

[185] L. F. Abbott and P. Sikivie, "A Cosmological Bound on the Invisible Axion," *Phys. Lett. B* **120** (1983) 133–136.

[186] G. R. Dvali, "Removing the cosmological bound on the axion scale," arXiv:hep-ph/9505253.

[187] R. Foot, H. Lew, and R. R. Volkas, "A Model with fundamental improper space-time symmetries," *Phys. Lett. B* **272** (1991) 67–70.

[188] C. G. Callan, Jr., R. F. Dashen, and D. J. Gross, "Toward a Theory of the Strong Interactions," *Phys. Rev. D* **17** (1978) 2717.

[189] D. J. Gross, R. D. Pisarski, and L. G. Yaffe, "QCD and Instantons at Finite Temperature," *Rev. Mod. Phys.* **53** (1981) 43.

[190] P. Fox, A. Pierce, and S. Thomas, "Probing a QCD String Axion with Precision Cosmological Measurements," *arXiv e-prints* (Sept., 2004) hep–th/0409059, arXiv:hep-th/0409059 [astro-ph].

[191] G. G. Raffelt, "Astrophysical axion bounds," *Lect. Notes Phys.* **741** (2008) 51–71, arXiv:hep-ph/0611350.

[192] F. Takahashi, W. Yin, and A. H. Guth, "QCD axion window and low-scale inflation," *Phys. Rev. D* **98** no. 1, (2018) 015042, arXiv:1805.08763 [hep-ph].

[193] E. Koutsangelas, "Removing the cosmological bound on the axion scale in the Kim-Shifman-Vainshtein-Zakharov and Dine-Fischler-Srednicki-Zhitnitsky models," *Phys. Rev. D* **107** no. 9, (2023) 095009, arXiv:2212.07822 [hep-ph].

[194] K. Choi and S. H. Im, "Realizing the relaxion from multiple axions and its UV completion with high scale supersymmetry," *JHEP* **01** (2016) 149, arXiv:1511.00132 [hep-ph].

[195] D. E. Kaplan and R. Rattazzi, "Large field excursions and approximate discrete symmetries from a clockwork axion," *Phys. Rev. D* **93** no. 8, (2016) 085007, arXiv:1511.01827 [hep-ph].

[196] T. Kobayashi, R. Kurematsu, and F. Takahashi, "Isocurvature Constraints and Anharmonic Effects on QCD Axion Dark Matter," *JCAP* **09** (2013) 032, arXiv:1304.0922 [hep-ph].

[197] R. Foot, "Mirror dark matter: Cosmology, galaxy structure and direct detection," *Int. J. Mod. Phys. A* **29** (2014) 1430013, arXiv:1401.3965 [astro-ph.CO].

[198] G. Dvali, "Entropy Bound and Unitarity of Scattering Amplitudes," *JHEP* **03** (2021) 126, arXiv:2003.05546 [hep-th].

[199] G. Dvali, "Bounds on quantum information storage and retrieval," *Phil. Trans. A. Math. Phys. Eng. Sci.* **380** no. 2216, (2021) 20210071, arXiv:2107.10616 [hep-th].

[200] C. O'Hare, "cajohare/axionlimits: Axionlimits." https://cajohare.github.io/AxionLimits/, July, 2020.

[201] B. Ratra and P. J. E. Peebles, "Cosmological Consequences of a Rolling Homogeneous Scalar Field," *Phys. Rev. D* **37** (1988) 3406.

[202] C. Wetterich, "Cosmology and the Fate of Dilatation Symmetry," *Nucl. Phys. B* **302** (1988) 668–696, arXiv:1711.03844 [hep-th].

[203] G. Hardy, E. Wright, D. Heath-Brown, and J. Silverman, *An Introduction to the Theory of Numbers*. Oxford mathematics. OUP Oxford, 2008. https://books.google.de/books?id=P6uTBqOa3T4C.

[204] E. Landau, *Handbuch der lehre von der verteilung der primzahlen*. No. Bd. 1 in Handbuch der lehre von der verteilung der primzahlen. B. G. Teubner, 1909. https://books.google.de/books?id=81m4AAAAIAAJ.

[205] **NOvA** Collaboration, M. A. Acero *et al.*, "Improved measurement of neutrino oscillation parameters by the NOvA experiment," *Phys. Rev. D* **106** no. 3, (2022) 032004, arXiv:2108.08219 [hep-ex].

List of Figures

List of Tables